

**CEREBELLAR AND CEREBELLAR
THALAMIC CONTRIBUTIONS TO MOTOR
ADAPTATION**

by

Haiyin Chen

A dissertation submitted to The Johns Hopkins University in conformity with the
requirements for the degree of Doctor of Philosophy.

Baltimore, Maryland

March, 2007

© 2007 Haiyin Chen

All Rights Reserved

Abstract

Motor control theories have proposed that the brain controls movements through internal models which perform two reciprocal computations: given the motor action, predict sensory consequences (forward model) and given the desired sensory states, generate the appropriate motor action (inverse model). To produce accurate movements, the brain must continually calibrate or adapt these models. In this thesis, I explore the critical role played by the cerebellum in the formation and adaptation of these internal movement models, in both the reaching motor system and the saccadic system.

For reaching movements it has been hypothesized that the cerebellum influences planned motor output through the cerebello-thalamo-cortical (CTC) pathway. We tested this hypothesis by studying patients with deep brain stimulation (DBS) electrodes placed in the cerebellar thalamus for the treatment of tremor. If the cerebellar thalamus relays both the normal signals related to motor adaptation as well as the abnormal oscillatory activity related to tremor, then stimulating the nucleus would produce both the desired tremor relief and the unintended disruption of motor adaptation. Indeed, we found that patients' ability to adapt their reaching movements to novel force fields was impaired by DBS in a voltage dependent fashion: the larger the stimulation voltage, the bigger the impairment.

We next investigated how the CTC pathway encodes motor adaptation by recording thalamic neural activities while patients made reaching movements during the microelectrode mapping phase of the DBS neurosurgery. We found preliminary evidence that thalamic activity is modulated by adaptation.

To further understand the mechanism of adaptation, we turned to the sac-

cadic system, where movement trajectory control relies heavily on internal feedback and estimation via the forward model. We trained healthy human subjects on a cross-axis adaptation paradigm and discovered that saccade trajectories became significantly curved with adaptation. Our stochastic optimal feedback control model suggests that curvature results from differential rates of adaptation between the forward and inverse models. Together, our data and model suggest that saccade accuracy is maintained via rapid adaptation of the forward model, which, based on anatomical evidence, is very likely carried out by the cerebellum.

Thesis Advisor: Dr. Reza Shadmehr

Thesis Readers: Drs. David Zee, Frederick Lenz, Amy Bastian, Eric Young

Acknowledgements

This thesis was truly a collaborative effort from multiple laboratories at the Johns Hopkins School of Medicine. First and foremost, I thank Reza Shadmehr, my adviser of five years at the Department of Biomedical Engineering, for giving me tremendous support and a wonderful environment to do science. I have learned and benefited fully from Reza's dedication, professionalism and infectious passion for science. I will never forget one Easter Sunday when I was programming the portable robot to prepare for my first surgery experiment scheduled for the following morning, Reza called me from home to invite me and other members of the lab to his house for dinner. After a wonderful meal, I told Reza that I needed to go back to lab to get ready for the big day, and was completely surprised that he had prepared to return to lab with me so he could help me debug the system. We stayed up all night working together, and began the next morning, with great excitement, our intra-operative research on the neurophysiology of the cerebellar thalamus.

So many people at Reza's lab had a great impact on my work, thinking, or general well-being as a graduate student: Maurice Smith, Opher Donchin, Joern Diedrichsen, Thrishantha Nanayakkara, Goran Djordjevic, EunJung Hwang, Vincent Huang, Maneesh Dewan, Jun Izawa, Arash Hadipour, Tushar Rane, Sang June Oh, Siavash Vaziri, Stephanie Wainscott, Bardia Behabadi, Minnan Xu, and Christine Lee. In particular, I thank Maurice Smith for being a great mentor and collaborator on the DBS project, for teaching me everything from smart data analysis to effective presentation for my thesis proposal. I also thank Arash Hadipour for assisting me with many surgery experiments. Most importantly, I thank members of the Shadmehr lab for their wonderful friendship, support and humor, without which I could never

have made it to graduation.

I thank Dr. Sherwin Hua and Dr. Frederick Lenz for initiating the collaboration between our lab and Dr. Lenz’s team of experts. I remember the day Sherwin and Dr. Lenz came to our lab and played for us video clips of rhythmic firing of human thalamic tremor neurons captured on the oscilloscope, I was so enthralled that I decided right then that I wanted to study these neurons for my Ph.D thesis. I am grateful for the opportunity to work on the projects that formed the first two parts of my thesis and the invaluable scientific and clinical knowledge I have gained through working with Dr. Lenz and Dr. Hua. Recording from the human brain while patients performed reaching tasks in the OR required tremendous team-work and support. I thank members of the Lenz lab — H. Chris Lawson, Lance Rowland, Shinji Ohara and George Hovey — for making this a fun and rewarding adventure.

I am indebted to all the patients who participated our studies and especially those who worked with us during surgery. I will always remember the smiles on these patients’ faces, some nervous, some brave, some even relaxed, and their reassuring words that they would like to do what they can to help advance research because someone else before them had contributed to the development of the DBS. Their generosity and commitment had been both inspiring and critical to my thesis research, and made my endeavor all the more worthwhile for me.

I had the fortune and privilege of working with Dr. David Zee during the last two years of my Ph.D research, and absolutely fell in love with oculomotor research. Working with Dr. Zee was fast-paced, challenging and tremendous fun. His depth and breadth of scientific and clinical knowledge were simply astounding, while his methodicalness and creativity turned every shadow of doubt into “just another control experiment”, which often opened up further inquiries that were worthy of investigation. The saccade project was conducted in collaboration with my fellow BME Ph.D student, Wilsaan Joiner. I thank both Wilsaan and Dr. Zee for teaching me how to use the eye-coil system, working tirelessly together on this project with me, and being a great source of encouragement during the last stretch of my Ph.D. I am also grateful to members of the Zee lab — Dale Roberts, Adrian Lasker, Jing Tian, Sarah Ying, Howard Ying, Xiaoyan Shan, Aasef Shaikh — for all the help I

received, especially Dale Roberts and Adrian Lasker, who generously assisted with the eye-coils in nearly all my experiments.

Last but not least, I thank my friends and family for giving me so many good memories and so much moral support for the past seven years. Every Ph.D tenure has its own “trials and tribulations”. My friends and family have not only sustained me throughout this journey, but also helped me grow into a more mature and confident individual. I thank my fellow BME Ph.D students — Vincent Huang, EunJung Hwang, Minnan Xu, Sulin Chen, Steve Chase, Steve Eliades, Wilsaan Joiner, Simil Roupe, Srivatsan Raghavan, Lina Reiss, Sheng Xu, friends from Princeton — Emily Lin, An-Lon Chen, Jennifer Bergsieker, Scott Humphries, Eric Peng, friends I met while at graduate school — Naomi Lesley, Poppy Crum, Yan Huang, Roger Peng, Chau Do, James Gordon, Aman Jetha, and friends from my middle school in China — Jin Shi, Liang Kun and Zhang Xin, for their unfailing love and support. I am especially grateful to my family — my mother, my sister, my grandparents, aunt Han Li-Ying, uncle Gu Lian-Chu, my husband Jason Harris and his family — who have put so much love, time and effort in my education, and make me feel special everyday of my life.

Contents

Abstract	ii
Acknowledgements	iv
List of Figures	x
List of Tables	xii
1 Introduction	1
1.1 Internal Model as the Computational Framework of Motor Control	1
1.2 Cerebellum and Motor Adaptation	4
1.3 The Cerebello-Thalamo-Cortical Pathway	4
1.4 Deep Brain Stimulation and Thalamotomy	5
1.5 Intra-Operative Recording of the Ventrolateral Thalamus	6
1.6 Cerebellum and Saccade Adaptation	7
1.6.1 The Local Feedback Loop	7
1.6.2 Cerebellar Activity During Saccade	9
1.6.3 Cerebellum Mediates Saccade Adaptation	9
2 Methods	11
2.1 Methods for DBS and Thalamotomy Psychophysical Studies	11
2.1.1 Subjects	11
2.1.2 Experimental Apparatus	12
2.1.3 Experimental Procedures	14
2.1.4 Data Analysis	15
2.2 Methods for Human Ventrolateral Thalamic Neurophysiology Studies	18
2.2.1 Subjects	18
2.2.2 Experimental Apparatus	18
2.2.3 Experimental Paradigm	19
2.2.4 Recording Quality and Criteria for Data Analysis	22
2.2.5 Anatomical Localization of Recorded Units	23
2.2.6 Data Analysis	23
2.3 Methods for Cross-Axis Saccade Adaptation Psychophysical Studies	25

2.3.1	Subjects	25
2.3.2	Experimental Apparatus	26
2.3.3	Experimental Paradigm	26
2.3.4	Random Target Jump Experiment	29
2.3.5	Multi-Day Cross-Axis Adaptation Experiment	29
2.3.6	Cross-Axis Adaptation to Two-Degree Target Jumps	29
3	Effects of Human Cerebellar Thalamus Disruption on Adaptive Control of Reaching	30
3.1	Effect of Vim Deep Brain Stimulation on Adaptive Control of Reaching . .	30
3.1.1	Effect of Stimulation on Movements in Null Field	31
3.1.2	Effect of Stimulation on Adaptation to Force Fields	39
3.2	Effect of Stimulation on Trial-to-Trial Sensitivity of Motor Error	44
3.2.1	Sensitivity to Motor Error: A State-Space Model of Adaptation . . .	44
3.2.2	Measuring the Goodness of Fit of the Model	46
3.2.3	Model Results: Effect of DBS on Error-Driven Motor Adaptation . .	47
3.3	Effect of Vim Thalamotomy on Adaptive Control of Reaching	50
3.3.1	Effect of Thalamotomy on Movements in Null Field	50
3.3.2	Effect of Thalamotomy on Adaptation to Force Fields	51
3.4	Discussion	51
4	Intra-Operative Recording of Human Ventrolateral Thalamus	57
4.1	Ventrolateral Thalamus and Reaching Movement Control	57
4.2	Summary of Database	59
4.3	Motor Adaptation Performance in the OR	59
4.4	Timing of VL Thalamic Activity With Respect To Movement	62
4.5	Directional Selectivities of VL Thalamic neurons	62
4.5.1	Directional Tuning During Eight-Direction Movement Block	62
4.5.2	Direction Selectivity During Two-Direction Adaptation Block . . .	64
4.6	Patterns of Task-related Activities	67
4.6.1	Velocity-Like Discharge Pattern	67
4.6.2	Inhibition Then Rebound-Excitation	71
4.7	Adaptation-Induced Change in VL Thalamic Neural Activity	72
5	Cross-Axis Saccade Adaptation	76
5.1	Magnitude of Cross-Axis Saccade Adaptation	76
5.2	Cross-Axis Saccade Adaptation Induces Curvature in Saccade Trajectories .	78
5.2.1	Quantifying Saccade Curvature	79
5.2.2	Curvature Results From Adaptation, Not Visual Feedback of Target Jump	80
5.3	Relative Timing of Saccade Component Velocities Changes With Adaptation	83
5.3.1	Component Velocities and Their Coordination During Normal Oblique Saccades	83

5.3.2	Characteristics of Component Velocities During Adaptation	84
5.4	Chord Slopes Display Multiple Timescales of Learning	85
6	Modeling Cross-Axis Saccade Adaptation	88
6.1	Simulating a Single Saccade Trajectory	88
6.1.1	Starting Point: Signal-Dependent Noise	88
6.1.2	New Framework: Stochastic Optimal Feedback Control	90
6.2	Modeling Adaptation	93
6.2.1	Trajectory Curvature Reflects Suboptimality in the Saccadic System	93
6.2.2	Adapting the Controller and the Forward Model	94
6.3	Characteristics of Forward Model Adaptation	98
6.3.1	Forward Model Involves Multiple Time-Scales of Plasticity	98
6.3.2	Error Interpretation Dictates Motor Learning	98
6.4	Neural Correlates of the Model	104
	Bibliography	107
	Curriculum Vitae	118

List of Figures

1.1	Comparison of internal models for the reaching system and the saccade system	3
2.1	Experimental design for the DBS psychophysics study.	13
2.2	Recording human ventrolateral thalamic activity during surgery	20
2.3	Experimental design for the cross-axis adaptation study.	27
3.1	Tremor reduction in DBS patients.	32
3.2	Example of reach trajectories from a DBS patient.	38
3.3	Effect of DBS on motor adaptation.	40
3.4	Relationship between stimulation voltage and adaptation impairment.	43
3.5	State-space model results for DBS patients and controls.	48
3.6	Effect of thalamotomy on tremor and motor adaptation.	52
4.1	Ascending pathways from the cerebellum and the basal ganglia to cerebral cortex	58
4.2	Sample neurophysiological recording from the OR	60
4.3	Psychophysical performance in the OR	61
4.4	Timing of VL thalamic activity with respect to movement	63
4.5	Examples of human VL thalamic neurons showing directional tuning	65
4.6	Human VL thalamic neurons are not generally cosine-tuned	66
4.7	VL thalamic neurons active during acceleration	68
4.8	VL thalamic neurons active during deceleration	69
4.9	VL thalamic units displaying activity correlated with movement speed	70
4.10	Vim units displaying inhibition then excitation	71
4.11	Changes in VL thalamic activity during adaptation	73
5.1	Cross-axis paradigm induces robust saccade adaptation.	77
5.2	Performance of a representative subject.	79
5.3	Progression of chord slopes during adaptation	81
5.4	Random target jump does not induce adaptation or curvature	82
5.5	Characteristics of primary saccade component velocities.	86
6.1	Comparison of optimization models for saccade trajectories	91
6.2	Comparisons of four implementations of cross-axis saccade adaptation.	96

6.3	Two Scenarios of how error drives forward model adaptation	100
6.4	Results of the two-state model	102
6.5	Results of the error-assignment model	105

List of Tables

3.1	DBS subjects information	33
3.2	Thalamotomy subjects information	34
3.3	Performance comparison between DBS patients and control subjects	35
3.4	Performance comparison between thalamotomy patients and control subjects	36

*For Jason,
who teaches me by example
to love with understanding
and to understand with love.*

*And for all my teachers,
for instilling a sense of wonder in me.*

Landing on one of those table-lands of the Sahara which fall away steeply at the sides, I found myself on the flat top of the frustrum of a cone, an isolated vestige of a plateau that had crumbled round the edges. In this part of the Sahara such truncated cones are visible from the air every hundred miles or so, their smooth surfaces always at about the same altitude above the desert and their geologic substance always identical. The surface sand is composed of minute and distinct shells; but progressively as you dig along a vertical section, the shells become more fragmentary, tend to cohere, and at the base of the cone form a pure calcareous deposit.

... I lingered there, startled by this silence that never had been broken. The first star began to shine, and I said to myself that this pure surface had lain here thousands of years in sight only of the stars. But suddenly my musings on this white sheet and these shining stars were endowed with a singular significance. I had kicked against a hard, black stone, the size of a man's fist, a sort of moulded rock of lava incredibly present on the surface of a bed of shells a thousand feet deep. A sheet spread beneath an apple-tree can receive only apples; a sheet spread beneath the stars can receive only star-dust. Never had a stone fallen from the skies made known its origin so unmistakably.

And very naturally, raising my eyes, I said to myself that from the height of this celestial apple-tree there must have dropped other fruits, and that I should find them exactly where they fell, since never from the beginning of time had anything been present to displace them.

Excited by my adventure, I picked up one and then a second and then a third of these stones, finding them at about the rate of one stone to the acre. And here is where my adventure became magical, for in a striking foreshortening of time that embraced thousands of years, I had become the witness of this miserly rain from the stars. The marvel of marvels was that there on the rounded back of the planet, between this magnetic sheet and those stars, a human consciousness was present in which as in a mirror that rain could be reflected.

— Antoine de Saint-Exupéry, *Wind, Sand and Stars*

Chapter 1

Introduction

1.1 Internal Model as the Computational Framework of Motor Control

Our limbs have inertial dynamics that dictate a complex relationship between joint motions and joint torques. In order to reliably produce a simple movement, such as flexion of the elbow, the brain must activate not only elbow flexors, but also shoulder flexors that counter the shoulder extension torque produced by acceleration of the elbow. To decelerate the elbow flexion and stop at a target, activation and precise timing of elbow extensors are required. Otherwise, the limb will overshoot the target and oscillate (Vilis & Hore, 1980). Current theories suggest that because of time delays in sensory feedback, the brain implicitly accounts for this physics when it composes motor commands (Shadmehr & Mussa-Ivaldi, 1994). To perform a voluntary movement, the brain appears to perform two kinds of computations: 1) given a desired change in the proprioceptively or visually defined sensory state of the limb, it predicts the motor commands that are likely to produce the desired change, and 2) given a planned motor command, it predicts the sensory consequences of that command. These sensori-motor and motor-sensory maps have been respectively referred to as the inverse and forward models of dynamics, and collectively called “internal models” of action (Wolpert & Ghahramani, 2000).

A schematic of how this computational system may operate to carry out a simple point-to-point reaching movement is shown in Figure 1.1A. Given a desired goal, the controller generates appropriate motor commands to initiate the movement. After some delay,

afferent feedback provided by vision and proprioception reaches the controller so that the motor output may be updated accordingly, or generated for the next time step, depending on the implementation. This process iterates until the limb reaches the desired end point. As in any control system, delayed feedback causes instability and oscillation. The forward model of the limb dynamics mitigates this problem by providing internal estimates about the current state of the limb to the controller, via efferent copies of the motor commands. Essentially, the forward model is an internal simulation of the external limb dynamics. Recently, Vaziri et al. (2006) showed that predictions from the forward model and actual measurements of the sensory state integrate optimally to facilitate movement planning and control.

Behaviorally, we know that two types of compensatory actions are engaged when the nervous system detects errors in limb movements. First, both short- and long-latency reflex are evoked by the unexpected proprioceptive inputs associated with error to generate an on-line corrective response. Second, when errors are experienced repeatedly, the on-line corrections, along with error, will serve as teaching signals for the internal model, so that subsequent motor commands produce movements with less error (Marsden et al., 1976; Kawato, 1989). These two systems, one feedback, the other feedforward, are both necessary to ensure accurate movements. Much of what we know about the internal model is thought to be related to the feedforward component — the inverse model of the internal model, also known as the controller. In fact, it has been very difficult to directly observe the influence of forward models in the control of reaching movements, because its effect, or predictions *are* integrated with the sensory feedback. Indeed, it is not known whether motor adaptation is primarily due to changes in the forward model that predicts the sensory consequences of motor commands, or the controller that generates those commands.

This problem — teasing apart sensory feedback and forward model's predictions — can be conveniently avoided if we turn to the saccadic system. Like reaching movements, saccades are also goal-directed point-to-point movements. However, typical saccades are too brief to be influenced by visual feedback. And it has been demonstrated that proprioception does not play a role in on-line control of saccade trajectory (Hopp & Fuchs, 2004). To monitor saccade trajectories, the brain must therefore rely on a forward model of the eye (Fig. 1.1B&C).

In this thesis, we have examined the role of the cerebellum in adaptation of the internal model through both the reaching motor system and the saccadic system.

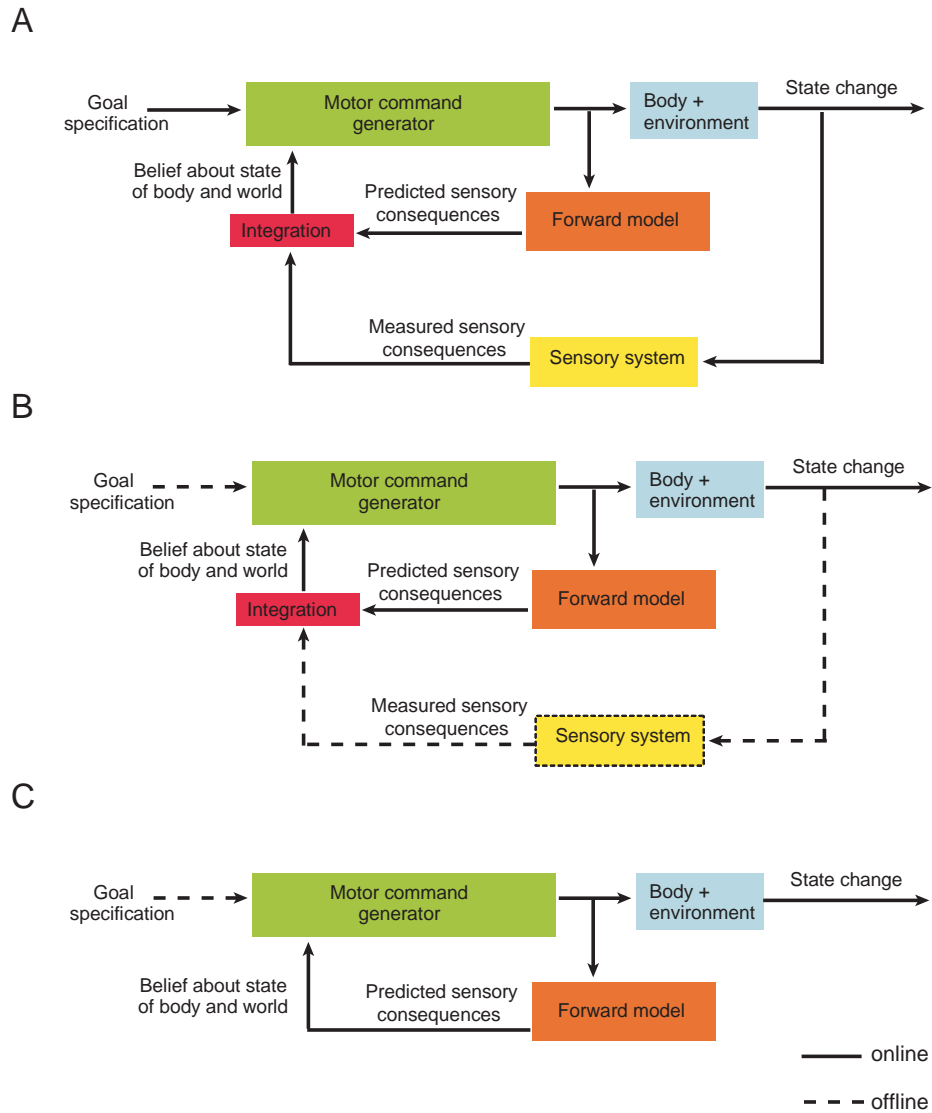


Figure 1.1 Comparison of internal models for the reaching system and the saccade system. **A.** Internal model for reaching system. **B. & C.** Internal model for the saccade system.

1.2 Cerebellum and Motor Adaptation

A fundamental characteristic of internal models is that when they are embedded into a control system, they reduce the reliance of the controller on sensory feedback. As a result, the accuracy of action is thought to be linked to the accuracy of internal models. For example, when internal models of reaching are inaccurate, simulations of reaching show ataxic symptoms (Schweighofer et al., 1998) like those recorded in cerebellar patients (Bastian et al., 1996). Indeed, psychophysical studies suggest that cerebellum is crucially involved in the formation of internal models of reaching. For example, patients with lesions in the posterior cerebellum were unable to adapt to visuomotor misalignments imposed by prism goggles (Weiner et al., 1983; Martin et al., 1996). Patients with global cerebellar degeneration were profoundly impaired in adapting to the novel dynamics of a force field (Maschke et al., 2004; Smith & Shadmehr, 2005). In contrast, patients with Huntington’s disease or Parkinson’s disease – diseases involving the basal ganglia – showed normal adaptation of reaching in force fields (Krebs et al., 2001; Smith & Shadmehr, 2005) and normal adaptation with prisms (Fernandez-Ruiz et al., 2003).

1.3 The Cerebello-Thalamo-Cortical Pathway

The dentate nucleus of the cerebellum projects to the ventro-lateral thalamus, which in turn projects to the motor areas of the frontal lobe (Sakai et al., 2002). In nonhuman primates, neural correlates of internal models of reaching have been recorded in the frontal motor areas, including the primary motor cortex (Li et al., 2001; Paz et al., 2003), supplementary motor area (Padoa-Schioppa et al., 2004), and premotor cortex (Padoa-Schioppa et al., 2002). In light of results in human patient studies, it seems likely that aspects of the internal models of reaching form in the cerebellum and influence descending motor commands via cerebello-thalamo-cortical pathways.

Current evidence, however, has not led to any consensus about the role of this pathway in motor learning. Martin et al. (1996) reported that two out of the three patients with lesions in the cerebellar thalamus learned to compensate for prism goggles normally, while the other patient did not pass criteria for either baseline performance or adaptation. On the other hand, animal lesion research has demonstrated that cerebellar thalamic nucleus is important for the acquisition of certain motor skills. Fabre & Buser (1979) reported that

bilateral lesion of the ventro-lateral thalamus in cats impaired learning of a reaching task that involved pointing to moving targets. Jeljeli et al. (2003) showed that lesion of the ventral thalamic nuclei in rats caused pronounced deficits in their ability to learn to walk on a rotating beam. The inconsistency between human and animal research could be the result of an inter-species difference in the role thalamus plays in adaptation. For example, the cerebellar nuclei project to the thalamus as well as to the spinal motorneurons through brainstem nuclei. It is plausible that in humans, the contribution of the cerebellum to adaptive control of reaching movements is primarily conveyed via brainstem pathways. However, it is difficult to make any conclusion based on the studies so far because of the paucity of available data and inconsistency among patients.

1.4 Deep Brain Stimulation and Thalamotomy

Programmable stimulation of the cerebellar thalamus provides a unique opportunity to explore the role of thalamus in human motor adaptation. We studied patients with essential tremor (ET) who had deep brain stimulators (DBS) stereotactically placed in the posterior aspect of their ventrolateral thalamus (VLp), also known as the ventral intermediate nucleus (Vim). ET is characterized by a 4-12Hz postural tremor (present during voluntary maintenance of steady posture) that usually affects both limbs. In advanced stages, this postural tremor is often accompanied with an intention tremor that intensifies as the hand approaches a target (Elble & Koller, 1990). There is growing evidence supporting the hypothesis that the pacemaker for ET is in the inferior olive-cerebellar circuits (for review, see Deuschl & Bergman 2002). The anomalous oscillation is believed to be then transmitted by the cerebello-thalamo-cortical pathway and manifest as tremor. In ET patients, pathological rhythmic discharges at the frequency of the tremor are seen in all three major nuclei of the ventrolateral thalamus: the cerebellar-recipient (Vim), the pallidal-recipient, and the principal somatosensory nucleus, with Vim having the highest concentration of such tremor-related neurons (Hua & Lenz, 2005). It has been shown that Vim DBS is highly effective for relief of ET (Koller et al., 2000). The success is made possible by accurate and individual localization of the region within Vim that is associated with limb tremor. The locus of Vim DBS implant is determined by the combination of finding Vim's stereotactic coordinates from MRI, neurophysiological mapping of the nucleus, and intra-operative confirmation of relief of tremor with micro- or macro- stimulation of the

identified region (Garonzik et al., 2002).

The mechanism by which DBS produces its therapeutic effect is still being elucidated. Mathematical modeling of the response of thalamocortical neurons to DBS suggests that with typical settings of the stimulator, axons of thalamic relay neurons within a 2mm region around the stimulating electrode are driven to fire at the stimulus frequency while cell bodies and the intrinsic activities of these neurons are inhibited (McIntyre et al., 2004). Indeed, PET imaging studies have shown that DBS leads to increased activation, hence blood flow, in the cortical regions that Vim projects to (Ceballos-Baumann et al., 2001; Perlmutter et al., 2002; Haslinger et al., 2003). Thalamic DBS also tends to drive local inhibitory interneurons in the Vim and may potentially drive the cerebellar nuclei antidromically (the dentate, interpositus and fastigial nuclei all project to VLp, (Macchi & Jones, 1997). The combined effect of thalamic DBS is thought to prevent the tremor-generating signal in the cerebellar nuclei from reaching the cerebral cortex. However, if cerebellar nuclei also convey information to the cerebral cortex related to internal models of reaching, then Vim stimulation might impair adaptive control of reaching.

We found evidence in support of this conjecture. In a reaching task known to induce adaptation, we observed that when DBS was turned on, patients tended to adapt slower than when no stimulation was given. To explore the possibility that this impairment in adaptation might have been primarily a result of indirect stimulation of cortical motor regions by thalamic DBS (Haslinger et al., 2003), we considered another group of ET patients, those with prior Vim thalamotomy. We found that while tremor was generally small or absent in the arm contralateral to the thalamotomy, adaptation was better with the arm ipsilateral to the thalamotomy. Together, these findings corroborate with our hypothesis that adaptation of reaching requires the integrity of the cerebellar thalamus.

1.5 Intra-Operative Recording of the Ventrolateral Thalamus

The success of thalamic DBS for tremor-relief is enabled by microelectrode neurophysiological mapping during neurosurgery which serves to delineate the cerebellar thalamus and to identify regions within the nucleus that are most responsible for tremor. For the mapping procedure, during which the patient is fully awake, single and multi-units

are recorded while the patients' limb is manipulated passively or voluntarily to define the receptive fields of the neurons. To our knowledge, responses of the human thalamic neurons to voluntary movements or perturbations have never been quantified. These mapping procedures offered an unprecedented opportunity to investigate the neurophysiology of the human cerebellar thalamus. In our second experiment, we recorded activities of thalamic neurons while patients made reaching movements using a robotic manipulandum that perturbed their movements in patterns known to induce adaptation. We then infer the nature of the adaptive control signal processing carried out in the cerebellar thalamus.

1.6 Cerebellum and Saccade Adaptation

1.6.1 The Local Feedback Loop

Saccades are rapid, conjugate eye movements that redirect the fovea toward targets of interest. The word *saccade*, French for *jerk*, was first introduced in 1891 by Edwin Landolt who noticed that when we read, the eyes do not move smoothly along a line of text but make little jerky movements, each followed by a short pause (Westheimer, 1989). Saccades are goal-directed point-to-point eye movements that we use to explore visual environments; they can be produced either voluntarily or reflexively. In comparison to reaching movements, saccadic movements are simpler to control. The eye has little inertia and relatively few degrees of freedom for movement – each eye is pulled by six extraocular muscles that form three complementary pairs to produce abduction-adduction, elevation-depression, and intorsion-extorsion.

The purpose of saccade is to move the eye as quickly as possible so that we can scan visual environments without sacrificing, most of the time, stability of retinal image and therefore a continuous visual percept. For example, 15° saccades only take ~ 60 ms. Such movement duration is too fast for visual feedback to play a role in the guidance of saccade trajectories. In fact, it has been shown that the brain actively suppresses visual processing during saccades to reduce the perception of the visual motion (Thiele et al., 2002). Because of this, saccades are often referred to as “blind”. One might think that proprioception, a faster sensory pathway, would play a role in the control of saccades. But Keller & Robinson (1971) showed that stretch reflex is absent in the extraocular muscles of the monkey.

In addition to being extremely fast, saccades are highly stereotyped. The peak

speed and duration of saccades increase monotonically with saccade amplitude, a property referred to as the “main sequence” relationship (Bahill et al., 1975). Because of such characteristics, it was thought that saccades may be preprogrammed, or produced ballistically. Zee et al. (1976) showed this was incorrect; abnormally slow saccades made by patients with spinocerebellar degeneration could adjust themselves mid-flight to track intra-saccadic target jumps. Furthermore, given the ever-present physiological noise in the nervous system, saccades are highly accurate. How, then, in the absence of sensory feedback, does the brain achieve such accuracy? To address this question, in 1975, D. A. Robinson proposed the “local feedback loop” model in which the saccadic system monitors the progress of movements through internal feedback mechanisms. The local feedback loop would derive online estimates about the state of the eye (e.g. position, velocity) through efferent copies of motor commands, update the error vector from the eye to the goal, and thus enable “real-time” trajectory control. In the current language of computational motor control, the local feedback loop is a forward model of the eye.

Several lines of work support this concept of saccadic trajectory control. Hallet & Lightstone (1975) showed that if a point source of light is briefly flashed during a saccade, the subject can make a saccade back to the point in space from where the light source emanated. This is possible only if the brain had information about the position of the eye in the orbit at the time of the flash. Sommer & Wurtz (2004) demonstrated with a memory-guided double-step paradigm that variabilities in size and direction of the first saccade are corrected by the second saccade without new visual information. These two studies confirm that the brain keeps track of the state of the eye along the saccade, as well as its position in reference to the saccadic goal, for future actions. Jürgens et al. (1981) showed that both natural and drug-induced (diazepam) variability of saccade velocity and duration had little influence on saccade amplitude, further supporting the idea of close-loop feedback control of eye position during saccades. Striking physiological evidence came from Robinson et al. (1993), who showed that, in monkeys, unilateral lesions in the caudal fastigial nucleus (cFN) of the cerebellum cause saccades made in all directions to become hypermetric toward the side of the lesion. In particular, the lesion caused attempted vertical saccades to veer toward the lesion direction and display pronounced curvature in the same direction during the latter portion of the saccades. This suggests that the cerebellum may play an important role in steering saccades and making them straight.

1.6.2 Cerebellar Activity During Saccade

Saccades are initiated by commands from the superior colliculus (SC) to neurons in the brainstem that generate premotor commands for saccades. The brainstem saccadic circuitry consists of a group of nuclei collectively known as the brainstem burst generator (BBG). Anatomically, there is also an indirect pathway from SC to BBG via the cerebellum. It is likely that the cerebellum receives efferent copies of the motor commands sent by the SC and uses its own output to the BBG to influence saccadic accuracy. Neurophysiological recording in the caudal fastigial nucleus (cFN), the main output nucleus of the oculomotor cerebellum, has revealed precisely timed activity in cFN neurons related to saccade onset and offset. Neurons in the contralateral cFN fire pre-saccade bursts, the duration of which correlates with the amplitude of the saccade, and neurons in the ipsilateral cFN fire bursts during the late portion of the saccade which presumably help to terminate saccades (Fuchs et al., 1993). Lesions to the cFN results in highly dysmetric eye movements (Vilis & Hore, 1981; Robinson et al., 1993; Iwamoto & Yoshida, 2002; Robinson et al., 2002).

In the framework of computational motor control, the direct pathway from SC may transmit the feedforward motor commands and the indirect pathway via the cerebellum provide either internal feedback or additive motor control signal to BBG.

1.6.3 Cerebellum Mediates Saccade Adaptation

The cerebellum is also critical for calibrating overall accuracy of saccades by adjusting continually the saccadic motor commands to match saccade goals, a process known as saccade adaptation (for review see Hopp & Fuchs 2004). Lesions of the oculomotor cerebellar vermis and the cFN in monkeys impair their ability to adapt saccades (Optican & Robinson, 1980; Goldberg et al., 1993; Takagi et al., 1998; Barash et al., 1999). Patients with Wallenberg's syndrome, a disease involving damage to the cerebellar input pathway from the inferior olive, show enduring dysmetria and reduced capacity to readjust saccadic amplitude (Waespe & Baumgartner, 1992). Patients with cerebellar degradation also show impaired saccade adaptation (Straube et al., 2001). A reversible inactivation study by Robinson & Noto (2005) supported the idea that saccade adaptation starts in the oculomotor vermis, and is later consolidated in the cFN. Very recently, Soetedjo & Fuchs (2006) showed that complex spike activities of subpopulation of purkinje cells in the oculomotor vermis encode error direction during saccade adaptation though not error magnitude.

These data all point to the cerebellum as a key component in saccade adaptation, yet still, the process by which the cerebellum carries out adaptation is not understood. If saccadic motor commands consist of both feedforward and internal feedback components, which component is modified by adaptation? Or if both components adapt simultaneously, how do they interact over time? It is possible that one component leads or even teaches the other in the process of adaptation; alternatively, they may also progress at similar rates. Furthermore, to what extent do the feedforward and feedback components share neuroanatomical circuitry? Answers to these questions would have broad implications on adaptation of other types of point-to-point movements such as reaching.

Chapter 2

Methods

2.1 Methods for DBS and Thalamotomy Psychophysical Studies

2.1.1 Subjects

Twenty ET patients were recruited from the Johns Hopkins Neurosurgery clinic (F.A. Lenz). Fifteen ET patients had either unilateral (11 patients) or bilateral (4 patients) Vim DBS implants (mean age: 63 y, range: 42–80 y). Thus, a total of 19 unique DBS sides were tested (mean time since procedure: 16 months, range: 1 day to 5 years, see Table 3.1) and they are considered as separate DBS cases in the data analysis. The other five patients had unilateral Vim thalamotomy (mean age: 66 y, range: 51–71y; mean time since procedure: 7 y, range: 4–12 y). Of these five patients, four had left Vim thalamotomy, one had right Vim thalamotomy. Of these 20 ET patients, 4 were left handed and 16 were right handed.

Twenty-six healthy adults were recruited to serve as control subjects for the two patient groups. Nineteen served as controls for the DBS patient group (mean age: 58 y, range 49–84 y) and seven as controls for the thalamotomy patient group (mean age: 58 y, range: 50–71 y). Of these 26 subjects, 3 were left-handed and 23 were right-handed. No difference in performance or adaptation level was found between the left- and right-handed controls subjects. Subjects gave written consent for the experiments and the experimental procedures were approved by Johns Hopkins Institutional Review Board.

2.1.2 Experimental Apparatus

We examined adaptive control of reaching in force fields. The experimental setup is shown in Figure 2.1A. Subject held onto the handle of a robotic arm and reached to targets that were displayed on a video monitor. A sling was used to support the subject’s arm and restrict movements to the horizontal plane. Each reach is called a ‘trial’. On odd number trials, the targets appeared at 10cm from the center of the screen at one of four angles 0° , -45° , -90° or -135° (measured clockwise from the horizontal axis). On even number trials, the target appeared back at the center of the screen. At the start of each trial, the subject held the cursor at a crosshair (1cm wide) indicating trial origin for 0.5s. The crosshair then disappeared and a square box (1cm wide) representing the target was displayed. At the end of each reach, the subject received color and sound feedback on the speed and duration of their reach. A pleasant ‘burst’ sound was played if the trial was completed within 0.5 ± 0.07 s and the peak movement speed was between 0.20 and 0.55 m/s. Criteria for movement completion and proximity to trial origin and target were relaxed to accommodate for patients’ tremor. At trial start, the target box would be given if the cursor had been held within 1.5cm from the center of the crosshair for 0.5s. Movements were considered complete either after movement speed had fallen below 0.03m/s for 0.5s or after the cursor had been within 1.5cm from the target center for 1s.

Trials were organized into sets of 96 targets. A single session consisted of 4 null sets, followed by 4 adaptation sets, followed by 3 washout sets. During the null sets, the robot arm was passive and the motors were turned off. During the adaptation sets, the robotic arm applied a viscous curl force-field at the handle to perturb the subject’s movements. The force applied at the hand, $\vec{F}(t)$, was proportional in magnitude and perpendicular in direction to the movement velocity of the hand $\vec{v}(t)$:

$$\vec{F}(t) = C\vec{v}(t) \tag{2.1}$$

where $C = [0 \ 13; -13 \ 0]$ Ns/m for the clockwise curl field and $C = [0 \ -13; 13 \ 0]$ Ns/m for the counterclockwise curl field. Also given within the adaptation sets are catch trials (probability of 1/6, randomly placed) where the force field was unexpectedly removed for the duration of the trial. During the washout sets, the robot motors were turned off with the intention of washing out the effect of motor adaptation induced by the force field. In total, subjects performed 11 sets of trials, or 1056 reaching movements in each session. A

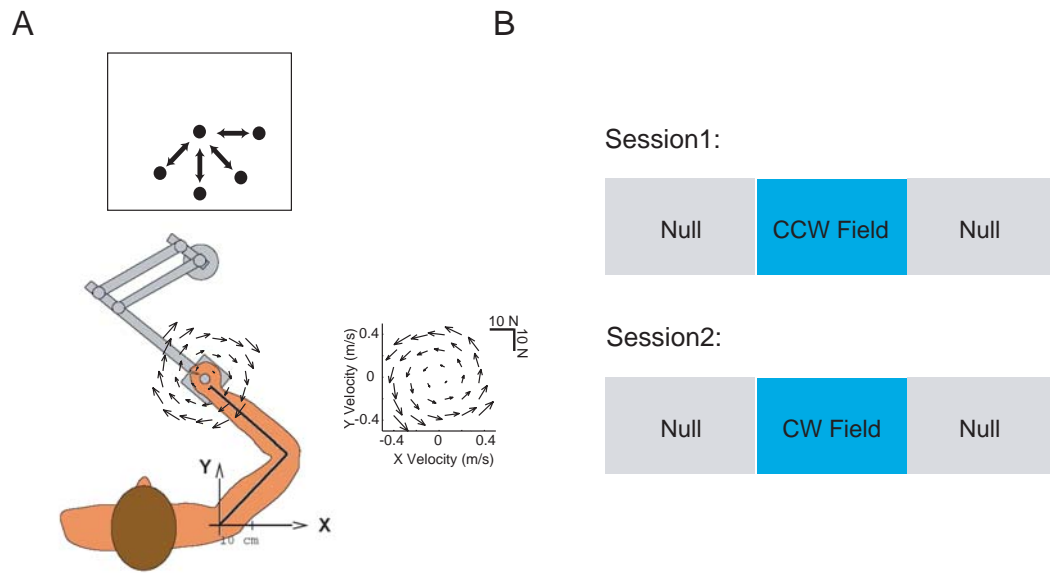


Figure 2.1 Experimental design for the DBS psychophysics study. **A.** Experimental apparatus. The vector fields are clockwise (left) and counterclockwise viscous curl force fields. **B.** Experimental procedure.

complete study consisted of two sessions.

2.1.3 Experimental Procedures

DBS patient group and DBS control group

Fifteen ET patients with DBS implants were trained in the curl fields under two conditions: DBS turned on vs. DBS turned off. The hand contralateral to the implant was used in each condition. For patients with bilateral implants, the effect of DBS was studied separately for each implant. The implant ipsilateral to the hand performing the reaching task was always turned off in order to eliminate possible interference. Subjects were randomly assigned to have DBS off during the first session or off during the second session. In 10 DBS sides/cases, DBS was turned on during the first session and off during the second session. In 9 DBS sides/cases, DBS on/off order was reversed. Among this later group, the first session was conducted one day before the surgery. Hence for these patients, the condition ‘no-stimulation’ was used in place of DBS off. Because we found an effect of stimulation voltage in the group data, we asked four DBS patients (pt. 1, 5, 10, 12) to return and repeat the study more than once, each time at a different DBS voltage setting. Only data from each patient’s first study is included for group analysis of motor learning. Patient 15 did not complete the washout sets in session 2 and was excluded from the trial-to-trial analysis (§3.2).

For both the patient and the control group, the counterclockwise field was given in the first session and the clockwise field was given in the second.

Programming the DBS

Programming of the DBS was performed by a trained physician. The adjustable parameters for DBS are stimulation voltage, pulse width, frequency, polarity at each of the 4 contacts, and polarity at the battery case. The optimal parameter combination for each patient was carefully searched based on reports and observations of stimulation response by both the patient and the physician. Tasks used to evaluate the response include postural hold (arm extension, drinking from a cup), pointing (finger-to-nose pointing), drawing (spiral and line drawing), and writing. The final DBS setting selected was the one that achieved maximum effectiveness on tremor reduction while inducing little, no or only transient side effects of stimulation such as paresthesia and dysarthria. In some patients, multiple param-

eter combinations achieved similar therapeutic results. We conducted multiple experiments in 4 such DBS patients, each time under a different stimulation parameter combination to assess the effect of stimulation parameter on motor learning (see Table 3.1).

Thalamotomy patient group and thalamotomy control group

We recruited five ET patients with Vim thalamotomy (see Table 3.2 and tested them in two sessions in a procedure similar to that of DBS patients. In the morning session, thalamotomy patients trained with the arm ipsilateral to the thalamotomy in the counterclockwise curl field. In the afternoon, they trained with the arm contralateral to the thalamotomy in a clockwise field. Control subjects for the thalamotomy patient group trained with their non-dominant arms in the counterclockwise field during the first session and the dominant arms in the clockwise field during the second session.

2.1.4 Data Analysis

Performance measures

For each trial, we measured general movement performance with four parameters: path length, movement duration, peak speed, and movement error in terms of angular deviation (defined below) 300ms after movement onset.

Movement onsets can be easily detected with a speed threshold when the speed profiles of the movements are relatively smooth and single-peaked. For ET patients, however, postural tremor can often prevent the hand from holding still at trial origin and add oscillatory irregularities to the movements. Thus a simple speed threshold can lead to false detection of movement onset. We took a number of steps to accurately detect movement onset. The trajectory of each trial was broken down to movement segments that exceeded 0.03m/s and only those segments longer than 300ms were selected. To select the correct movement segment, the starting point of the segment had to be no farther than 1cm from the origin and the net displacement toward the target for the segment had to be at least 4.5cm. This precluded erroneous inclusion of looping trajectories resulting from postural tremor while patients attempt to hold still at origin, as well as trials in which sudden dips in speed occurred on route to target.

To analyze motor adaptation, we focused on the movement error made in the first 300ms of each reach. We defined angular error as the angle of trajectory deviation from

the target direction at a fixed time after movement onset, with the convention that counterclockwise errors were positive. Another frequently used measure of error is displacement in the direction perpendicular to target direction. Results from analysis performed with perpendicular displacement at 250ms or 300ms, and angular error at 250ms or 300ms were consistent. We chose to use angular error at 300ms.

During the adaptation and washout trials, we measured movement error with respect to errors recorded at the end of the null sets – after subjects had completed nearly 300 practice trials. That is, a baseline movement error for each direction was estimated from the last null set by taking the median angular error of all trials made in that direction. All subsequent analyses on motor adaptation were based on these median-corrected angular error measurements.

Learning index

To reduce motor errors while unfamiliar forces are applied at the hand, the motor system could adopt either one of two strategies: co-contracting the muscles to increase the stiffness of the arm, or predictively compensate for the force fields by developing an internal model. Both strategies lead to the reduction of trajectory deviations during field trials, however they result in very different catch trial behaviors. Co-contraction would keep errors small in catch trials just as it does field trial. Internal model, on the other hand, would cause catch trial trajectories to become more deviated in the opposite direction as it evolves to better compensate the external forces (Shadmehr & Mussa-Ivaldi, 1994). Hence the measure that quantifies learning must capture changes of trajectory errors in both field and catch trials. A learning index, LI, (Donchin et al., 2002; Smith & Shadmehr, 2005) is calculated for each set as follows:

$$LI = \frac{\bar{y}_{catch}}{\bar{y}_{catch} - \bar{y}_{field}} \quad (2.2)$$

where \bar{y}_{catch} and \bar{y}_{field} are the median angular error for all catch trials and all field trials in the set, respectively. Since \bar{y}_{catch} and \bar{y}_{field} have opposite signs, their difference is the combined angular error of field and catch trials, which corresponds to the net effect of the force field on movement trajectories. This effect depends on the magnitude of the force field as well as compliance of the subject’s arm. By normalizing \bar{y}_{catch} with the force-field effect, we allow the learning index to be independent of arm compliance. Note that the

index is non-negative. Zero angular error in catch trials yields a zero learning index. When the force field is fully compensated, the learning index attains the maximum 1.0.

We used the average learning index for the second half (3rd and 4th sets) of the adaptation sets as a measure of the overall level of motor adaptation achieved during each experiment session. We also used the denominator in equation 2.2 as a measure of each subject’s arm compliance. The average compliance in the second half of the adaptation sets is presented in Table 3.3.

Tremor Analysis

We obtained tremor information by analyzing each patient’s movement trajectories in the task. This approach imposed several constraints. First, tremor recorded by the robot arm was restricted to the horizontal plane. Second, because the trial lengths were short and the frequency resolution of any spectral analysis is the inverse of the data duration, we were not able to measure tremor with high degree of precision. For most patients, the average recording duration – the sum of time waiting at the origin for target, on route to target, and time at the target– was around 2 seconds. Trials with large tremor had significantly longer recording duration as more time was spent at the origin waiting for the hand velocity and deviation from origin to decrease below thresholds.

Because of the above limitations, we did not attempt to separately resolve *postural tremor* — oscillations produced at the origin and target box while patients are attempting to hold still, and *kinetic tremor*— oscillation produced on route to the target. Rather, we measure the amount of tremor present in each trial on the whole. For the first null set of each session, we computed the 1024-point power spectral density (PSD) of each trial’s acceleration profile. The average PSD of the set was then normalized by its integral so that comparisons could be made across subjects. To assess the effects of thalamotomy and DBS on essential tremor, we computed for each subject’s normalized PSD the fractional power occupied by the frequency range from 3Hz to 10Hz. Besides being a relevant frequency range for ET, the 3Hz–10Hz band was chosen so that task-related movement power was excluded. The acceleration profile of a point-to- point movement cycles through a peak and a trough much like a sine function does over one period. Since in our task, the average time it takes for subjects to make the 10cm movement is between 0.5s and 1s, the associated acceleration power will concentrate in the 1Hz to 2Hz range. As illustrated in Fig 3.1A,

the large peaks below 3Hz in all PSD are task-related. The same spectral analysis was performed on control subjects and the averaged PSD between the two sessions was used for comparison with patients.

2.2 Methods for Human Ventrolateral Thalamic Neurophysiology Studies

2.2.1 Subjects

We studied 23 patients (age range: 44-80) who underwent stereotaxic neurosurgery to receive either a thalamic DBS implant or thalamotomy for the treatment of various neurological disorders (18 had ET, 2 had Parkinson’s disease, 1 had central pain, 1 had multiple sclerosis, and 1 had post-traumatic stress disorder). Four of these patients received bilateral DBS implants. The research protocol was discussed with the patient and a family member by neurosurgeon F.A. Lenz after the patient has been approved and agreed to the surgery. We proceeded with research only if the patient gave both written consent prior to surgery and verbal consent in the operating room (OR). Every research session (lasting ~10 minutes) was conducted with additional verbal consent from the patient and approval from the neurosurgeon. All protocols were approved by the Johns Hopkins Institutional Review Board.

The day before surgery, if the patient was available, he or she was introduced to the experimental setup and trained to make movements with the robot. This was so that patients could become familiar with the task. Patients were not exposed to force fields before surgery.

2.2.2 Experimental Apparatus

Figure 2.2A depicts an OR experiment in progress. The experimental setup is essentially the same as that used for the DBS psychophysics study (Fig. 2.1A), with two modifications:

1. The subject performed the experiment in supine position (with head slightly elevated) and therefore had limited range of motion in the shoulder joint. Subject’s elbow was not supported by a sling as it was in the psychophysics study.

2. The robot arm was actuated by pneumatic pistons which had significantly more delay (~ 50 ms) compared to the conventionally-used electric motors. This means that the viscous curl field produced by this robot was not as smooth and consistent compared to the one produced by the robot with electric motors.

Data Acquisition

Neurophysiologic, electromyographic (EMG) and movement data were collected simultaneously during these experiments. Extra-cellular recordings from a single micro-electrode was high-pass filtered (cutoff frequency: 300Hz) and sampled at 25KHz. Spike sorting was performed offline with commercial software (AlphaSort, Alpha-Omega Engineering, Nazareth, Israel) that employed principal component analysis. EMGs from six limb muscles — flexors and extensors for the wrist, shoulder and elbow — were recorded at 3KHz. Movement data — two-dimensional position and velocity — were collected at 200Hz by a different computer which sent time stamps to the physiological data record to provide synchronization.

2.2.3 Experimental Paradigm

During the microelectrode Vim mapping phase of the surgery, recording sites were selected according to the strength of the response to passive movements, voluntary resistance to those passive movements, as well as activity during voluntary movements. If the site responded to shoulder, elbow or wrist movements, we immediately began the neurophysiological recording and asked the patient hold the handle of the robot and make visually-guided reaching movements. Each set of experiment consisted of three blocks of trials: eight-direction null trials, two-direction adaptation trials, and a repeat of the eight-direction null trials (Fig. 2.2D). All movements were organized in out-and-back pairs. Stimulus presentations for each trial were as follows. At the start of the trial, a crosshair was shown to indicate the starting location and subject was to keep the cursor on the crosshair for 500ms. After another short delay (mean 200ms, range 0–400ms), a square target was presented 9cm away from the origin at one of the four peripheral locations. Subject was instructed to move as quickly as possible to the target and stay inside the square for another 400ms before it turned into a crosshair and became the starting point of the next trial.

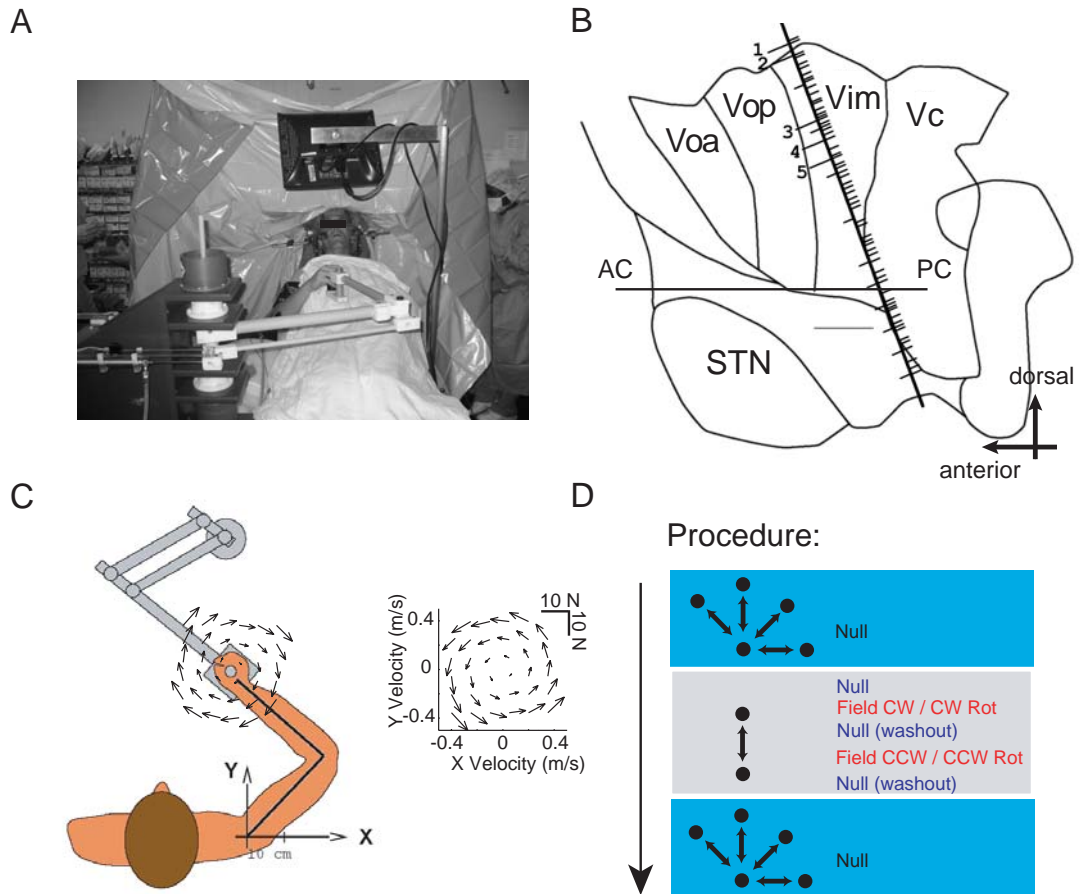


Figure 2.2 Recording human ventrolateral thalamic activity during surgery. **A.** Experimental setup during neurosurgery. The patient's hand was placed on the handle of a robot actuated with pneumatic pistons. Targets were displayed on a LCD monitor. A stereotaxic frame was mounted on the patient's head and secured to the OR table. **B.** Trajectory of the microelectrode overlaid on an atlas of the human ventrolateral thalamus. This track centered in Vim and ended at the border of sensory thalamus, Vc. Numbers to the left of the track indicate recording sites where subject performed the visuomotor task. Voa: ventralis oralis anterior. Vop: ventralis oralis posterior. Vim: ventralis intermediate. Vc: ventral caudal nucleus. STN: substantia nigra. PC: posterior commissure. AC: anterior commissure. **C.** Clockwise and counterclockwise viscous curl force fields. **D.** Experimental design for the intra-operative recording study.

The eight-direction null trial blocks were designed to assess neurons' directional tuning properties, hence they were referred to as *tuning* blocks. Each tuning block consisted of 40 null trials, in which targets for each of the four peripheral locations (0° , 45° , 90° , 135° , see Fig. 2.2D) were presented five times either consecutively (early design) or in random order (later design).

The adaptation trial block consisted of five short blocks of trials — *null1*, *pert1*, *null2*, *pert2* and *null3* — during which targets were only presented at 0° and 90° locations. One of two types of perturbation were given to induce motor adaptation: curl force field or visual rotation.

For the force field paradigm, *null1* consisted of 10 trials while *null2* and *null3* consisted of 16 trials each. The *pert* blocks each consisted of 42 two-directional movements (24 pairs), during which either a clockwise (*pert1*) or a counterclockwise (*pert2*) force field was imposed by the robot. Seven catch trials are randomly interspersed among the force trials. Trial block *null1* served to establish both baseline neural and behavioral activity in the two directions, blocks *null2* and *null3* to washout the behavioral effect of adaptation induced by the perturbation blocks.

During the visual rotation paradigm, subjects had to learn to move the robot while a clockwise or a counterclockwise rotation was imposed on the cursor. Movements were also paired in out-and-back fashion, but because the rotation was with respect to the 0° target, the task required the subject's arm be brought back to the origin by the robot without visual feedback. Hence all voluntary movements in the adaptation block were upward movements. In this paradigm, *null1* consists of 8 trials while *null2* and *null3* consist of 12 trials each. The rotation blocks (*pert1* and *pert2*) consisted of 24 trials each. Four catch trials were randomly interspersed among the adaptation trials.

Length of Experiment Varied Depending on the Patient

The force field paradigm and the visual rotation paradigm described above consisted of 206 trials and 140 trials, respectively. Each experiment took 10-12 minutes to complete. Although these paradigms were significantly shorter compared to that used in the DBS psychophysics study (§2.1.2) and could only lead to partial adaptation even in healthy subjects, often it was necessary to shorten the paradigm still to reduce the total amount of time required to complete an experiment. Sometimes the patient would be interested

to perform the experiment and move with good speed early on during the task, but slow down significantly toward the end due to fatigue in the arm (no sling was used to support the arm). To accommodate this, we modified the length of the trial blocks depending on how soon the patient needed to rest his or her arm (hence the trial numbers provided above were only approximate). The modifications included: eliminating the catch trials so that more adaptation could be achieved in the same number of perturbation trials, shortening each trial blocks, and eliminating one or both of the tuning blocks since our goal was to study VL thalamic activity during adaptation.

2.2.4 Recording Quality and Criteria for Data Analysis

Besides fatigue in the arm, several other factors affected the stability and the quality of data collection:

1. Tremor in the limb: occasionally, a patient's tremor could be(come) too large for the patient to hold on to the robot handle, much less to move it according to visual instruction and hold still at the target. This could happen either consistently for a patient, in which case we stopped the research protocol completely, or sporadically, in which case we waited to see if the tremor would subside. If we found that tremor was minor in null trials but intensified by the force perturbation, we stopped data collection and used the visual rotation paradigm in the next experiment.
2. Heart-rate artifact: the burr-hole opening required for the DBS/thalamotomy surgery was approximately the size of a quarter. The loss of cerebral spinal fluid from the burr-hole caused the brain tissue to become much more susceptible to motion created by arterial pressure. Often during the experiment the microelectrode would pick up background firing modulated at the frequency of the heart beat (cross-checked with EKG) and overwhelm the neural signal being studied.
3. Electrode impedance: the impedance of the custom-made platinum-iridium (80%/20%) glass-coated electrodes were generally 1-1.5M Ω before insertion, but decreased significantly along the track (often to \sim 0.5M Ω) as they were also used to micro-stimulate the tissue for physiological confirmation. This meant that the signal-to-noise ratio of the recording dropped along track with penetration depth. For this reason, much of our existing data were multi-unit recording where units could not be easily sorted.

4. Recording stability: although the patient’s head was fixed to the OR table via the stereotaxic head-frame, not all movements were eliminated. Occasionally, recording was interrupted by speech or coughing from the patient.

All of the above factors led to compromises in either the quality or the length of the recording. We therefore have chosen to analyze only the experiments where we have stable recording for at least 60 trials.

2.2.5 Anatomical Localization of Recorded Units

Units were localized post-surgery by overlaying the trajectories of the microelectrode on an atlas of the human ventrolateral thalamus (Fig. 2.2B). The two are registered by matching known neurophysiological characteristics of the region with the response fields found along the trajectory. These characteristics include:

1. Response fields transition from motor to sensory at the border between Vim and Vc.
2. Neurons responding to cutaneous stimuli are found in Vc.
3. Neurons firing at tremor frequency are more likely to be found in Vim.

This localization procedure provides a best physiological *estimate* on the anatomical location of the recorded units.

2.2.6 Data Analysis

Learning Index

To quantify motor adaptation, we calculated the learning index (LI) using three methods depending on the availability of data. When both catch and perturbation trials were performed, LI was computed using Eq. 2.2 over trials from the second half of the perturbation block. When only perturbation trials were performed and were followed by washout trials, we used:

$$LI = \frac{\bar{y}_{washout}}{\bar{y}_{washout} - \bar{y}_{pert}}, \quad (2.3)$$

where y is movement angular error 300ms after movement onset, $\bar{y}_{washout}$ is the average error from the first two washout trials, which, theoretically, should exhibit similar amount of aftereffect as catch trials, and \bar{y}_{pert} is the average error from the last four perturbation

trials. Lastly, if the experiment ended before any washout trials could be collected, a third method was used:

$$LI = \frac{\bar{y}_{early} - \bar{y}_{late}}{\bar{y}_{early}}, \quad (2.4)$$

where \bar{y}_{early} and \bar{y}_{late} correspond to the average error during the first and last four trials in the perturbation block, respectively.

Spike Density Function

To visualize the neural data, rasters of neuronal discharge and a continuously varying spike density function (SDF) were aligned at one of the key time points during the trials, e.g., target display, movement onset, peak velocity, etc. SDFs were constructed by convolving the spike train with a Gaussian filter ($\mu = 0, \sigma = 20ms$). This method was an adaptation of the double exponential filter in Pare & Hanes (2003).

Latency of Activity With Respect to Movement Onset

For each trial block (tuning and adaptation), we computed the latency of peak activity with respect to movement onset (referred to as time of peak activity). For every tuning block, a mean firing rate, f_0 , was defined as the average firing rate for all trials and all directions during a 3sec window around movement onset time. Next, the peri-stimulus time histogram (PSTH) was computed over all trials during the 3sec window, and compared with f_0 . If the PSTH exceeded f_0 by 1 standard error (SE, bin-wise) of the PSTH for a consecutive 240ms, the time at which the neuron’s activity peaked during this response epoch ($E_{z>1}$) was taken as the latency of neural response to movements during the *tuning* block.

To find the response latency of a unit during the adaptation block, a slight variant of the above procedure was carried out. For each voluntary movement direction, we constructed a PSTH aligned at movement onset for all trials in that direction. The time-span of the PSTH was $\pm 1.5sec$ and bin widths were 50ms. Both the mean firing rate, f_0 , and the bin-wise SE of the PSTH were computed. If the PSTH remained outside the 2 SE window, either above or below f_0 , for at least 200ms, then the neural response was considered movement-related. The latency of neural response was taken as the point at which the PSTH first crossed the 1 SE window around f_0 . The duration of this epoch ($E_{z>1}$) was referred to as the neuron’s response duration. The average latency between the two

directions (if the force field paradigm was used) was used to represent the overall latency for the unit during adaptation.

Preferred Direction

Neurons’ directional tuning properties were assessed using the conventional cosine-tuning method (Georgopoulos et al., 1982; Schwartz et al., 1988; Coltz et al., 1999). The mean firing rates over $E_{z>1}$ (defined above) for all movement directions, $\theta = 0^\circ, \dots, 315^\circ$, were fit to a cosine function:

$$f = \beta_0 + \gamma_1 \cos(\theta - \theta_{PD}) + \epsilon \quad (2.5)$$

The peak of the cosine function corresponds to the direction in which cell discharge rate was highest and is referred to as the preferred direction (PD, θ_{PD} in the equation) of the cell. The regression coefficients β_0 and γ_1 represent the mean discharge rate over all directions and the discharge modulation as a function of direction, respectively; ϵ represents the fitting residual error. To evaluate the strength of directional tuning, we adopted the convention of Georgopoulos et al. (1982) by calculating an index of the depth of neuron’s discharge modulation with direction (termed *depth of modulation*), defined as

$$D_{mod} = \gamma_1 / \beta_0. \quad (2.6)$$

Tuning is considered significant if the r^2 for the regression exceeds 0.7, which corresponds to $p < 0.05$.

2.3 Methods for Cross-Axis Saccade Adaptation Psychophysical Studies

2.3.1 Subjects

Subjects were recruited from the Johns Hopkins medical community. Seven subjects (including three of the investigators of the project: HC, WJ, and DZ) performed the cross-axis adaptation experiments twice - clockwise adaptation paradigm on one day and counterclockwise adaptation paradigm on another day. The order in which the two paradigms were given was counterbalanced across subjects. Four additional subjects (in-

cluding investigator RS) were trained on only one of the two paradigms (two on clockwise and two on counterclockwise adaptation) over three consecutive days (§2.3.5). Data from all 11 subjects were pooled in the analysis of the one-day experiment data. Two of the seven subjects (WJ and DZ) who performed the one-day adaptation experiment later also performed the random target jump experiment (§2.3.4). Four subjects (including WJ and a subject who did the three-day experiment) performed the two-degree cross-axis adaptation experiment (§2.3.6). All subjects gave written consent to protocols approved by the Johns Hopkins Institution Review Board.

2.3.2 Experimental Apparatus

We used the scleral search coil system (Robinson, 1963) to measure eye movements. Subjects sat in a dark room facing a vertical screen on which light emitting diodes (LEDs) were presented as targets. The seat and head position of the subject was adjusted so that the mid-point between the subject’s eyes was at the center of the coil-system magnetic field, and aligned with the LED located at the center of the vertical target screen ($0^\circ, 0^\circ$). Bite bars were used to minimize head movements. A single directional scleral search coil (Skalar Medical BV, Delft, Netherlands) was used to record horizontal and vertical eye movements at 1000Hz, from either the left or the right eye.

2.3.3 Experimental Paradigm

Each experiment consisted of four trial blocks given in the following order: oblique control trials, pre-adaptation catch trials, adaptation trials interspersed with catch trials, and post-adaptation catch trials (Fig. 2.3A). The pre- and post-adaptation catch-trial blocks were identical. Targets for oblique trials and adaptation trials lay either in the first and third quadrants or in the second and fourth quadrants of the visual space, depending on whether the target jump under investigation was in the counterclockwise or clockwise direction.

Figure 2.3C illustrates oblique control trials for the counterclockwise adaptation experiment. The entire oblique trial block consisted of 50 trials and was given in two sets: 25 trials to five targets located in the first quadrant, five repetitions to each target, followed by another 25 trials to five targets located in the third quadrant, also five repetitions to each target. Target appearance within the set was random. The target locations were 15° lateral to the center LED and $0^\circ, 1^\circ, 2^\circ, 3^\circ$, or 5° above (in the first quadrant) or below (in

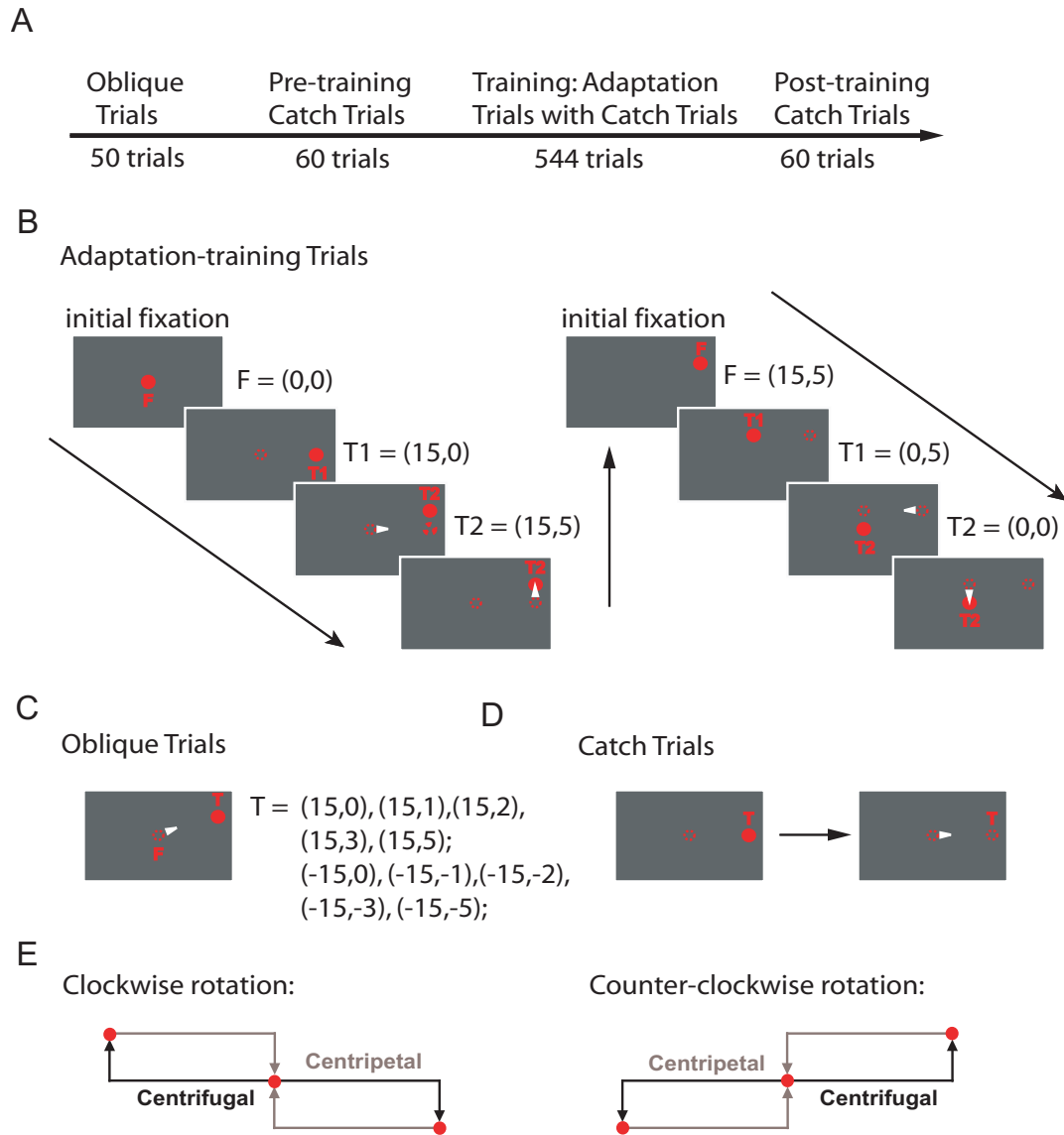


Figure 2.3 Experimental design for the cross-axis adaptation study. **A.** Chronology of each experiment. **B.** Target presentation sequence for a pair of adaptation trials during a counterclockwise adaptation experiment. Filled circles indicate currently illuminated LEDs and open circles indicate previously illuminated LEDs. White arrows indicate the commencement of a saccade. **C. & D.** Example target presentation sequence for oblique and catch trials. **E.** Target configurations for clockwise and counter-clockwise cross-axis saccade adaptation experiments.

the third quadrant) the meridian. Each trial began with fixation at the center LED ($0^\circ, 0^\circ$) for a random interval of 1-2s, after which the center LED was extinguished and the target LED was turned on for 1s. The inter-trial interval was 500ms. During clockwise adaptation experiments, targets were presented in the second and fourth quadrants 15° lateral to the center with vertical eccentricities of $0^\circ, 2^\circ, 3^\circ, 4^\circ$, and 5° (instead of $0^\circ, 1^\circ, 2^\circ, 3^\circ$, and 5° , due to constraints of the LED array used).

The catch trial block contained 60 trials (Fig. 2.3D). On odd-numbered trials, the center fixation LED was turned on for a random period of 1-2s, a target then appeared either 15° to its left or its right. This target LED was extinguished when the subject began to saccade - specifically, as soon as the subject's gaze moved outside of a 2° window surrounding the center fixation LED - and was turned back on 750ms later. This relit target then became the fixation LED for the next trial. Thus, the odd-numbered catch trials were all centrifugal and began at the center LED, while the even-numbered catch trials were all centripetal and began at $\pm 15^\circ$ lateral to the center. These centrifugal and centripetal trial pairs were repeated 15 times in each direction (left or right) randomly during the catch trial block. There was no break between trials.

Trials in the adaptation block were also organized in centrifugal-centripetal pairs. During a counterclockwise adaptation experiment (Fig. 2.3B), odd trials began with fixation at the center LED (F) for 1-2s. A target 15° to the left or the right of the center then appeared (T1). As soon as the subject began to saccade (gaze angle leaving the 2° window surrounding F), the target jumped 5° vertically to a new location (T2). The jump direction was consistently counterclockwise to the orientation of T1, i.e. when T1 was $(15^\circ, 0^\circ)$, T2 was $(15^\circ, 5^\circ)$, and when T1 was $(-15^\circ, 0^\circ)$, T2 was $(-15^\circ, -5^\circ)$. The T2 LED was given for 1s then continued to stay on to serve as the fixation point (F) for the centripetal-even trial. T1 for these even trials were at either $(0^\circ, 5^\circ)$ or $(0^\circ, -5^\circ)$. Once the primary saccade began, T1 jumped to $(0^\circ, 0^\circ)$. Each of the two possible centrifugal-centripetal trial pairs was presented 15 times within an adaptation set. Four catch trial pairs were randomly interspersed among the adaptation trials during training. Altogether, an adaptation set consisted of 60 adaptation trials and 8 catch trials. The adaptation set was repeated eight times and a short break (10sec - 1min) was given between sets.

In the clockwise adaptation experiment, targets were jumped clockwise vertically from the meridian to the second and fourth quadrants of visual space (Fig. 2.3E). All other aspects of the training block were identical to those for the counterclockwise experiment.

2.3.4 Random Target Jump Experiment

We conducted a control experiment to determine whether any effect that we observed in the adaptation experiment was due to real time visual feedback of the target jumps. The random target jump experiment consisted of a block of 500 target jump trials; no other trial types were given. During each trial, the target T1 jumped either up or down at random. Trials were organized in two groups: leftward and rightward sets. Trials in the leftward sets began with fixation at $(25^\circ, 0^\circ)$. On any one trial, T1 could be either $15^\circ, 25^\circ, 30^\circ, 45^\circ$ or 50° to the left of fixation. As soon as the subject's eye left the 2° fixation window, T1 disappeared and a target (T2) appeared either directly above or below T1 at $-10^\circ, -5^\circ, 0^\circ, 5^\circ$, or 10° . Each leftward set consisted of 50 trials, with each of the 25 possible T1-T2 combinations appearing twice. Trials of the rightward sets began with fixation at $(-25^\circ, 0^\circ)$ and had symmetrical target configurations as the leftward trials. Both types of target sets were repeated five times, resulting in a total of 500 trials.

2.3.5 Multi-Day Cross-Axis Adaptation Experiment

The one-day adaptation experiment was repeated over three consecutive days in four subjects to examine long term cross-axis adaptation. Procedures for day 2 and day 3 were identical with that of day 1 except that no oblique control trials were given on these days. Eye coils were worn alternately on the left and right eye for the 3-day experiment.

2.3.6 Cross-Axis Adaptation to Two-Degree Target Jumps

We conducted a variant of the above cross-axis adaptation experiment in which the intra-saccadic target jump size was 2° instead of 5° . Four subjects were recruited for this experiment. Quality of the data was poor in two of the subjects and they were excluded from analysis: one subject had poor eye sight and showed strong directional bias in all saccades; the other subject's saccades were abnormally slow with large amounts of drifts.

Chapter 3

Effects of Human Cerebellar Thalamus Disruption on Adaptive Control of Reaching

3.1 Effect of Vim Deep Brain Stimulation on Adaptive Control of Reaching

We studied the ability of the brain to adapt control of reaching to changes in the dynamics of the environment. Our task is a well studied paradigm where subjects hold the handle of a robotic arm and reach to visually displayed targets (Shadmehr & Mussa-Ivaldi, 1994). The robot either produced no active forces (null trials) or produced a pattern of forces that depended on hand velocity (force field trials). We began our study by examining a group of ET patients that had a DBS implant at the anterior aspect of the thalamic cerebellar nucleus (Vim) of the thalamus (n=15). The basic paradigm involved two sessions of testing. In session 1, subjects performed 384 trials in the null sets (baseline training), then 384 trials in a force field sets (adaptation training), and finally 288 trials in the null sets (washout). Session 2 was identical to session 1 except that forces in the field were rotated by 180°. Patients were randomly assigned to one of two groups: one group had no stimulation in session 1 while another group had no stimulation in session 2. Table 3.1 provides information on stimulation settings and the times at which experiments were conducted relative to the patients' implant surgery dates.

3.1.1 Effect of Stimulation on Movements in Null Field

Stimulation reduced tremor in the initial null set

Oscillations of the hand at 4-12 Hz are a typical feature of ET when the arm is held up against gravity. DBS is very effective in treating this tremor (Vaillancourt et al., 2003). Indeed, our patients displayed clear benefits from the DBS during routine neurological exam consisting of tasks such as postural hold (arm extension, drinking from a cup), pointing (finger-to-nose pointing), drawing (spiral and line drawing), and writing. Because we were interested in quantifying the effect of thalamic stimulation on learning control of reaching, we assessed the effect of stimulation on tremor during the same task.

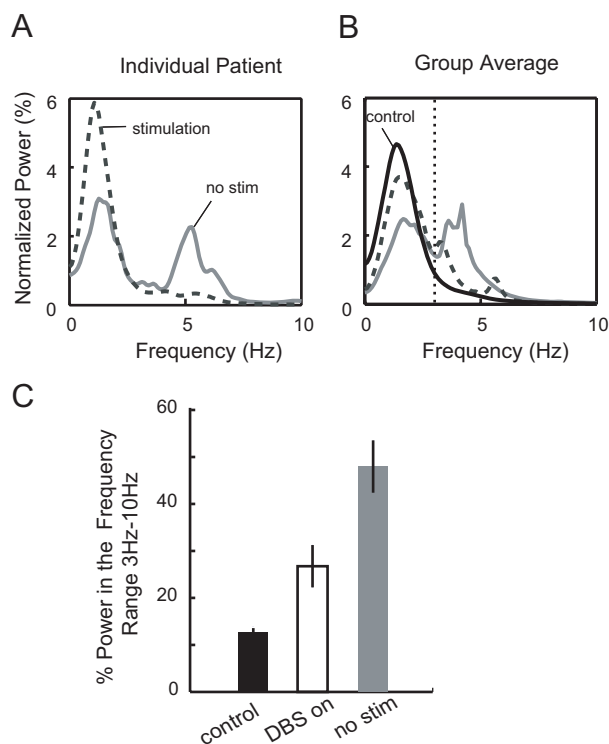


Figure 3.1 Tremor reduction in DBS patients. **A**. Normalized average power spectral density (PSD) for trials in the first null set of each experimental session for a DBS patient. With no stimulation, the PSD exhibited a peak centered at 5Hz. With stimulation, this tremor-associated peak was absent. **B**: Group averages of the normalized PSD measured under each stimulation condition were plotted along with the group average PSD for the control subjects (averaged over the two sessions). Dotted vertical line marks 3Hz. The fraction of power in the range of 3-10Hz (tremor frequency range) was used to quantify tremor amplitude. **C**. Average fraction of power in the tremor frequency range for the control group, DBS patients with stimulation and DBS patients with no stimulation, respectively. Error bars are SE. Stimulation resulted in significant reduction of tremor power ($p=0.0051$).

Table 3.1 DBS subjects information

Case ID \star	DBS Setting				Time of Experiment Relative to Surgery		Δ LI $\star\star$
	Electrodes 0 1 2 3 case	voltage (v)	PW (μ s)	Freq. (Hz)	No stimulation	DBS ON	
1R	0 - - - +	2	270	185	3.3 mo.	5.3 mo.	-0.028
1R	0 - - - +	1.8	270	185	23 mo.	23mo.	-0.205
1R	0 - 0 0 +	1.8	270	185	23.5mo.	23.5mo	-0.112
2R	0 - - - +	6.7	120	185	6 mo.	6 mo.	-0.300
3R	+ - 0 0 0	4.9	120	185	11 mo.	11 mo.	-0.354
4R	+ - - - 0	4.3	60	185	37 mo.	37 mo.	-0.074
5R	+ - - - 0	4.1	210	185	-1 day \dagger	2 days	-0.342
5R	+ - - - 0	3	210	185	-1 day \dagger	9 days	-0.192
5R	+ - - - 0	3.8	210	185	-1 day \dagger	5 mo.	-0.043
5R	+ - - - 0	2.8	210	185	16 mo.	16mo.	-0.046
5L	0 0 - + 0	2.5	210	185	-1 day \dagger	10 days	0.149
6R	0 - - + 0	4.5	60	145	12 mo.	12 mo.	-0.313
6L	+ - - - 0	1.8	120	185	-1 day \dagger	5 days	0.028
7R	+ - - - 0	3.2	150	185	9 mo.	1 day	-0.187
7L	0 0 0 - 0	2.5	60	185	1.3 mo.	1.3 mo.	-0.054
8R	0 0 0 - 0	4	60	185	1.5 mo.	1.5 mo.	-0.049
9R	- 0 0 0 +	2	60	185	1.7 mo.	1 mo.	-0.043
9L	0 - 0 0 +	3.5	90	185	30 mo.	29.5 mo	0.003
10R	0 0 - 0 +	3.5	150	185	4.3 mo.	4.3 mo.	0.126
10R	0 - - - +	2.9	210	185	6 mo.	6 mo.	0.100
11R	- 0 0 0 +	3.2	90	185	28 mo.	28 mo.	0.129
12L	0 0 0 - +	3.5	90	185	33 mo.	33 mo.	-0.006
12L	0 - - - +	2.1	90	185	34 mo.	34 mo.	-0.106
13R	- 0 0 0 +	3.6	120	185	24 mo.	24 mo.	-0.156
14R	0 + - 0 0	3.3	60	185	61 mo.	61 mo.	0.103
15R	- + 0 0 0	3	60	185	8 mo.	8 mo.	-0.121

\star Case ID: number identifies the patient, letter identifies the arm used in the experiment

$\star\star$ Δ LI denotes the average change in learning index between DBS on and no stimulation sessions for the last two adaptation sets.

\dagger Patient was tested the day before surgery.

Table 3.2 Thalamotomy subjects information

Patient	Locus of Thalamotomy	Date of Surgery
1	Left Vim	1999
2	Left Vim	1998
3	Left Vim	1991
4	Left Vim	1996
5	Right Vim	1993

Table 3.3 Performance comparison between DBS patients and control subjects

Performance Measure	DBS Patients	DBS Controls	% Change From Controls
Group Size	19	19	—
Peak Speed (m/s)	0.29 (0.05)	0.31 (0.04)	-8% (24%*)
Path Length (cm)	10.70 (1.34)	10.06 (0.7)	6%*** (91%****)
Movement Duration (s)	1.55 (0.33)	1.11 (0.17)	39%*** (95%**)
AE at 300ms (deg)	0.59 (6.85)	-0.18 (4.44)	-433% (53%***)
Arm Compliance (deg)	16.55	15.19	9%

Note: With the exception of arm compliance, performance measures in the table are computed using trials from the last null set (before adaptation sets began) of each experimental session. The across-trial mean and standard deviation of each performance measure are averaged across sessions for each subject, then compared between the DBS patient group (n = 19) and the control group (n = 19). The group means of the two statistics for each measure are displayed in separate rows with the mean standard deviation shown in parenthesis. The columns, from left to right, show mean values for the patient group, mean values for the control group and % change of the patient group mean from the control group mean. Arm compliance is measured as the average difference between catch trial and field trial angular errors (at 300ms) during the last two adaptation sets, hence given in units of degrees. Standard deviation was not calculated for arm compliance as arm compliance was derived per set rather than per trial. AE: raw angular errors, before corrections for bias.

Asterisks indicate significance of the patient group mean difference from controls using two-sided t-test: *P<0.05, **P<0.01, ***P<0.001, ****P<0.0001.

Table 3.4 Performance comparison between thalamotomy patients and control subjects

Performance Measure	Thalam. Patients	Thalam. Controls	% Change From Controls	All ET Patients	All Controls	% Change From Controls
Group Size	5	7	—	24	26	—
Peak Speed (m/s)	0.26 (0.04)	0.34 (0.06)	-23.4%** (-23.8%**)	0.28 (0.05)	0.32 (0.05)	-12%** (10%)
Path Length (cm)	10.43 (1.40)	10.49 (1.13)	-0.5% (22.7%)	10.65 (1.35)	10.18 (0.82)	5%** (65%***)
Movement Duration (s)	1.52 (0.36)	1.23 (0.22)	24.1%* (65.0%)	1.54 (0.34)	1.14 (0.18)	35%***** (85%***)
ae at 300ms (deg)	0.23 (6.14)	-0.08 (5.18)	-388% (12.9%)	0.52 (6.70)	-0.15 4.64	-441% (44%*****)
Arm Compliance (deg)	16.83	16.66	1.0%	16.61	15.59	7%

Table 4 follows the same convention as Table 2.

All ET patients - combining DBS and thalamotomy patients;

all controls - combining the respective control subject groups.

Asterisks denote significance level of t-test: *P<0.05, **P<0.01,

P<0.001, *P<0.0001, *****P<0.00001.

We focused on the effect of DBS on tremor during reaches in the first null set. We measured tremor in each trial by computing a power spectral density (PSD) of the hand acceleration profile and then normalized this measure by its integral. We then compared this normalized PSD between the DBS on condition and the no stimulation condition. Figure 3.1A shows this measure for a representative patient. With no stimulation, the PSD was bimodal, showing a task-relevant peak at 1-2Hz and a tremor-related peak at about 5Hz. Thalamic stimulation almost completely eliminated the tremor, resulting in an increase of percent power in the task-relevant 1-2Hz (see Methods). The group average plot (Fig. 3.1B) indicated a consistent pattern of tremor reduction in our patients. To quantify this effect, we computed the fraction of power in the 3-10Hz range for each subject (Fig. 3.1C). Stimulation reduced the fractional power in the tremor frequency range by 44% (paired t-test, $p = 0.0051$).

After a period of practice in the null sets, movement kinematics were comparable between stimulation conditions

We found that for almost all patients, in the no stimulation condition the tremor was largest during the initial null set, but then decreased substantially with time and practice. The initial large tremor may in part have been due to nervousness associated with exposure to a novel task, as ET can be aggravated by stress (Gengo et al., 1986). With practice and familiarity, patients may have been able to assume a more relaxed posture and mental state.

Figure 3.2 provides example reaching movements of a DBS patient during early and late null sets with and without stimulation. Figure 3.2A shows that with no stimulation, the patient's movements in the first null set exhibited significant tremor both while the hand was waiting at the origin and while the hand was moving. In the later null sets during the same no-stimulation session (Fig. 3.2B), the patient's tremor was mostly confined to the waiting period and its magnitude was greatly reduced so that the total movement time was shortened almost by half. Surprisingly, tremor in late null set with no stimulation was comparable to tremor with DBS turned on (Fig. 3.2C and D). Indeed, across all patients, we found that by the last null set tremor magnitude (in terms of fraction of power in the 3-10Hz range) in the no-stimulation condition had been reduced from the first null set by an average of 32%. This compares to the 44% tremor reduction by DBS (from the first null

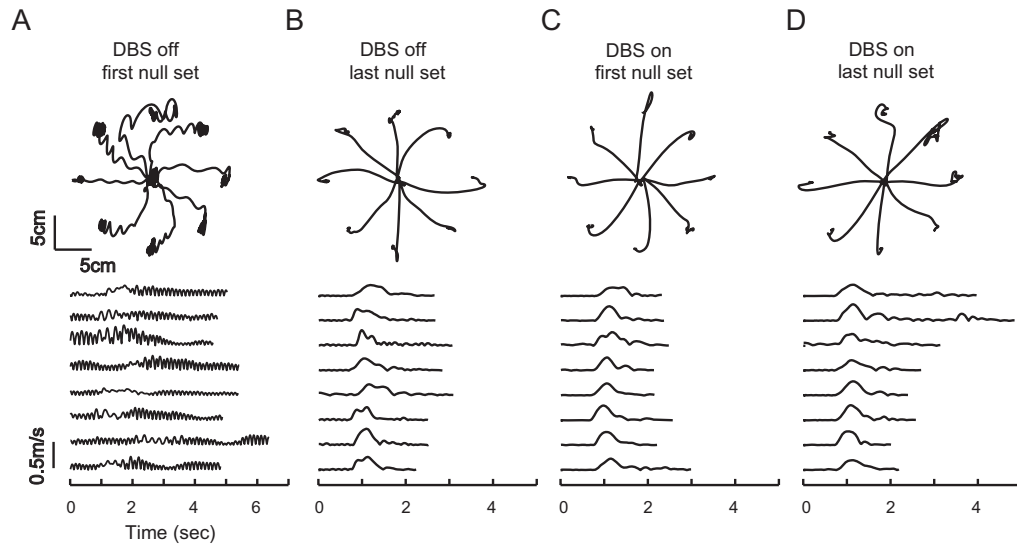


Figure 3.2 Example of reach trajectories from a DBS patient. Top row: paths of the first movements made in each direction during selected sets. Bottom row: speed profiles of the movements in the top row, corresponding to directions 0° , 45° , ..., 315° (from top to bottom). **A.** Trajectories from the first null set of the no-stimulation session. **B.** Trajectories from the last null set of the no-stimulation session. **C.** Trajectories from the first null set of the DBS on session. **D.** Trajectories from the last null set of the DBS on session. With DBS on, the first null set began with dramatically less tremor than the no-stimulation condition. However, in the no-stimulation condition, with the support of the sling at the elbow and increasing familiarity with the task, tremor subsided to levels comparable to DBS on.

set of the no-stimulation condition to the first null set in the DBS on condition). Therefore, regardless of the stimulation condition, tremor had substantially decreased by the last null set of each experimental session.

Once the tremor had subsided, did DBS affect other aspects of reaching? We focused on trials made in the last null set of each session and used four parameters to characterize movement trajectories: path length, angular errors at 300ms after movement onset, peak speed, and movement duration. The mean and standard deviation values of these parameters were used to compare both across stimulation condition and subject group. Surprisingly, we found that with stimulation there was no significant within subject change in the mean value of any of the four kinematic parameters. DBS also did not change patient’s arm compliance. In fact, performance with DBS turned on showed a significant increase in standard deviations of path length (24%, two-sided paired t-test, $p = 0.0085$) and peak speed (8%, $p = 0.013$). Thus, while DBS effectively suppressed tremor, it did not improve the average movement kinematics, and actually resulted in increased trial-to-trial variability of the movements. As compared to control subjects, ET patients had increased mean path length (6%) and movement duration (39%) (Table 3.3). Performance by patients also showed significantly increased inter-trial variability in all parameters.

3.1.2 Effect of Stimulation on Adaptation to Force Fields

Vim Stimulation impaired reaching adaptation

Adapting to altered dynamics of reaching requires changes in motor commands that initiate the reach (Thoroughman & Shadmehr, 1999). These changes are due to feed-forward mechanisms because in catch trials where the dynamics are unexpectedly removed, the limb over-compensates, resulting in aftereffects. Figure 3.3A shows the average size of aftereffects achieved by a control subject and a DBS patient, toward the end of trainings in the adaptation sets. For the control subject, aftereffects from the two experimental sessions were comparable, indicating similar amounts of adaptation. The DBS patient, however, showed significantly larger aftereffects in the no stimulation session than in the DBS session.

Figure 3.3B shows for the same DBS subject the time course of angular-errors (trajectory deviation at 300ms into the movement) during each experimental session. For a system that learns to predict the dynamics of the task we would expect to see decreasing

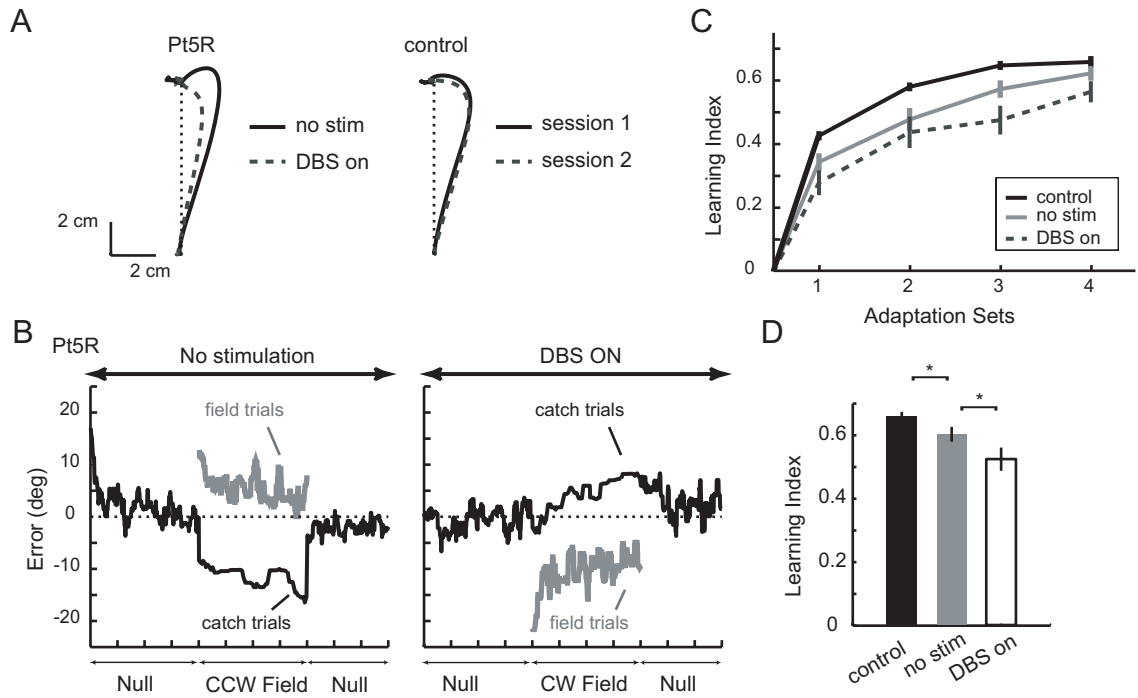


Figure 3.3 Effect of DBS on motor adaptation. **A**. Average catch trial trajectories of a DBS patient and a control subject. Trials were taken from the last adaptation set of each session and were rotated to a canonical direction before averaging. Trials from the session where a clockwise force field was given are inverted for ease of visual comparison. **B**. Performance of a DBS patient with stimulation (left) and without stimulation (right). Shown here are moving averages (window size = 15) of angular error for all trials in each session. The patient achieved significantly higher catch trial errors and lower field trial errors with DBS off than DBS on. **C**. Average learning index for each adaptation set is shown for the control group and each stimulation condition for the patient group. Error bars are SE. **D**. Summary of performance: the average learning index over the last two adaptation sets for each subject group. With no stimulation, patients showed reduced learning index compared to control subjects ($p=0.025$). With DBS turned on, an additional reduction in learning was observed ($p=0.024$).

field trial errors along with increasing catch trial errors (aftereffects). This patient exhibited the expected error pattern both with and without thalamic stimulation. However, training without stimulation led to significantly larger aftereffects (as seen in Fig. 3.3A) and smaller force field errors than training with stimulation. We used the ratio of catch trial errors to the difference between catch and field errors as a learning index (Donchin et al., 2002; Smith & Shadmehr, 2005). As errors in catch trials increase and errors in field trials decrease this index increases from 0 to 1, with unity value reflecting complete adaptation (Eq. 2.2). Figure 3.3C plots the distribution of this index for each subject group. Without stimulation, patients were impaired in adaptation with respect to controls. However, stimulation further degraded this performance. Figure 3.3D quantifies this effect by averaging performance in the last two training sets. When no stimulation was applied, ET patients showed on average an 8% reduction in learning index compared to controls ($p = 0.025$). However, with stimulation the patients showed an additional 13% reduction in the learning index ($p = 0.024$ when comparing DBS on and no-stimulation; 20% reduction comparing DBS on to control, $p = 0.0007$).

Acquisition of internal models involves error-dependent trial-to-trial changes in motor commands. For adaptation to take place, error experienced in a given movement to a given target needs to influence subsequent motor commands for that movement direction; this corrective influence may “spill over” to other movement directions as well, resulting in generalization of adaptation. We can quantify this pattern of direction-dependent trial-to-trial adaptation via an error generalization function (Thoroughman & Shadmehr, 2000; Donchin et al., 2003; Smith & Shadmehr, 2005). The rate of adaptation also depends on the strength of motor memory retention. It is possible that patients do not adapt as well because the trace of motor memory somehow decays faster. In Section 3.2, we characterized these properties of adaptation for our subject populations with an autoregressive linear state-space model that has been previously applied to study both healthy subjects and movement disorder patients (Thoroughman & Shadmehr, 2000; Donchin et al., 2003; Smith & Shadmehr, 2005). Our goal was to use the model to identify components of the adaptive computation that were affected by either ET itself or stimulation, which led to the overall reduction in learning we observed with learning index. We found that neither ET nor thalamic stimulation significantly affected the general shape of the error generalization function or motor memory retention. Rather, they significantly reduced the strength of generalization in several key movement directions relative to the direction in which error

was experienced. Compared to controls, ET patients without stimulation learned over 30% less at the movement direction where error was experienced. Thalamic stimulation led to an additional 37% reduction in this sensitivity to errors.

Adaptation impairment was correlated with stimulation voltage

Thalamic stimulation does not simply switch off a subcortical-cortical neuronal relay. Rather, variation of stimulation parameters (voltage amplitude, frequency, pulse duration, and electrode selection) produces a complex pattern of activity in the thalamo-cortical circuitry. A recent study found that while increased stimulation voltage was consistently associated with increased tremor relief, pulse duration had only a small effect, and frequency change had no significant effect (O’Suilleabhain et al., 2003). If the degree of tremor reduction depends on parameter settings, then do deficits in motor learning also depend on parameters of stimulation? Fig. 3.4A and B illustrate the performance of two patients with two different stimulation voltage settings. With the DBS off, both subjects demonstrated motor adaptation (the exact levels of adaptation vary from patient to patient). When DBS was turned on, performance of the subject with higher voltage (Fig. 3.4A) was significantly reduced, while performance of the subject with lower voltage (Fig. 3.4B) remained similar to that of the off state. Figure 3.4C plots the relationship between the magnitude of within-subject percent change in the learning index and the stimulation voltage. We found a significant correlation (Pearson’s correlation, $r = -0.67$, $p = 0.0018$, Spearman rank correlation, $r = -0.62$, $p = 0.0044$) between stimulation voltage and the degree of impairment in motor adaptation. The voltage sensitivity was somewhat stronger when the electrode configuration was in bipolar mode (stimulating with respect to one of the four electrodes, Fig. 3.4E) than unipolar mode (stimulating with respect to the battery case, Fig. 3.4D).

In contrast, we did not observe a correlation between learning impairment and pulse width of DBS (frequency of stimulation was identical in all but one of our patients). The partial correlation between percent change in learning index and stimulation voltage, controlling for stimulation frequency, pulse width, stimulation mode (bipolar or unipolar), number of cathodes activated, number of all activated contacts, time of the study relative to each patient’s implant surgery and time lag between the DBS-on session and no-stimulation session (see Table 3.1), was $r = -0.75$ ($p = 0.005$, $df = 10$, two-tailed). This indicates that in our study, voltage was the only parameter in the above eight factors that plays a significant

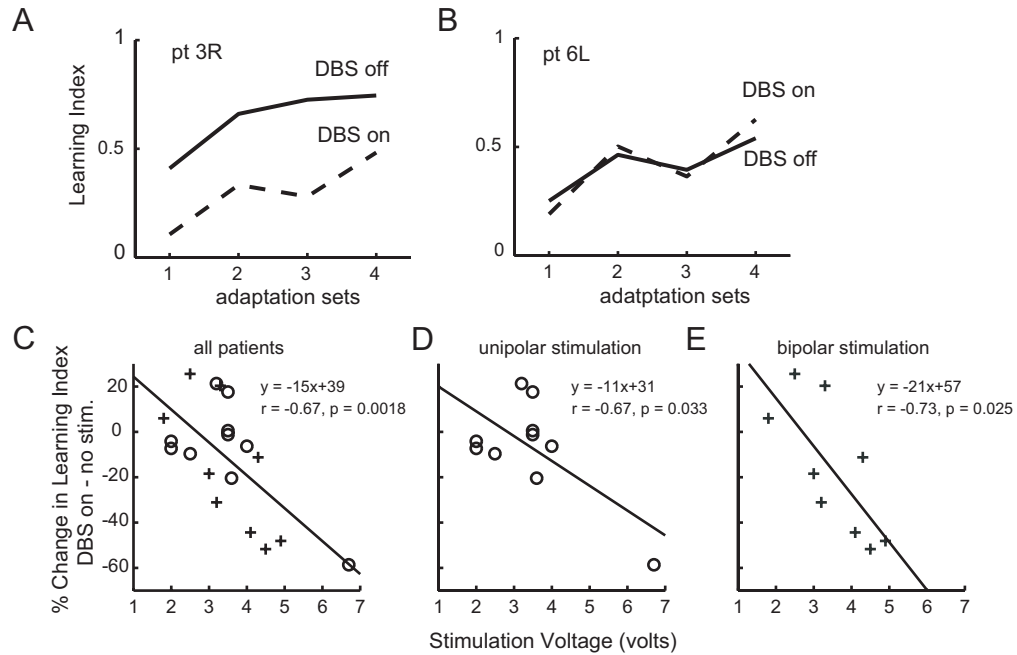


Figure 3.4 Relationship between stimulation voltage and adaptation impairment. **A**. Performance by a patient whose stimulation voltage for the DBS was set at 4.9V. **B**. Performance by a patient whose stimulation voltage was set at 1.8V. **C**. Percent change in learning index (DBS on - no stim.) as a function of stimulation voltage for all 19 DBS cases. Circles indicate patients with unipolar stimulation and pluses indicate patients with bipolar stimulation. **D**, **E**. Relationship between stimulation voltage and percent change in learning index fit separately for patients with unipolar and bipolar stimulations.

role in motor adaptation impairment. We further performed stepwise regression to examine the effect of interaction between stimulation voltage and pulse width which is related to total current output from the DBS and found no significant improvement of fit between learning index reduction and voltage.

While each of the linear regressions in Figs 3.4C, D and E reveal strong correlation between percent reduction in learning index and stimulation voltage, the intercepts of the regression are 39%, 31% and 57% for the combined, unipolar stimulation and bipolar stimulation groups respectively, predicting a facilitation of adaptation at 0 volt stimulation. However, when DBS is programmed to stimulate at 0 volts, we should not expect any change in the level of adaptation between DBS on and no stimulation. The inter-session learning index change for control subjects was $-1\% \pm 11\%$ (mean and standard deviation), rendering it unlikely that there exist some forward interference or facilitation of performance from session one to session two. We speculate that the relationship between adaptation impairment and voltage may be better characterized by a nonlinear function. One possibility is a sigmoid-type function that gradually decreases from 0% reduction near 0 volts, then decreases more steeply beyond 3 volts, and finally saturates somewhere beyond 7 volts. It is also possible that the relationship between adaptation reduction and voltage is non-monotonic. At low stimulation voltage, patients may adapt better than the no stimulation condition given that the abnormal tremor signal is a source of noise that can be disruptive to normal neuronal processing. Our finding that, on average, ET patients adapt less than control subjects (Fig. 3.3) when no stimulation is given lends support to this hypothesis. Given limited patient population, it is difficult to conclude the true relationship between adaptation reduction and voltage. It is clear however, that at stimulation voltage beyond 4 volts, adaptation is greatly reduced.

3.2 Effect of Stimulation on Trial-to-Trial Sensitivity of Motor Error

3.2.1 Sensitivity to Motor Error: A State-Space Model of Adaptation

We quantified the sensitivity of the motor system to errors that were experienced in a given trial and how those errors affected the motor commands that initiated the subsequent trial. Recent theories developed by Thoroughman & Shadmehr (2000) and Donchin et al.

(2003) describe this incremental learning process with a discrete state space model. We used a similar model to fit the sequence of trial-to-trial angular errors for each individual subject.

$$\hat{y} = D_{\theta}F[n] - z_{\theta}[n] \quad (3.1a)$$

$$\mathbf{z}[n + 1] = A\mathbf{z}[n] + \mathbf{B}\hat{y}[n] \quad (3.1b)$$

In Eq. 3.1, $\hat{y}[n]$ is the estimated angular error measured in trial n , θ is the target direction for that trial, D_{θ} is the arm’s compliance in target direction θ , and $F[n]$ is the force magnitude the robot applied in trial n at 300ms into the movement. The variable $z_{\theta}[n]$ is defined as

$$z_{\theta}[n] \equiv D_{\theta}\hat{F}[n] \quad (3.2)$$

where $\hat{F}[n]$ is the magnitude of force the internal model expects to experience in that trial. Thus $z_{\theta}[n]$ is the amount of error compensation the internal model produces when the target direction is θ . The scalar $z_{\theta}[n]$ is an element in the 8-by-1 vector $\mathbf{z}[n]$, which represents the internal model’s compensatory output in each of the 8 target directions in trial n . Eq. 3.1a can be rewritten as $\hat{y} = D_{\theta}(F[n] - \hat{F}[n])$, which simply states that the estimated hand path deviation in trial n , $\hat{y}[n]$, results from the difference between the force actually experienced and the force compensation from the internal model.

The process of adaptation, the mechanism by which errors experienced in any one trial modify the internal state of the learning is modeled with a generalization function. In Eq. 3.1b, \mathbf{B} is an 8-element vector that represents this generalization. Its properties are better revealed in the following scalar form:

$$z_{\varphi}[n + 1] = Az_{\varphi}[n] + B(\varphi - \theta)\hat{y}[n], \quad \varphi = 0^{\circ}, \dots, 315^{\circ} \quad (3.3)$$

Essentially, \mathbf{B} specifies a set of gains by which error experienced in one direction θ changes the internal model in all 8 possible target directions. Note that \mathbf{B} is constrained to only depend on the angular difference between the target direction in which error was experienced θ , and the direction of the internal model it updates, φ .

The state space model presented here is identical to that in Smith & Shadmehr (2005), except that we have added the parameter A , which represents a “forgetting factor”;

a degradation of internal model through the passage of time between trials. With $A = 1$, the internal model maintains its state in between trials with perfect memory. As A decreases from 1 to 0, the internal model loses more and more representation. Therefore, parameter A models a process of forgetting from trial to trial.

D_θ in Eq. 3.2 represents compliance of the arm. It is a one-dimensional function reduced from the classical two-dimensional compliance matrix. It contains 3 parameters: $D_\theta = D_1 + D_2 \cos(2\theta) + D_3 \sin(2\theta)$, and only describes compliance in the direction perpendicular to target direction (see Smith & Shadmehr 2005 for a mathematical derivation). To reduce the number of parameters in the model, we also force symmetry around zero angular difference on the generalization function $B(\varphi - \theta)$, so that $B(\Delta\theta) = B(-\Delta\theta)$, for $\Delta\theta = 45^\circ, 90^\circ, 135^\circ, 180^\circ$.

In summary, a total of 9 parameters were present in the state space model: 5 for B , 3 for D and 1 for A . We estimated these 9 parameters for each subject by fitting Eq. 3.1 to the data sequence of 480 trials (4 adaptation sets and 1 washout set). A nonlinear least squares solver is used to obtain the parameter set that minimizes the squared error between the model fit and the data. Search of the best parameter set always began with the initial condition $A = 1, \mathbf{B} = \mathbf{0}$ and $\mathbf{D} = \mathbf{0}$.

3.2.2 Measuring the Goodness of Fit of the Model

We assessed the goodness of fit of the state space model for each individual subject by calculating the statistic r^2 , the fraction of the observed variance accounted for by the model:

$$r^2 = 1 - \frac{\sum_{n=1}^N \|y[n] - \hat{y}[n]\|^2}{\sum_{n=1}^N \|y[n] - \bar{y}[n]\|^2} \quad (3.4)$$

where \hat{y} is the sequence of estimated angular error associated with any parameter set (\mathbf{B} , \mathbf{D} , A), and \bar{y} is the average of the data, y , which represents a baseline model that serves to compare with the state space model. In addition, we calculate the partial r^2 for the generalization function and the forgetting factor. We define

$$r_{\mathbf{B},\mathbf{A}}^2 = 1 - \frac{\sum_{n=1}^N \|y[n] - \hat{y}[n]\|^2}{\sum_{n=1}^N \|y[n] - \hat{y}_{\mathbf{D}}[n]\|^2} \quad (3.5)$$

where $\hat{y}_{\mathbf{D}}$ is the sequence of estimated angular error resulting from fitting the arm compliance \mathbf{D} alone when \mathbf{B} is set to $\mathbf{0}$. (Note that if $\mathbf{B} = \mathbf{0}$, the value of A does not affect model

prediction). $r_{\mathbf{B},\mathbf{A}}^2$ is the percent of variance accounted for by \mathbf{B} and \mathbf{A} after having fit \mathbf{D} . This represents the variance accounted for by learning related changes in motor output. $r_{\mathbf{D}}^2$ is calculated similarly.

The average r^2 for the control group, the patient group with no stimulation and the patient group with DBS on are 0.73, 0.61 and 0.59, respectively. The average $r_{\mathbf{D}}^2$ for these groups are 0.58, 0.52 and 0.52, in the same order, and the average $r_{\mathbf{B},\mathbf{A}}^2$ for each group are 0.36, 0.20, and 0.14 in the same order. The estimated compliance function accounted for similar amounts of the observed variance, while the variance captured by the generalization function and the forgetting factor decreases with the strength of the generalization function.

Next, we performed a bootstrap analysis to verify that the $r_{\mathbf{B},\mathbf{A}}^2$ obtained above in fact represent levels of trial-by-trial adaptation. We artificially removed the adaptation component of the data by shuffling the sequence of 480 angular errors while preserving the order of target directions and force magnitude (force/catch trials) given in the experiment. This procedure roughly maintains the explanatory power of \mathbf{D} . From these constructed data sequences, we can bootstrap (50 iterations) a distribution of $r_{\mathbf{B},\mathbf{A}}^2$ for each subject when no motor adaptation takes place and make comparisons with the $r_{\mathbf{B},\mathbf{A}}^2$ obtained from actual data sequences. The average z-scores of the actual $r_{\mathbf{B},\mathbf{A}}^2$ for the control group, the patient group with no stimulation and the patient group with DBS on are 14, 9.6 and 6.8, respectively, with standard deviations of 2.8, 4.5 and 2.8, in the same order. These highly significant z-scores indicate that the model captured the trial-by-trial adaptation in the data.

3.2.3 Model Results: Effect of DBS on Error-Driven Motor Adaptation

We fit the state space model to individual subject data taken during the five training sets when adaptation is most actively induced - the four adaptation sets and the first washout set. The resultant model parameters are averaged across each group and presented in Fig. 3.5. As shown in Fig. 3.5A, the average arm compliance (D1) for the patients during DBS on was not different from that during no-stimulation ($p=0.147$, two-sided paired t-test). The arm compliance for the control group was not different from the patient group under either the no-stimulation condition or DBS-on condition ($p = 0.054$ and $p = 0.414$, respectively, two-sided t-test). The forgetting factor \mathbf{A} in the Eq. 3.1 characterizes how well the internal model is maintained between trials. When $\mathbf{A} = 1$, the

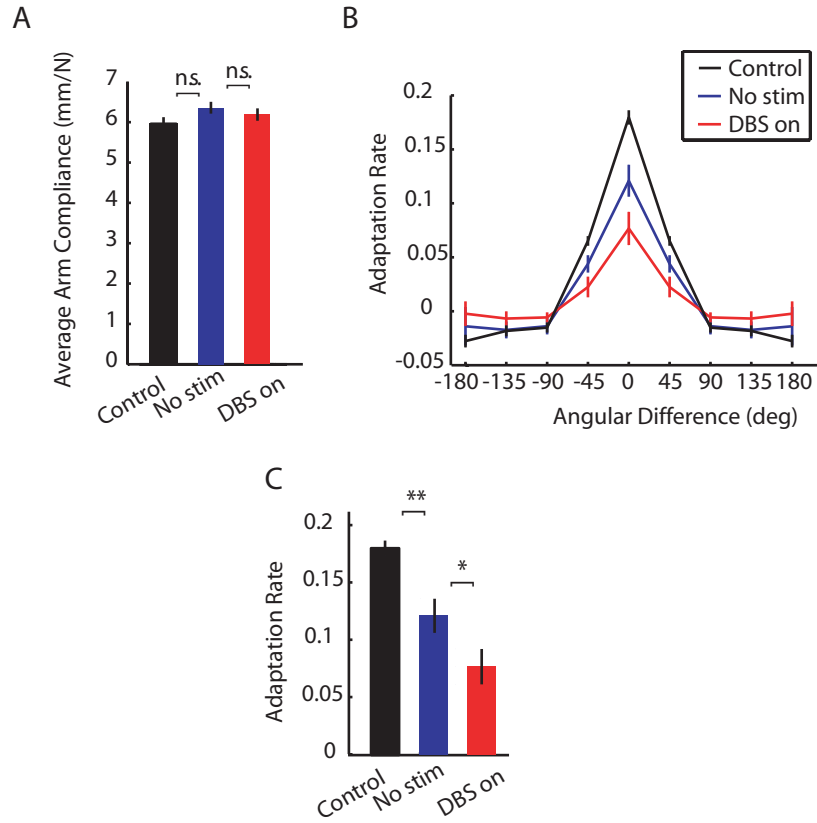


Figure 3.5 State-space model results for DBS patients and controls. **A**. Average arm compliance for each subject group. With no stimulation, DBS subjects show higher compliance than controls ($p=0.026$). **B**. Generalization function for each subject group. **C**. Average generalization strength at zero angular difference for each subject group. With no stimulation, DBS group show significantly reduced generalization compared to control subjects at 0° angular difference ($p=0.0003$), and $\pm 45^\circ$ angular difference ($p = 0.011$). With DBS on, generalization is further reduced compared to no stimulation at 0° ($p=0.014$) and $\pm 45^\circ$ angular difference ($p = 0.024$). All error bars indicate SE.

internal model is remembered perfectly from one trial to the next; when $A = 0$, any changes made to the internal model are completely lost between trials. Average forgetting factor was found to be between 0.99 and 1 for both stimulator conditions for the patient group as well as the control group. Therefore, stimulation did not affect the process of maintaining memory. However, as we show below, it did affect the process of memory acquisition.

Fig. 3.5B displays the average generalization patterns for the control subjects, the patients under the DBS-on condition, and the patients under the no-stimulation condition. The shapes of these generalization functions are similar to those previously derived in other work (Thoroughman & Shadmehr, 2000; Donchin et al., 2003; Smith & Shadmehr, 2005). Characteristically, generalization was maximum at zero angular difference, which means that the internal model for a particular movement direction was most affected by the error experienced in that same direction. Generalization from neighboring movement directions fell off quickly as a function of angular difference, reaching near zero at 90° and becoming slightly negative at 180° . The actual strengths of generalization, however, were markedly different from group to group. Compared to the control group, the no-stimulation group showed an average decrease of 33% at both ($p=0.0003$) and angular difference ($p = 0.011$, one-sided t-test). Furthermore, when DBS was turned on, patients showed an additional 37% reduction at angular difference ($p = 0.014$) and 49% reduction angular difference ($p = 0.024$, one-sided paired t-test). Figure S1C summarizes peak point of the generalization function for each subject group. Note that while the learning rate decrease associated with ET (comparing no stimulation condition to control), and that associated with stimulation (comparing no stimulation to DBS on) were greater than 30%, the corresponding changes measured by learning index were only 8% and 13%. This suggests that ET and DBS each affects the rate of trial-to-trial learning more than the asymptotic performance level achieved.

We calculated learning indices (LI, Eq. 2.2) from the state space model fits, and found them to correlate very well with learning indices computed from the experimental data. Combining LI obtained from all four adaptation sets and all subjects in each group, we find that the predicted LI and actual LI have correlation coefficient values of 0.94, 0.85 and 0.91 for control group, no-stimulation condition, and DBS-on condition, respectively.

In summary, the state space model offered additional insights to the impairment we observed with learning index. Several possible factors may have contributed to the reduction of learning index. For example, stimulation may have caused impairment in retaining

information relevant to learning control. Stimulation may have affected limb compliance. Finally, stimulation may have affected the sensitivity of the adaptive process to errors that were experienced in a given trial. Our results from the state space model demonstrate that poor learning under thalamic stimulation was not due to decreased motor memory retention or abnormal limb compliance. Rather, stimulation made the motor commands that initiated a given movement far less responsive to errors that occurred in the previous trial.

3.3 Effect of Vim Thalamotomy on Adaptive Control of Reaching

Was the impairment of adaptation due to the fact that Vim thalamic stimulation indirectly stimulated motor regions of the cerebral cortex? To explore this question, we recruited five ET patients who had undergone unilateral Vim thalamotomy (Table 3.2) and tested them in the same paradigm as the DBS patients. The important difference was that in one session, the patient used the arm ipsilateral to the thalamotomy and in the other session the contralateral arm.

3.3.1 Effect of Thalamotomy on Movements in Null Field

Because ET is generally a bilateral disease, one expects to find significant tremor in the arm ipsilateral to the thalamotomy as compared to the contralateral arm. Fig. 3.6A plots our measure of tremor during reaches in the null field for a representative patient and for the entire group. For the patient, the hand ipsilateral to the thalamotomy exhibited a clear peak in PSD at 5 Hz while no such peak was evident in the contralateral hand. As expected, the fraction of power in the 3-10Hz range was lower on average when the patients used the arm contralateral to the thalamotomy than the ipsilateral arm (Fig. 3.6B). In terms of movement kinematics, thalamotomy did not significantly affect either the mean or the standard deviation of peak speed, path length, movement duration or angular error of movements made in the last null set. Additionally, thalamotomy had no significant effect on arm compliance measured during adaptation sets. Compared to control subjects, thalamotomy patients showed significant reduction in peak speed (23%) and increase in movement duration (24%) (Table 3.4). Patients also showed reduction of standard deviation

for peak speed (24%), though numerically it was not different from that of the control subjects for DBS patients (Table 3.3) and thus this reduction in inter-trial peak speed variability may be an artifact of the small sample size. To test this, we compared the data of all ET patients ($n = 24$: 5 thalamotomy subjects and 19 DBS cases) to the data of all control subjects ($n = 26$) (Table 3.4). We found that ET patients showed significantly increased inter-trial variability in path length (65%), movement duration (85%) and angular errors (44%), but not in peak speed. ET patients on average moved significantly slower than control subjects - they achieved 12% smaller peak speed, their movement path lengths and durations were 5% and 35% longer, respectively. Our measures of movement kinematics indicated that ET patients moved slower than healthy control subjects and their trajectories tended to be more variable across trials.

3.3.2 Effect of Thalamotomy on Adaptation to Force Fields

Vim thalamotomy impaired reach adaptation in force fields

Fig. 3.6C plots the learning index for all the thalamotomy patients. Switching from contralateral to ipsilateral arm produced a noticeable improvement in adaptation in four of the five patients. Control subjects, on the other hand, showed no difference in adaptation between the two arms (Fig. 3.6D). We calculated the between-arm performance (learning index) difference in the last two training sets and found that the difference was significantly greater in patients than controls (one-sided paired t-test, $p = 0.038$). This demonstrates that the thalamotomy patients as a group were significantly better in learning the task when they used the arm that exhibited more tremor (i.e., the arm ipsilateral to the thalamotomy).

3.4 Discussion

We tested the hypothesis that the cerebello-thalamo-cortical pathway plays a crucial role in adaptation of reaching movements by studying ET patients in whom this pathway was disrupted by Vim DBS or thalamotomy. We found that while both DBS and thalamotomy effectively reduced tremor during posture and reaching, they significantly impaired the rates of adaptation. In addition, we observed a significant correlation across the patients between stimulation voltage and the amount of adaptation impairment induced by stimulation. Patients with larger stimulation voltage tended to show greater adaptation

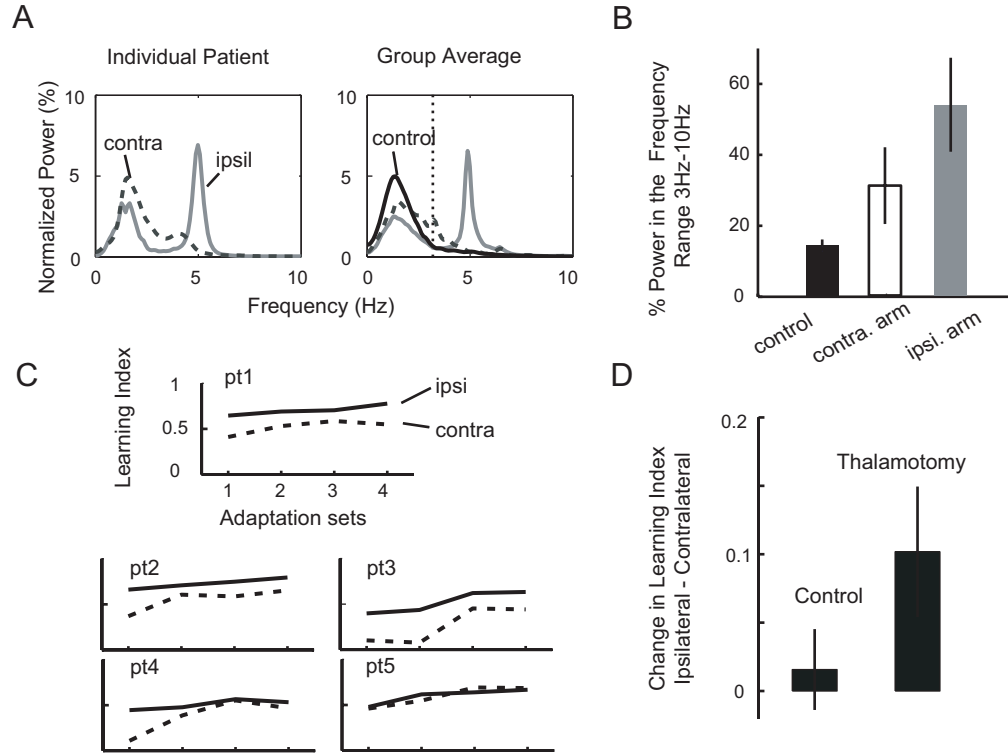


Figure 3.6 Effect of thalamotomy on tremor and motor adaptation. **A**. Left: normalized average PSD for all trials in the first null set of each session for a thalamotomy patient. PSD for the untreated arm, ipsilateral to the thalamotomy, has a tremor-associated peak at 5Hz. In the treated arm, contralateral to thalamotomy, this peak is greatly reduced. Right: group averages of normalized PSD for the patients' ipsilateral arms and the contralateral arms, as well as the control subjects (average of the two arms). Dotted vertical line marks 3Hz, as in Figure 3.1A. **B**. Group average of fractional power in the tremor frequency range (3-10Hz) for the control subjects, the ipsilateral and the contralateral arms of the patients. Error bars are SE. **C**. Performance of each thalamotomy patient quantified by learning index. Solid line indicates performance of the ipsilateral arm and dotted line contralateral arm. **D**. Average between-arm change in learning index for the patient group (ipsilateral - contralateral) and the control group (session1 - session2). Only learning indices from the last two adaptation sets are used. Thalamotomy patients show a significant decrease in adaptation in the contralateral arm ($p=0.038$).

impairment. The cerebellum has long been associated with motor adaptation. A number of psychophysical patient studies have found that damage to the cerebellum can profoundly impair the ability to adapt to novel kinematics or dynamics of reaching (Weiner et al., 1983; Martin et al., 1996; Maschke et al., 2004; Smith & Shadmehr, 2005). It is thought that the cerebellum has the ability to rapidly form internal models and “correct” the motor commands that are planned by the cortical motor areas by supplying information that predicts and compensates for constraints of the task (Conrad et al., 1974; Vilis & Hore, 1980). Alternatively, the cerebellum may compute signals that are crucial for forming an internal model (such as motor errors), and convey these signals to the cortical motor areas where motor memories form. In humans, the cerebellum directs most of its output to the cerebellar thalamus and only a small number of fibers to the red nucleus (Nolte & Angevine, 2000), thus from the anatomical standpoint, the cerebello-thalamo-cortical pathway should play a significant role in human motor adaptation, particularly reaching adaptation. However, until now, there has been very little empirical evidence directly supporting the importance of the cerebellar thalamus in human reaching adaptation (Martin et al., 1996). In the present study, we found evidence for this hypothesis using a within-subject design. We found that reversible disruption of the cerebellar thalamus produced adaptation deficits.

Additionally, we showed that during the no stimulation condition ET patients with DBS implants had an intermediate amount of adaptation impairment between stimulation and healthy controls. This suggests an underlying adaptation deficit associated with ET, a finding that is consistent with the current understanding that ET results from abnormal oscillatory activities in the inferior olive-cerebellum neural network (Elble, 2000; Deuschl & Bergman, 2002). Animal models of ET have shown enhancement of olivary rhythmicity with injection of β -carboline drugs which produces a tremor that resembles ET (Elble, 1998). Clinically, it has been observed that ET can disappear after lesions of the cerebellum (Dupuis et al., 1989), the pons (Urushitani et al., 1996; Nagaratnam & Kalasabail, 1997), or the thalamus (Duncan et al., 1988). PET studies of ET have shown hyperactivity in the cerebellum (Jenkins et al., 1993), the inferior olive as well as the thalamus (Hallett & Dubinsky, 1993). These work, along with the well-established surgical success of Vim DBS and thalamotomy for the suppression of ET, support the theory that tremor-related oscillations originate in the olivocerebellar circuits and propagate to the motor cortex by the cerebello-thalamo-cortical pathway. Taken together, it seems that in the untreated state of ET, functional disturbance of the cerebello-thalamo-cortical pathway caused by tremor-

related oscillations compromises the relay and processing of information pertaining to reach adaptation. Thalamic lesion or stimulation disrupts the transmission of this oscillation and relieves ET, but can further impair motor adaptation.

What is the nature of the information contained in the cerebellar outflow to the thalamus? One possibility is that the cerebellum forms internal models that compensate for specific dynamics of the task (forces produced by the robot) and correct the motor cortical commands. That is, the site of plasticity is in the cerebellum. Alternatively, the cerebellum may be involved in generating certain critical components of the internal model to be used by cortical motor areas. In particular, the cerebellum is well situated for computing motor errors. The intermediate zone of the cerebellar cortex receive afferents about the limbs from both the motor cortex and the spinal cord, allowing it to compare the desired motor output with the results of motor action. Both hypotheses on the cerebellum's role in internal model formation can explain the gross impairments in movement control and motor adaptation seen in cerebellar patients (Martin et al., 1996; Smith & Shadmehr, 2005). However, since motor error is a crucial training signal for adaptation of internal models, these two possible functional roles of the cerebellum cannot be distinguished with the current experiments.

Recently, Diedrichsen et al. (2005a) showed with an fMRI study that when reaching motor errors were generated by either force field, visual rotation or target jump and resulted in similar patterns of on-line feedback correction, the cerebellum became activated regardless the nature of the error and whether the error led to adaptation. This suggests that the cerebellum may be involved in error-correction even when no new internal model is forming, and supports the possibility that internal models form in motor cortical regions but depend on information supplied by the cerebellum through the thalamus. On the other hand, it has been shown that patients with cerebellar degeneration show somewhat preserved on-line error feedback correction when given force perturbations (Smith et al., 2000), whereas they are profoundly impaired in tasks that involve trial-to-trial error-driven learning (Smith & Shadmehr, 2005). These studies on cerebellar degeneration patients suggest that their ability to generate motor errors and to compensate accordingly is not completely abolished, rather, it is the ability to use these errors to drive adaptive changes to motor command that is abolished. Thus while it is clear that the cerebellum plays a critical role in motor plasticity, we do not yet understand the relative contributions of the cerebellum, the thalamus and the motor cortices in reaching motor control and adaptation.

How does thalamic stimulation affect the brain? High frequency stimulation pro-

duces a complex pattern of excitation and inhibition, and its influence can reach beyond the stimulating nucleus. That is, thalamic stimulation is likely to affect downstream and upstream neurons via orthodromic and antidromic stimulation of the nearby axons (Perlmutter et al., 2002; Anderson et al., 2003; Hashimoto et al., 2003; Haslinger et al., 2003; McIntyre et al., 2004). Indeed, imaging studies have demonstrated increased activity in the thalamus, M1, and SMA in resting ET patients with DBS on vs. off (Haslinger et al., 2003; Perlmutter et al., 2002). Although no significant changes were found in the cerebellar nuclei, it is possible that thalamic stimulation might artificially generate action potentials in the cerebellar-thalamic axons, which could travel antidromically to the cerebellar nuclei without causing large changes in synaptic activity. Thus, thalamic stimulation is likely to disrupt neuronal activity in three locations: the motor cortex, the thalamus, and the cerebellar nuclei.

Given this, an alternate interpretation for our DBS study is that adaptation impairment associated with thalamic stimulation was not due to the disruption of the cerebellar thalamus. Rather, it was a result of indirect stimulation of the motor cortical regions via the thalamocortical neurons in Vim. However, we found that thalamotomy and stimulation affected adaptation similarly. Therefore, this suggests that impaired adaptation cannot be exclusively attributed to indirect stimulation of the motor cortex or the cerebellar nuclei.

Our finding that DBS impairs motor adaptation is consistent with recent reports showing that stimulation of the sub-thalamic nucleus in Parkinson's disease impairs performance in certain cognitive or declarative memory tasks. Halbig et al. (2004) compared the DBS on vs. off condition and found that stimulation impaired recall in a declarative memory task. Hershey et al. (2004) found that sub-thalamic stimulation in Parkinson's disease impaired performance in a task that required spatial working memory. It seems that stimulation, whether in the sub-thalamic nuclei or in the cerebellar thalamus, has the potential to produce certain side effects in addition to its known therapeutic actions.

Previously known side effects associated with Vim DBS and thalamotomy in ET patients include paresthesia, dysarthria, persistent and transient arm ataxia and gait disturbance (Mohadjer et al., 1990; Shahzadi et al., 1995; Schuurman et al., 2000; Dowsey-Limousin, 2002). For patients who have DBS, these side effects can often be reversed by turning the stimulator off. Still, many patients who experience side effects choose to leave the stimulator on during the day, for the benefit of tremor suppression far outweighs the side effects. Comparative studies of the effects of thalamic DBS and thalamotomy on ET

and two other movement disorders associated severe tremor (Parkinson's disease, multiple sclerosis) have shown that while the two surgical therapies are equally effective for tremor suppression, DBS tends to give fewer side effects and greater improvement in function as measured by patients' ability to perform daily life activities, self-assessment of surgical outcome, and neuropsychological evaluations (Schuurman et al., 2000). For patients with bilateral drug-resistant tremor, bilateral thalamotomy is no longer used in clinical practice while bilateral thalamic stimulation is a viable therapy. In the present study, we found that while thalamotomy produced motor adaptation deficits, DBS impaired adaptation in a voltage-dependent fashion. This means that at low stimulation voltage, DBS has the potential to eliminate tremor without affecting motor adaptation, further suggesting that DBS may be advantageous over thalamotomy.

Chapter 4

Intra-Operative Recording of Human Ventrolateral Thalamus

4.1 Ventrolateral Thalamus and Reaching Movement Control

The psychophysical results presented in the previous chapter demonstrate that the cerebello-thalamo-cortical pathway carries information related to motor adaptation from the cerebellum to the cortex. Disruption of the pathway impairs either adaptation or the manifestation of adapted behavior. However, the kind of adaptive information which is conveyed by the ascending cerebellar efferents remains unclear. Recordings from the cerebellar thalamus in monkeys during wrist movements have found that neuronal discharge tends to lead (in time) both movement onset (Butler et al., 1992) and activity of sensory thalamic neurons (Butler et al., 2000). Very importantly, the discharge of cerebellar thalamic neurons is sensitive to force perturbations to the arm (Butler et al., 1998) as well as visuo-motor gains required of the task – both are salient cues that must be represented by the brain in order for adaptation to take place. Further downstream, recording in both M1 and SMA has revealed adaptation-related plasticity, in terms of changes in tuning properties across behavior epochs of baseline, force field adaptation and washout (Li et al., 2001; Padoa-Schioppa et al., 2002, 2004). Specifically, one subpopulation of neurons present in both M1 and SMA, classified as “dynamic cells”, show tuning changes only during the force field training. While other subpopulations of neurons, classified as “memory I” and “memory

II” cells, seem to either sustain the tuning changes occurred during the force field epoch in the washout epoch or show no modification until the washout epoch, respectively. Combining the psychophysical and neurophysiologic findings, there is strong evidence that during adaptation, the motor cortices undergo active transformations to incorporate new internal models of limb movements and that this transformation may be guided or facilitated by the cerebello-thalamo-cortical pathway. We hypothesize that patterns of activity in the cerebellar thalamus will reflect changes associated with motor learning, particularly, it might contain information associated with movement error. Previous cerebellar thalamus studies

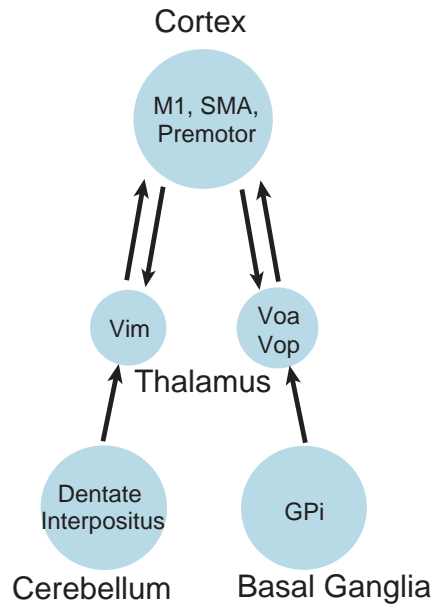


Figure 4.1 Ascending pathways from the cerebellum and the basal ganglia to cerebral cortex. Left: The cerebello-thalamo-cortical pathway and reciprocal projections from the cortex to the cerebellar thalamus. Right: The equivalent pathways between the basal ganglia and the cortex.

that involved motor adaptation have mostly focused on comparing neural activities in the untrained state and the fully adapted state – after the animals behavior had achieved stability or stereotype. The transient process of learning when most error is present has seldom been explored. Thoroughman & Shadmehr (2000) have shown that adaptation is reflected in behavioral trial-to-trial changes in movement trajectory. They found that the error experienced in a given movement has a measurable influence on the subsequent movement.

This suggests that error may drive learning by changing the motor commands generated in anticipation of forces in the upcoming movement. We examined Vim thalamus neural activity during adaptation and ask whether discharge is correlated with error.

4.2 Summary of Database

We participated in 27 thalamic surgeries and were able to collect data in 20 cases. In 10 of the cases we collected sufficient data for analysis (see §2.2.4 for criteria), yielding 61 ventrolateral (VL) thalamic units (16 single units and 45 multi-units), recorded during 36 adaptation experiments. In 28 of the 36 experiments, subjects adapted to curl force fields and in the remaining 8, subjects adapted to visual rotation. Of the 61 units, post-surgery anatomical localization (see §2.2.5) showed that 35 were in Vim, 12 were at the border of Vim and Vop, 10 were in Vop and 4 in Voa. Units in Voa and Vop were combined for analysis.

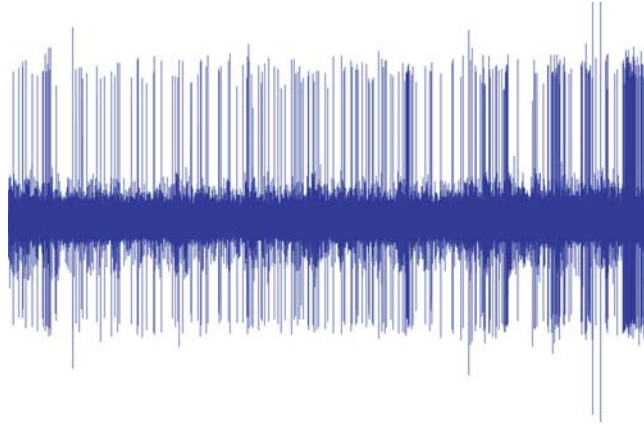
Figure 4.2 provides sample spike trains with high and low signal-to-noise ratio. The mean firing rates (FR) for all units, units in Vim, Vim-Vop border units, and units in Voa/Vop were: 17.9Hz, 19.2Hz, 18.8Hz and 14.9Hz, respectively. FR were not statistically different for these regions. The maximum FR recorded was 48.6Hz and the minimum, 2.0Hz (we did not explicitly exclude units with low FR, but units (8) with $FR < 4\text{Hz}$ were automatically rejected by later analyses that required sufficient response to movements).

4.3 Motor Adaptation Performance in the OR

Figure 4.3A illustrates the psychophysical performance by a patient during a force field adaptation experiment. Angular deviation at 300ms into the movement was used as the behavioral gauge for adaptation. This error was large early in the perturbation blocks, but decreased with practice. Also when the forces were turned off during the washout blocks, the patient demonstrated aftereffect. The learning indices (LI) for this experiment were 0.60 (*pert1*) and 0.34 (*pert2*). In general, when two opposing perturbation patterns are learned in succession with very little time in between, adaptation to the second perturbation pattern will tend to be worse than the first, due to anterograde interference. We found this to be true in 18 of the 28 experiments where subjects performed both *pert1* and *pert2* blocks.

The distribution for LI for all experiments is shown in Figure 4.3B. The mean

A



B

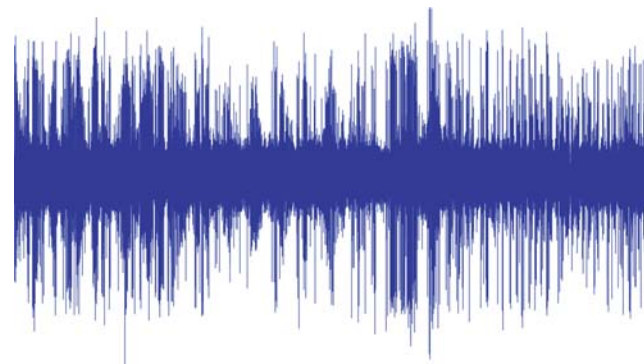


Figure 4.2 Sample neurophysiological recording from the OR. **A.** Thirty-second spike train with large SNR, containing two single units. **B.** Thirty-second spike train with small SNR, containing multi-units.

and standard deviation of the average LI, whenever there were two adaptation blocks, were 0.26 and 0.15, respectively. If we took the larger LI of the two blocks, the mean and standard deviation were 0.37 and 0.17, respectively. Although these statistics about LI seem comparable to that found for ET patients during the first training set (96 trials) in the DBS psychophysics study (Fig. 3.3C), the OR paradigms were significantly simpler – subjects only adapted to perturbation in two movement directions. Factors that contribute to the low level of learning and high level of variance in the LI of OR experiments include:

1. lack of weight-support for the arm, hence no relief for postural tremor
2. small number of training trials
3. the actuation of the robot arm was not as regular as that used in the psychophysics experiments (see §2.2.2).

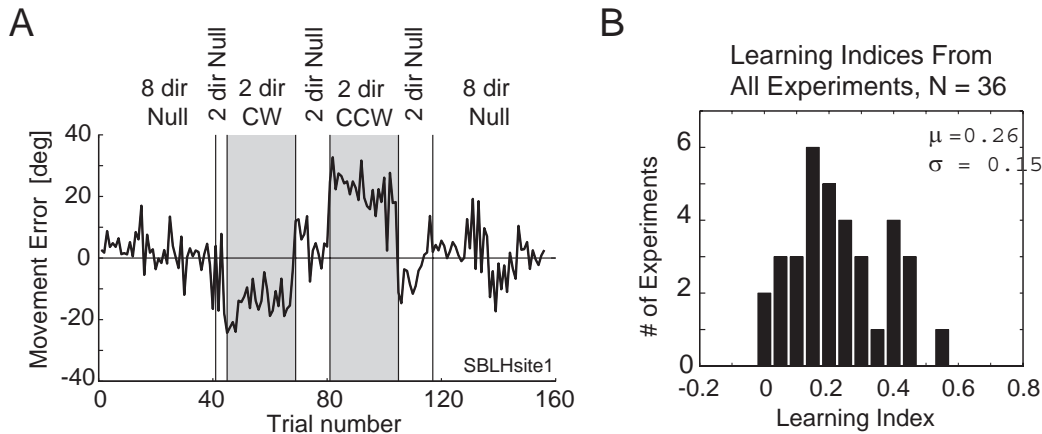


Figure 4.3 Psychophysical performance in the OR. **A.** Performance during a force field adaptation experiment. Error is the angle of deviation from straight trajectory at 300ms after movement onset. Errors in field trials became smaller with practice and errors in null (washout) trials that followed the field trials showed field-specific aftereffects. Therefore, the patient partially adapted to each field. **B.** Distribution of learning indices from all 36 experiments. In the 28 experiments where subjects performed both *part1* and *part2* blocks, the average LI between the two blocks is displayed.

4.4 Timing of VL Thalamic Activity With Respect To Movement

We examined whether the activities of the recorded units were related to voluntary reaching movements by detecting, for each unit, a response epoch during which the neural discharge was significantly different from the overall activity ($E_{z>1}$ defined in §2.2.6). A unit was considered movement-related if such a response epoch was found. Latency of movement-related activity was expressed as time relative to the onset of movement, and was measured separately for the *tuning* block and adaptation block.

Figure 4.4 displays the latency response for all units and units within each region of VL thalamus. Among all 61 units, we found 36 units to be movement-related: 25 units were movement-related during the *tuning* block and 29 during the adaptation block. The mean response latency of the cerebellar thalamus tended to be later than the basal ganglia thalamus — on average, the response latency of units in Vim was 0.295sec after movement onset, about 300ms later than the average for units in Voa/Vop (-0.020sec). This difference, however, was not significant (two-sided Wilcoxon rank sum test). Also, including the units at the Vop-Vim border into either group did not affect the result. This finding was surprising given that anatomically, Vim neurons project predominantly to the primary motor cortex, and Voa/Vop neurons to SMA.

4.5 Directional Selectivities of VL Thalamic neurons

4.5.1 Directional Tuning During Eight-Direction Movement Block

Figure 4.5 provides examples of activities of VL thalamic neurons activity during the eight-direction *tuning* block of the experiment. The neuron in Fig. 4.5A was from the Voa region, while the neuron in Fig. 4.5B was from the Vim region. Both neurons displayed sensitivity to movement direction. The Voa unit was most active during a pre-movement period before the target came on. In this experiment each of the four peripheral targets was presented five times (paired with the target at the origin, see §2.2.3) before moving onto the next target location. The predictability of the target sequence is clearly reflected in the neuron's activity. Its FR was the highest when expecting a target at the upper-right hand corner of the screen, or preparing for an impending arm movement in that direction.

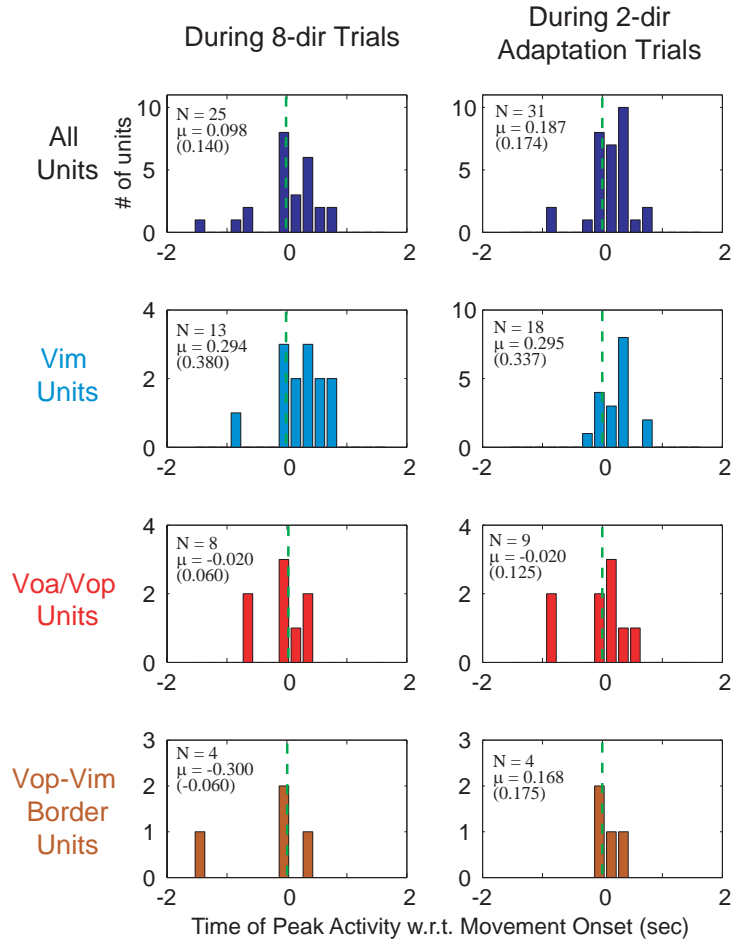


Figure 4.4 Timing of VL thalamic activity with respect to movement. Left column: time of peak-activity with respect to movement onset during tuning blocks for all units (row 1), Vim units (row 2), Voa/Vop units (row 3), and Vop-Vim border units (row 4). Right column: Latency of response with respect to movement onset during the adaptation block in each experiment. Numbers on the upper left corner of each plot indicate the number of neurons in each population, the population mean and median (in parenthesis).

The Vim unit in panel B was most active at the onset of movements involving flexion of the elbow, though its modulation with movement direction was not as strong as the Voa unit described above.

We quantified VL thalamic neurons’ directional tuning properties by the conventional method developed by Georgopoulos et al. (1982), which fits a cosine function to the neuron’s FR in different movement directions. The results are summarized in Figure 4.6. A statistically significant cosine-fit ($p < 0.05$) between discharge and movement direction required an r^2 value > 0.7 (Eq. 2.5). The r^2 obtained from our VL thalamic neuronal population are almost entirely below 0.7.

The left column of Figure 4.6 displays the depth of modulation (D_{mod}) for each population of units. As with the r^2 measure, D_{mod} characterizes how strongly movement direction modulates FR. On average, this index is near 20%. The outlier of the population, $D_{mod} = 68\%$, corresponds to the Voa unit described in Fig. 4.5A. Together, these results suggest that, overall, unlike the primary motor cortex (Georgopoulos et al., 1982; Schwartz et al., 1988), VL thalamic neurons do not seem to be cosine-tuned.

One caveat of this finding may be that we do not have sufficient data. Among the 61 units we recorded, experiments for 2 of the units did not include any *tuning* trials. Of the remaining 59 units, only 21 showed movement-related activity during the *tuning* block. Most of the units did not show a significant time of peak-activity, $E_{z>1}$ (defined in §2.2.6), which is a prerequisite for calculations of the cosine-fit. Furthermore, we only gave five trials for each movement direction during the *tuning* block, which may have been insufficient for studying direction selectivity given the noise level in the data (§2.2.4).

4.5.2 Direction Selectivity During Two-Direction Adaptation Block

Next, we examined the directional selectivity of VL thalamic neurons during adaptation to force fields. This was done by visual comparison of the overall shapes of the movement-onset aligned PSTHs for the two directions. Of the 29 movement-related units, 23 units were recorded during force field adaptation. (The remaining 6 were recorded during visual rotation experiments, which involved voluntary movements to only one-direction, and hence were excluded from this analysis.) Among these 23 units, 18 showed difference in their response between upward and downward movements.

We further categorized these units according to the phase of the movement in

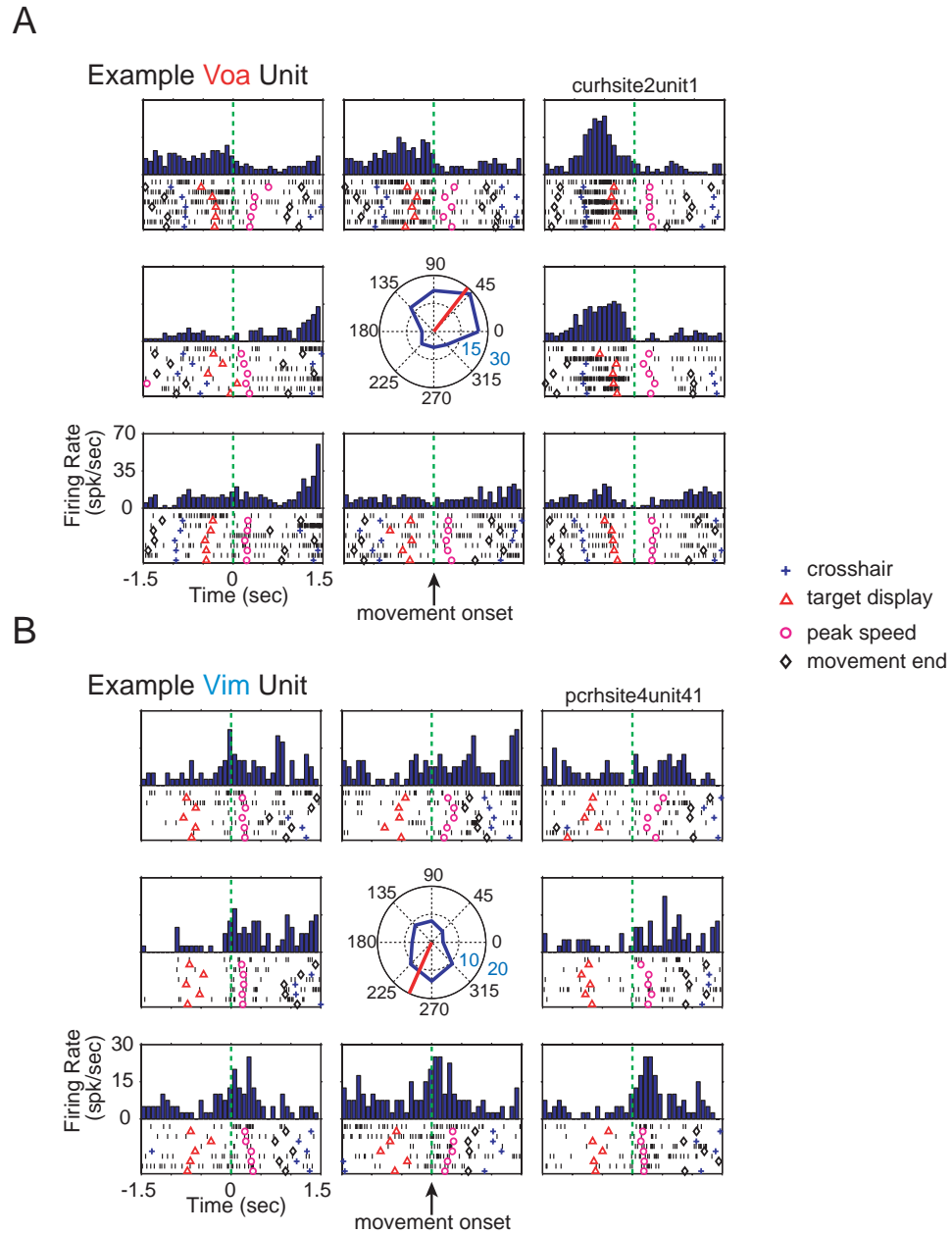


Figure 4.5 Examples of human VL thalamic neurons showing directional tuning. Rasters and PSTH are aligned to movement onset for each movement direction. Center plot summarizes in polar coordinates the mean firing rate over $E_{z>1}$ (see §2.2.6) for each movement direction. The red line indicates the neuron’s “preferred direction” (PD). **A.** A cosine-tuned *Voa* unit. PD=51°, $r^2 = 0.83$, $D_{mod} = 68\%$ **B.** Example *Vim* unit. PD=246°, $r^2 = 0.44$, $D_{mod} = 15\%$.

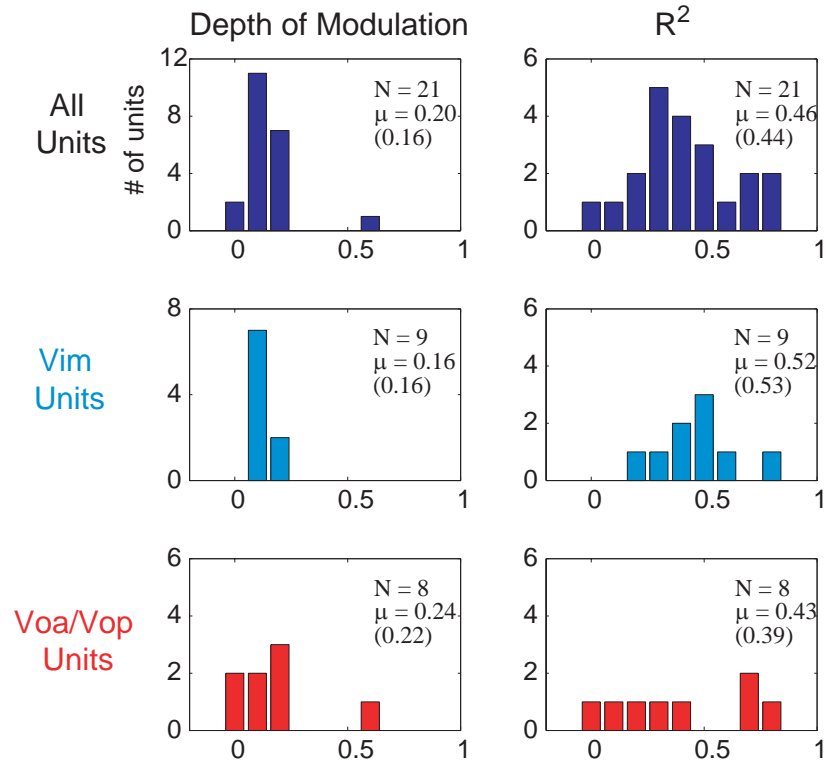


Figure 4.6 Human VL thalamic neurons are not generally cosine-tuned. Left column: distribution of D_{mod} for all units (row 1), Vim units (row 2) and Voa/Vop units (row 3). Right column: distribution of r^2 of the cosine fitting for all units (row 1), Vim units (row 2) and Voa/Vop units (row 3). Numbers on the corner of each plot indicate the number of neurons in each population, the population mean and median (in parenthesis). Units (4) found at the border of Vim and Vop were not included for this analysis.

which their response patterns were different. Three movement phases were distinguished: pre-movement reaction time period (500ms period before movement onset), acceleration and deceleration. We found 9 units were asymmetric in their discharge patterns during reaction time, 12 during acceleration and 12 during deceleration (these numbers are not mutually exclusive). The discharge patterns were different throughout the movement period (including reaction time) in 4 units.

Figure 4.7 rows 1–3 display the units whose response patterns for upward and downward movements were asymmetric during movement acceleration. The asymmetry indicates that VL units are direction-selective, some of them respond predominantly to movements in only one direction. Half of these 12 units resided in Vim and the other half in Voa/Vop. Figure 4.7 row 4 provides an example where the unit was responsive during movement acceleration, but does not care which direction the arm was accelerating.

Figure 4.8 rows 1–2 display 6 units whose discharge patterns for upward and downward movements were asymmetric during movement deceleration (6 other units were displayed in Fig. 4.7 rows 1–2 as they also exhibited asymmetric during acceleration). Among the 12 units, 6 resided in Vim, 5 in Voa/Vop and 1 at the Vop-Vim border. Rows 3–4 display additional units active during the deceleration phase of the movements in visual rotation experiments.

An additional 9 units demonstrated direction-selectivity during reaction time of movements. Examples are displayed in Fig. 4.7 (row 2, columns 1, 3, & 4) and Fig. 4.8 (row 2). Discharge prior to movement onsets are not confounded by movement kinematics. These units therefore reflect direction-selectivity in the efferent motor commands. Of the 9 units, 5 resided in Vim, 2 in Voa and 2 in Vop.

4.6 Patterns of Task-related Activities

4.6.1 Velocity-Like Discharge Pattern

Besides the direction-selectivity described above, a significant fraction of the units exhibited one of two discharge patterns in relation to movements. One pattern bore strong resemblance to velocity profiles of movements. Figure 4.9 displays five units whose firing rates are correlated (or anti-correlated) with either movement speed (panel A) or velocity in one direction (panels B–E). Anatomically, just posterior to Vim is the main sensory thalamic

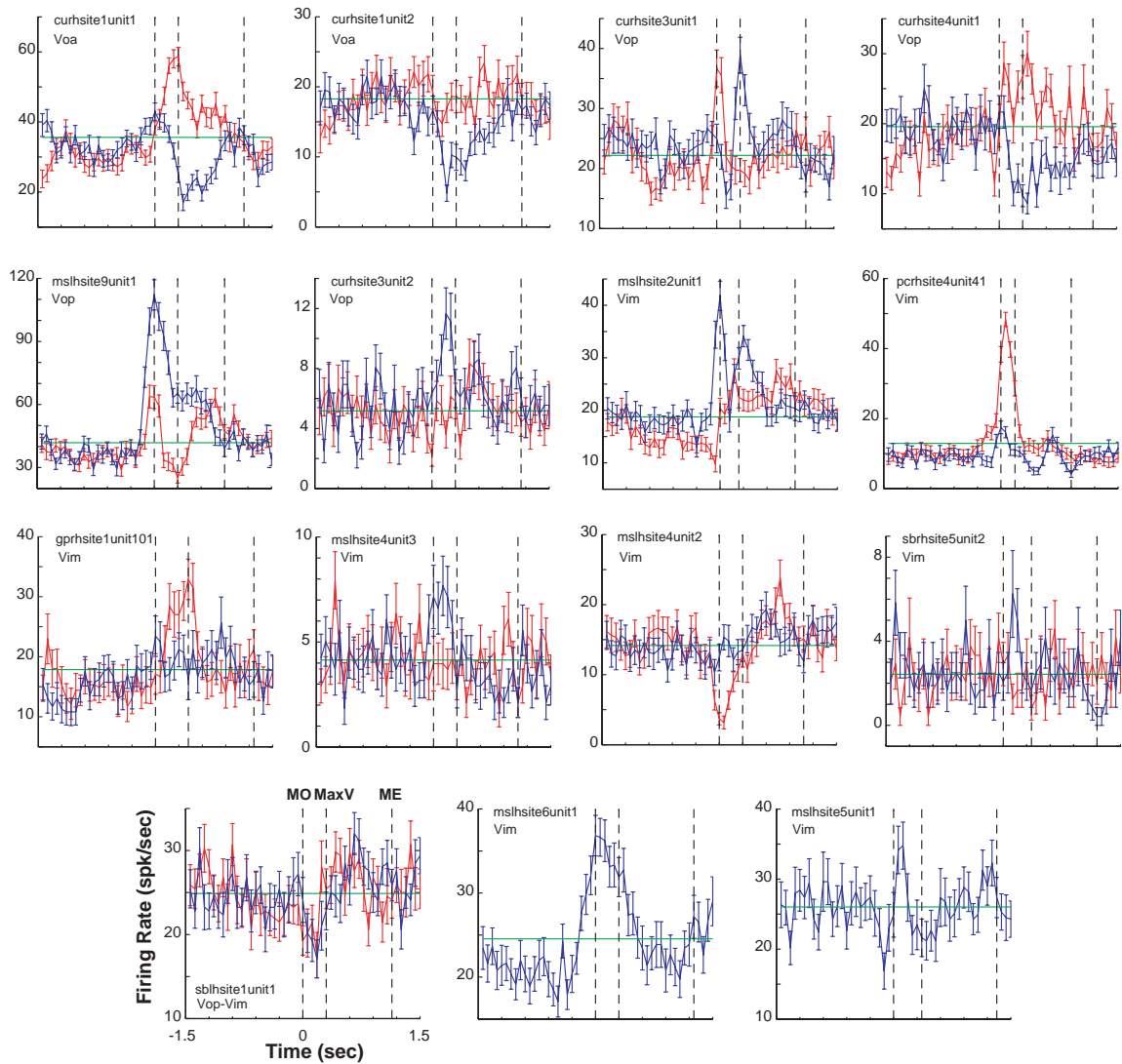


Figure 4.7 VL thalamic neurons active during acceleration. Each plot shows average PSTHs during upward (blue) and/or downward (red) movements over all trials in the adaptation block. Error bars indicate SEM. The three vertical dashed lines, from left to right, correspond to time of movement onset, average time of peak speed and average time of movement end, respectively. Horizontal line indicates the mean firing rate of the neuron. **Rows 1–3:** units that showed difference in discharge pattern between upward and downward movements during acceleration in force field adaptation experiments. **Row 4 left:** a unit that showed decreased activity during acceleration but no difference between upward and downward movements in force field adaptation experiment. **Row 4 middle & right:** units that showed changes in activity from baseline during the acceleration phase of upward movements in visual rotation experiments.

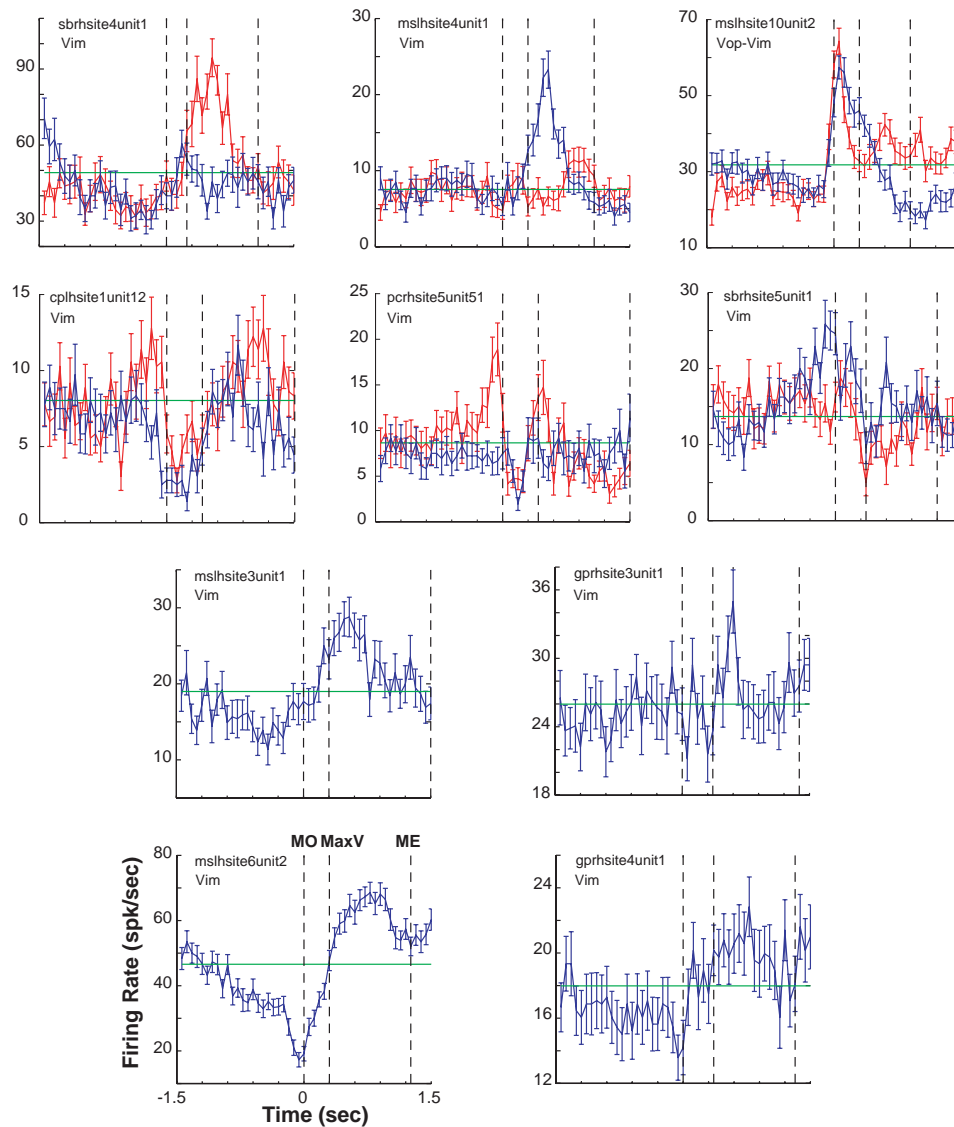


Figure 4.8 VL thalamic neurons active during deceleration. Plots follow the same convention as Figure 4.7. **Rows 1–2:** units that showed difference in discharge pattern between upward (blue) and downward movements (red) during deceleration in force field adaptation experiments. **Rows 3–4:** units that showed changes in activity from baseline during deceleration phase of (upward) movements in visual rotation experiments.

relay nucleus, ventralis caudalis (Vc, also known as ventral posterolateral nucleus, or VPL), which carries inputs from the dorsal column-medial lemniscus tract to the primary sensory nucleus. Vc thus receives proprioceptive information such as muscle spindle afferents from limbs. The velocity-like discharge pattern may very well have been found in Vc. However, discharge of muscle spindle is a nonlinear combination of all aspects of limb state, position, velocity, acceleration and even higher derivatives (Hasan, 1983). Recordings of stretch response of muscle spindles are not similar to the velocity-like profile we observed in VL thalamic units. Furthermore, although some proprioceptive afferents do terminate in Vim, they do not project so far as the basal ganglia thalamus, located in anterior VL. Three of these five units we found were located in Voa/Vop, which also suggests that such velocity-like discharge pattern may not be pure sensory feedback.

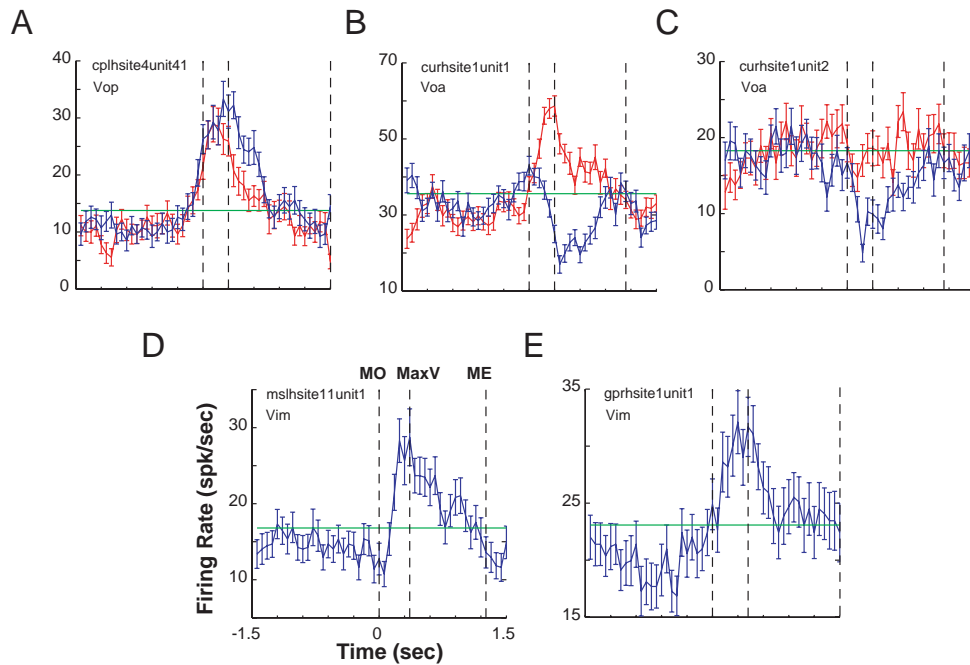


Figure 4.9 VL thalamic units displaying activity correlated with movement speed. Plots follow the same convention as Figure 4.7. Units displaying activity profile that correlated with either movement speed (A.) or velocity (B, D & E). In C. the unit's activity during upward (blue) movement was anti-correlated with movement velocity. **Row 1:** force field adaptation experiments. **Row 2:** visual rotation adaptation experiments.

4.6.2 Inhibition Then Rebound-Excitation

Figure 4.10 displays 7 units that showed inhibition then rebound excitation. The inhibition took place prior to or at movement onset, while the excitation began near peak velocity. The shape of these discharge patterns resembles a time-derivative of the profiles shown in Fig. 4.9.

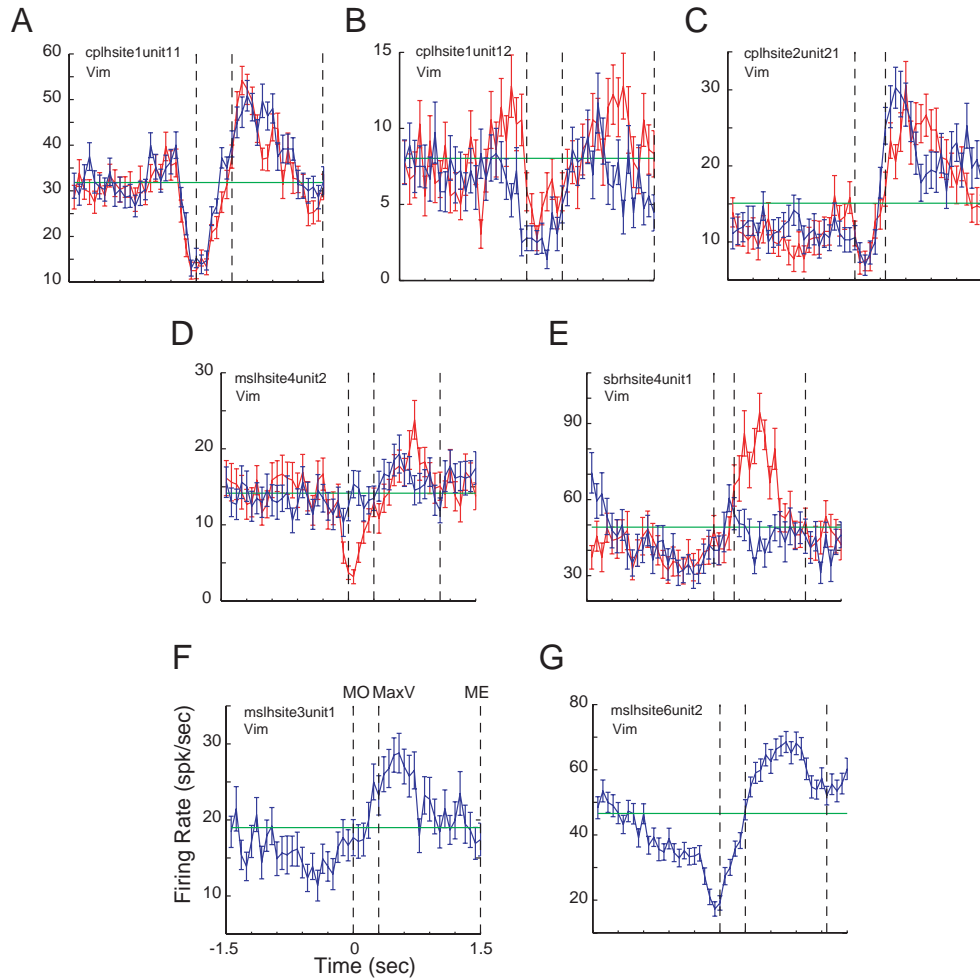


Figure 4.10 Vim units displaying inhibition then excitation. **A–E.** Force field adaptation experiments. **F&G.** Visual rotation adaptation experiments.

4.7 Adaptation-Induced Change in VL Thalamic Neural Activity

The goal of this study was to determine whether activities of VL thalamic neurons in the CTC pathway reflect error-driven motor adaptation. What features about adaptation do we expect these neurons to encode? Behaviorally, we know that two types of compensatory actions are engaged when the nervous system detects errors in limb movements. First, both short- and long-latency reflex are evoked by the unexpected proprioceptive inputs associated with error to generate an on-line corrective response. Second, when errors are experienced repeatedly, the on-line corrections, along with error, will serve as teaching signals for the internal model, so that subsequent motor commands produce movements with less error (Marsden et al., 1976; Kawato, 1989). These two systems, one feedback, the other feedforward, are both necessary to ensure accurate movements. For limb movements, it has been demonstrated that feedforward control and adaptation depend critically on the cerebellum (Smith & Shadmehr, 2005; Morton & Bastian, 2006).

Besides cerebellar inputs, Vim also receives some sensory inputs from the lemniscal tract (Berkley, 1980) and spinothalamic tract (Stepniewska et al., 2003). This convergence of inputs could mean that the nucleus is involved in both feedback and the feedforward control. But as shown earlier, VL thalamic neurons are highly sensitive to movement kinematics — movements in different directions evoke distinct discharge patterns during either acceleration, deceleration, or both. Hence, during movement, the presence of error could not be clearly dissociated from movement kinematics, nor from any online corrective response. We therefore have focused on neural activity during a “feedforward” epoch which includes the pre-movement reaction time period (500ms window before movement onset) and peri-movement-onset period ($\pm 100ms$ around movement onset). Any changes observed during this epoch should reflect error-driven changes in the feedforward motor plan, and be exempt from confounds relating to sensory feedback or feedback control. We predict that motor adaptation would modulate VL thalamic neural activity during this feedforward epoch. Indeed, response of several units during adaptation supports our prediction. Figure 4.11A presents activities of a Vim unit while the subject adapted to CCW visual rotation. During upward movements in the *null2* block (black), this unit consistently produced phasic bursts during the deceleration. When CCW rotation (red) was imposed, upward movements unexpectedly caused the cursor path to deviate to the left. To correct this, the hand must

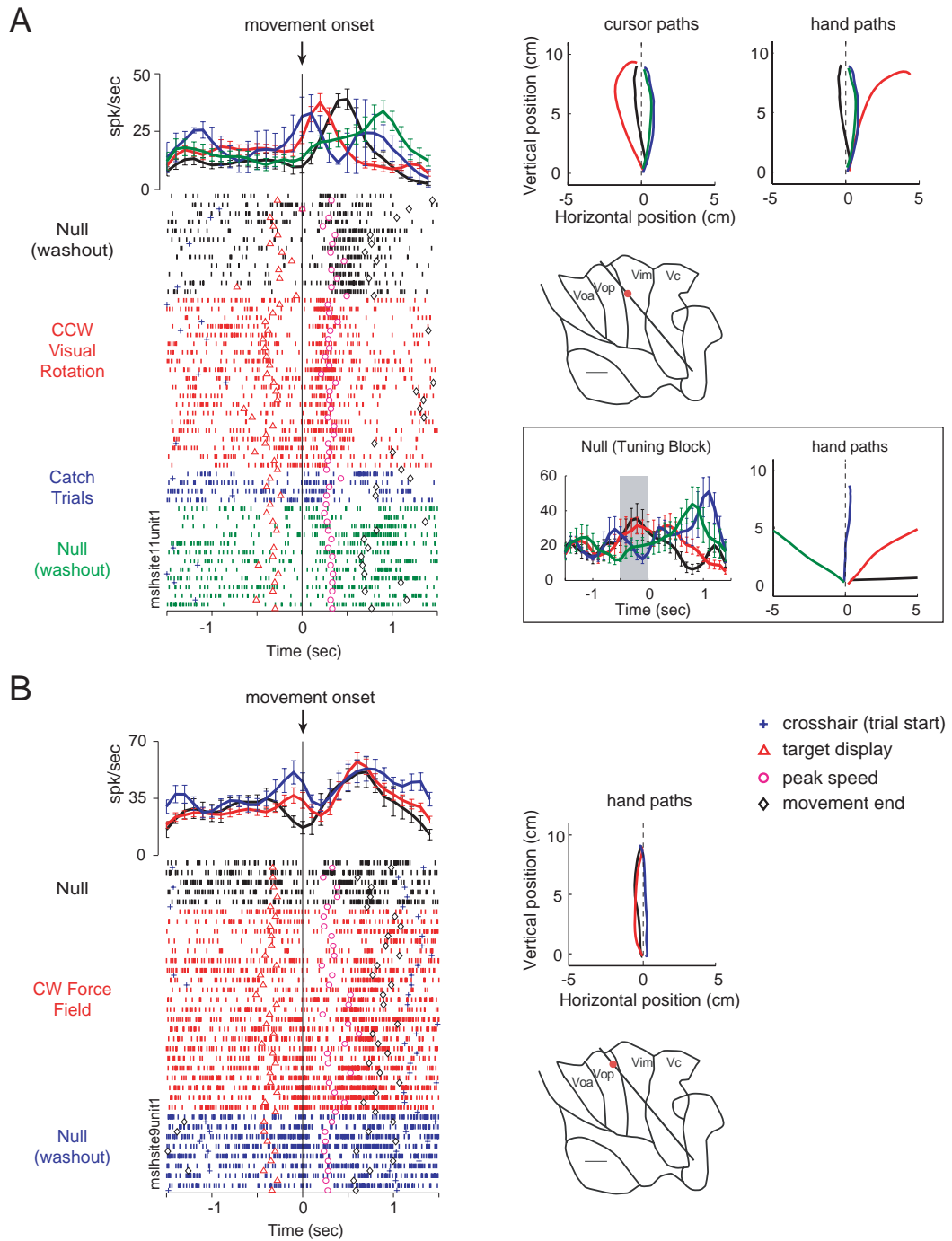


Figure 4.11 Changes in VL thalamic activity during adaptation. **A.** Activity of a Vim unit during visual rotation experiment. **B.** Activity of a Vop unit during force field adaptation. Rasters, SDFs as well as average movement paths from each trial block, labeled on the left, are plotted with the same color. Errorbars on SDF are SEM calculated over 100ms bins. Post-surgery anatomical localization for each unit is provided on the right.

move to the right. Note the onset of the phasic burst shifted to an earlier time — during acceleration. With training, the hand began to point rightward from the start. At the same time, the unit’s phasic discharge continue to shift earlier in time such that by the end of training, it occurred at movement onset. The same pattern could be observed in the rasters of catch trials (in blue; catch trials were randomly interspersed during the adaptation block, but grouped together here for ease of comparison) — the phasic burst shifted from acceleration to movement onset. Finally, during *null3* washout trials (green), the shift reversed its direction so that the unit discharged late in the movement again, though not in the same pattern as *null2*.

The boxed inset in Figure 4.11A presents the unit’s activity and average hand paths during the *tuning* block. No rotation was imposed in this block, hence the hand paths and cursor paths were identical. When we compared activity to the four peripheral targets during the 500ms prior to movement onset (shaded area), we noticed that movements with a rightward component (black and red) evoked higher levels of activity than upward and leftward movements. The unit tended to fire late during movement for upward and leftward movements. This is consistent with its discharge pattern during the adaptation block where upward movements (*null2*) elicited response in deceleration and increase in the rightward movement component caused the response to shift toward movement onset. The unit’s activity at and before movement onset indicates that it is not simply reporting the state of the limb, rather, its activity may reflect the motor intent. The “leftward” shift in the timing of the unit’s activity is reminiscent of the changes in electromyographical (EMG) output during reaching adaptation to force field observed by Thoroughman & Shadmehr (1999). In their study, Thoroughman & Shadmehr transformed EMG from four arm muscles into a composite trace to reflect muscle activation that specifically compensated for the imposing field. They discovered that with training, activation of this “field-appropriate” EMG gradually shifted from a delayed error-feedback response to a predictive feedforward response. While the paradigm we used for the unit in Figure 4.11A was visual rotation, hence no physical perturbation was applied to the arm, this mechanism of error-driven adaptation should still hold — error compensation should transition from reactive to predictive with learning.

Figure 4.11B presents activities of a Vop unit while the subject adapted to CW curl force field. At the start of the experiment, on downward null trials (black), this unit was most active during the deceleration phase of the movements. When the force field came

on (red), activity first dropped down then recovered to the original level. During the second half of the adaptation block, another phasic burst began to emerge near movement onset, so that the unit now fired biphasically at movement onset and deceleration. This pattern was sustained in the washout period (blue).

In summary, we found units in both parts of the motor thalamus displaying change in activity with respect to adaptation of reaching movements.

Chapter 5

Cross-Axis Saccade Adaptation

5.1 Magnitude of Cross-Axis Saccade Adaptation

We measured the progress of adaptation by tracking the vertical amplitude of the primary saccade. The average time course of adaptation roughly followed an exponential function with the time constant of ~ 200 trials (Figure 5.1A). By the end of the adaptation block (last 10% of the trials), the subjects' primary saccades had achieved 2.4° vertical amplitude, or 48% (mean, median 46%, SEM 4%) of the 5° vertical target jump. This level of adaptation is comparable to that found in the conventional in-axis gain-increase or -decrease adaptation studies (reviewed in Hopp & Fuchs 2004). The rate of the cross-axis adaptation may seem slower than the typical 30–60 trials found for in-axis adaptation, but our task design required subjects adapt both leftward and rightward saccades originating at three distinct locations (Fig. 2.3E), hence involved greater complexity.

During adaptation the primary saccade's end point shifted from the first target (T1) toward the second target (T2). Previous study of the two-dimensional double-step saccade paradigm (Findlay & Harris, 1984) had demonstrated that when a visual target shifted to a new location while the brain was still preparing for saccades to the original target location, the resulting saccade was pulled by the new visual stimulus and landed between the old and the new target location. The new target location was considered as a visual distractor. Although in our task the target jump occurred intra-saccadically, and in general, saccades are too fast to be influenced by such visual input, under special circumstances, they can be modified online (Zee et al., 1976; Van Gisbergen et al., 1987). To verify that the added vertical component in the primary saccades we described above truly results from

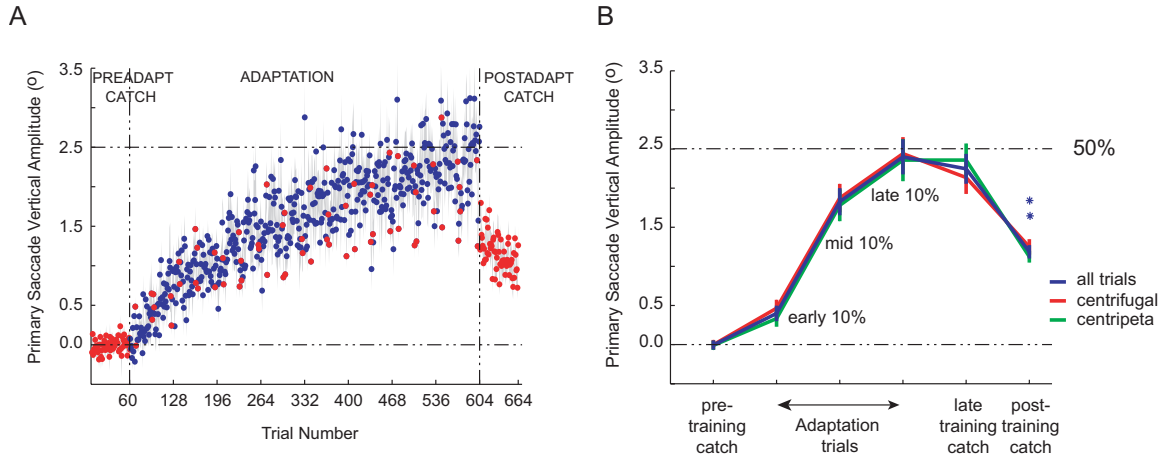


Figure 5.1 Cross-axis paradigm induces robust saccade adaptation. **A.** The time course of cross-axis saccade adaptation measured by the vertical component of the primary saccade amplitude. Data from clockwise and counterclockwise adaptation experiments are pooled and the directions of saccades are inverted appropriately before averaging. Blue dots correspond to adaptation trials and red dots correspond to catch trials, gray shades indicate standard error of the mean (SEM) for each trial ($n = 11$ subjects). **B.** Average primary saccade vertical amplitudes (blue) of trials in the pre-adaptation catch trial block, the first, middle and last 10% adaptation trials during the adaptation block, catch trials during the adaptation block and the post-adaptation catch trial blocks. Error bars indicate SEM. There is no significant difference between the vertical components of centrifugal (red) and centripetal (green) saccades before adaptation and during adaptation trials. But they are borderline ($p = 0.046$) and significantly ($p = 0.0067$) different in catch trials during adaptation and after adaptation (two-tailed paired t-test).

motor adaptation rather visual distractors, we gave catch trials throughout the experiment in which T1 did not jump to T2 but rather disappeared upon saccade initiation. As shown in Fig. 5.1A (red dots), while pre-training catch trials showed no vertical component, during training the catch trials followed the same time course as adaptation trials. This result demonstrates that the brain did not require the visual input from the target jump to program vertical components into the primary saccade. Following training, however, the level of adaptation in the catch trials showed an immediate reduction to 1.3° in just the first six trials, and then gradually decreased to approximately 1.1° (last 6 trials) over 60 trials. We will return to this rapid decline in adaptation later when we examine more closely the effect of rest period between sets in §5.4.

The figure-eight target configuration (Fig. 2.3B) that we used during adaptation limited the randomness of target presentation. While odd trials required centrifugal saccades to an unpredictable location - T1 appeared with equal likelihood to the left or the right of the origin, even trials always produced centripetal saccades back toward the origin (Method). We wondered if subjects' cognitive awareness of both the initial (T1) and final location (T2) of the targets during the even trials enhanced their level of adaptation in centripetal saccades as compared to centrifugal saccades. However, we found that the vertical components of centrifugal (red) and centripetal (green) saccades were virtually identical during all phases of training (Fig. 2.3). They were slightly different ($p=0.046$, two-sided paired t-test) by 0.29° (with centripetal trials having bigger values) in catch trials during adaptation and significantly different ($p=0.0067$, two-sided paired t-test) by 0.12° (centrifugal trials with larger values) in catch trials after adaptation. It is possible that centripetal trials did confer slight cognitive advantage during training that might have then led to slightly worse retention post-training, but the effect was extremely small and only existed in catch trials and not in adaptation trials.

5.2 Cross-Axis Saccade Adaptation Induces Curvature in Saccade Trajectories

Figure 5.2 provides performance of a typical subject during the experiment. The subject's primary saccade trajectories from the first, middle and last 10 trials in the adaptation block of the experiment are shown in blue, green and red, respectively (Fig. 5.2A).

They demonstrate with training, the subject's primary saccades became increasingly curved toward the final target position, a result more pronounced for saccades in the rightward direction in this subject (this variability between left- and rightward saccades in both adaptation level and trajectory curvature was common among subjects.) The average primary saccade trajectories of this subject during each phase of the experiment are presented in Fig. 5.2B; trajectories were rotated appropriately so they all start at (0,0) and move toward the upper right direction. In comparison to the oblique control trials with similar amplitude and direction executed before adaptation, the average saccade trajectories during adaptation trials showed significant curvature toward the final target.

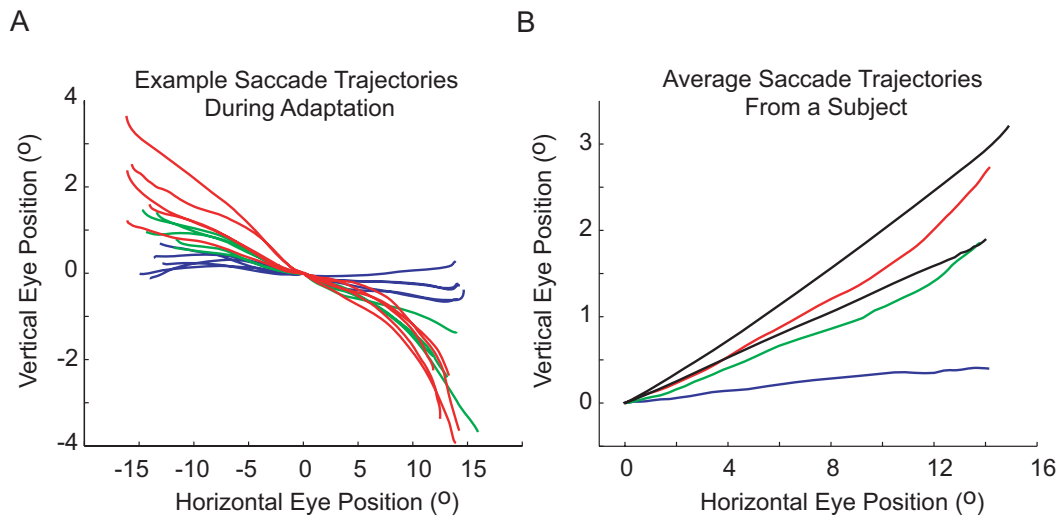


Figure 5.2 Performance of a representative subject. **A.** Primary saccade trajectories of the first, middle and last 10 adaptation trials are shown in blue, green and red, respectively. The origins of the saccades have been re-centered so that they begin at (0, 0) regardless where the actual fixation point was. As the level of adaptation increased, trajectories developed increasing curvature toward the secondary target. **B.** Average saccade trajectories during pre-adaptation control trials to oblique targets at $(15^\circ, 2^\circ)$ and $(15^\circ, 3^\circ)$ (in black), overlaid with average primary saccades of the first, middle and last 10% of adaptation trials (in blue, green and red, respectively).

5.2.1 Quantifying Saccade Curvature

We quantified this curvature for all 11 subjects by measuring the slope of the saccade trajectories. As illustrated in the inset of Figure 5.3A, each primary saccade was

divided into four equal segments along the horizontal direction and the slope of the straight line extending the ends of each segment (chord) was computed. The four chord slopes are referred to as S1, S2, S3 and S4. Consistent increases in chord slopes from S1 to S4 indicate curvature toward the final target, while consistent decreases indicate curvature away from the final target. Figure 5.3 displays average chord slopes across subjects before, during and after cross-axis adaptation as well as during the oblique control trials. Prior to adaptation, catch trials and oblique control trials showed no difference in chord slopes, indicating that these saccades were relatively straight. During adaptation, all four chord slopes rose with training, but at distinctly different rates: from the first to the last chord, the slopes rose progressively faster, with S4 increasing the fastest. In fact, S4 became significantly different from all previous chord slopes within the first 50 adaptation trials (S4 was significantly greater than S3 during the first, middle and last 10% adaptation trials at $p = 0.002$, $p = 0.0003$, $p = 0.000003$, one-tailed paired t-test); it becomes twice the size of S1 at the end of the block (mean S4/S1 ratio: 2.1). In terms of absolute vertical component contributed by the curvature, at the end of the adaptation block, the slope of the initial component of the saccade trajectory, S1, reached average value of 0.12 (mean, SEM is 0.01). If this initial slope was maintained throughout the saccade, the primary saccade would reach (15° , 1.8°), 75% of the 2.4° vertical eccentricity actually achieved in our experiments. Therefore, curvature accounted for 0.6° (an additional 33%), or 25% of the total cross axis adaptation.

5.2.2 Curvature Results From Adaptation, Not Visual Feedback of Target Jump

Figure 5.3A also shows the average behavior during catch trials in the last third of the adaptation block. The chord slopes of these late catch trials had essentially identical profiles to those of the late training trials. This result indicates that absence of the intra-saccadic target jump did not eliminate trajectory curvature, and the curvature was not a result of intra-saccadic visual input. Similarly, in a control study where target jumps were random, i.e., T1 had an equal chance of jumping up or down intra-saccadically, we found that the primary saccade trajectories were straight and showed no bias from the direction of the target jump (Figure 5.4). Together, these two types of control trials show that intra-saccadic target jumps are neither necessary nor sufficient to cause curvature in saccade trajectories. Rather, the curvature occurs when targets jump in a predictable fashion.

Progression of chord slopes during cross-axis adaptation

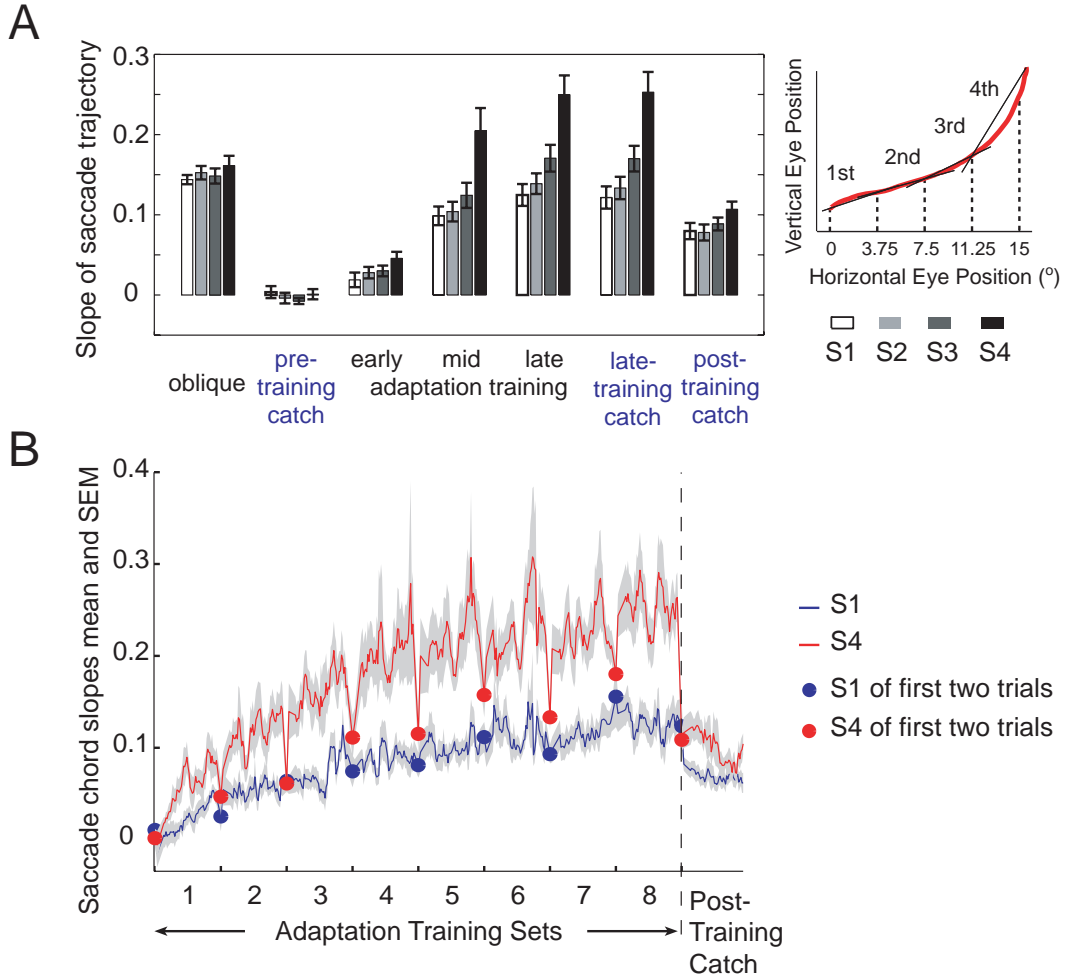


Figure 5.3 Progression of chord slopes during adaptation. **A.** Saccade curvature before, during and after cross-axis adaptation. Each primary saccade trajectory is divided into four segments (inset) and the slopes of the chords are denoted S1, S2, S3 and S4. Curvature is represented as relative change in slope from initial segment (white, S1) of the saccade to the final segment (black, S4). “Late-training catch” refers to the 10 catch trials given during the last one-third of the adaptation block. **B.** Moving average of the time course of S1 and S4 during adaptation (480 trials) and post-training catch trials (60 trials). Variable bin width (bw) was used to capture the transient dynamics at the start of each set: bw=2 trials for the first two trials, bw = 4 for the next four trials, then bw=6 for the rest of the set. Blue and red circles indicate for S1 and S4, respectively, the average chord slope for the first two trials of each set. Grey shades indicate standard error of mean.

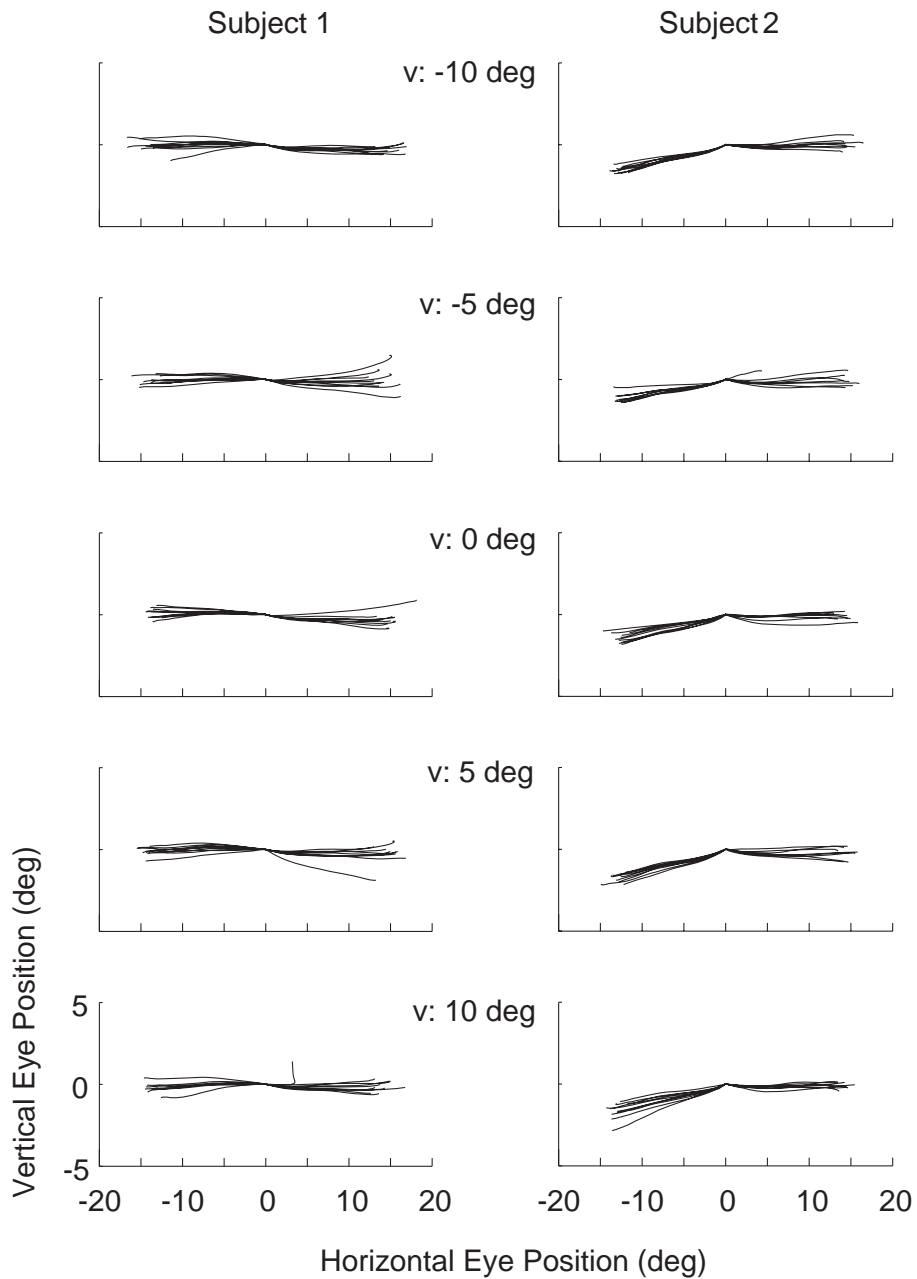


Figure 5.4 Random target jump does not induce adaptation or curvature. Individual primary saccades made during the random target jump experiment by two subjects are shown in the left and right columns. Trials are sorted and grouped according to the vertical target step size and direction. Row 1-5: trials where the vertical jump was -10° , -5° , 0° , 5° , 10° , respectively.

How long can the brain sustain this saccade curvature in the absence of external target jumps? The last set of bars in Figure 5.3A describes chord slopes of saccades from the post-adaptation catch trials. As noted earlier, the overall adaptation level was reduced during this block (Figure 5.1). The change in trajectory slope or saccade curvature was substantially reduced though not totally abolished. Across subjects, S4 was still significantly larger than S3 ($p=0.002$).

5.3 Relative Timing of Saccade Component Velocities Changes With Adaptation

In addition to analyzing changes in the path of the primary saccade trajectories during adaptation, we also characterized information relating to velocity of the saccades.

5.3.1 Component Velocities and Their Coordination During Normal Oblique Saccades

In the saccade literature, the horizontal and vertical velocity components of a saccade are referred to as ‘component velocities’ (Smit et al., 1990). This Cartesian decomposition of the velocities is physiologically based: while the superior colliculus represents saccades vectorially in terms of amplitude and direction, in the premotor circuitry just a few synapses downstream, the saccadic signal is broken down into horizontal and vertical components and carried out separately by the excitatory burst neurons (EBNs) in the paramedian pontine reticular formation (PPRF) and EBNs in the mesencephalic reticular formation (mRF), respectively. These independent control signals then drive the horizontal and vertical eye muscles through the ocular motor nuclei. When saccades are purely horizontal or purely vertical, both the peak velocity and duration of saccades increase monotonically with saccade amplitude in a stereotyped fashion known as the “main sequence” relationship (Bahill et al., 1975). However, in daily life the horizontal and vertical channels must be synchronized in order to direct the eye to targets diagonally offset from fixation. For example, a 15° saccade typically takes 60ms while a 5° takes only 40ms. During a saccade to a target at $(15^\circ, 5^\circ)$ from fixation, the vertical channel must operate differently than it would if the target was at $(0^\circ, 5^\circ)$, otherwise, the vertical component would be completed before the horizontal, resulting in a curved trajectory. In reality, the saccadic system per-

forms “component stretching” during oblique eye movements: (1) the peak velocity of the smaller component is reduced from what would normally be required for a purely vertical or horizontal saccade of the same amplitude and (2) the duration of the smaller component is prolonged to match the duration of the larger component (Guitton & Mandl, 1980; King et al., 1986; Becker & Jurgens, 1990; Smit et al., 1990). Therefore, when the two components are aligned correctly in time the oblique movement is straight and when they are misaligned the resulting eye movements can have varying degrees of curvature (Thomas & O’Beirne, 1967; Bahill & Stark, 1977; Becker & Jurgens, 1990; Smit et al., 1990). This alignment can be revealed by comparing metrics associated with each component velocity such as time of peak velocity and skewness of the velocity profile. When a velocity profile is symmetric, the time of peak velocity appears at the midpoint (50% point) of the total saccade duration. A skewed velocity profile would have peak velocity appearing either earlier or later than the midpoint.

5.3.2 Characteristics of Component Velocities During Adaptation

For each saccade, we measured the times at which each component velocity reached its peak. Figure 5.5A displays the across-subject average peak times of the component velocities throughout the course of the experiment. The peak time of horizontal velocity occurred at about 30ms into the saccade both before and during adaptation. The peak time of vertical velocity also occurred at 30ms during pre-training oblique trial blocks (saccades during pre-training catch trials were almost purely horizontal, thus had little vertical component) but as adaptation took place, the vertical velocity peak time began to lag the horizontal. This lag reached 10ms by the third adaptation set and stabilized for the remainder of the training block (Fig. 5.5B). An 8ms time lag by the peak vertical velocity was observed in post-training catch trials. Concomitant with the observed peak component velocities misalignment, primary saccade duration showed a slight increase with training. This was an expected result considering saccades became increasingly curved and hence longer in path. But it could also have resulted from reduction in the speed of the saccade. Indeed, saccade peak horizontal velocity decreased with training (Fig.5.5E) and since it is the dominant component, the overall peak speed followed the same pattern of decrease (data not shown).

Next, we examined the shape of the velocity profiles. Under normal circumstances,

speed profiles of saccades become increasingly skewed with saccade amplitude (Collewyn et al., 1988): peak speed of the saccade occurs increasingly ahead of the midpoint of the saccade duration and the profile has a longer tail. Our data showed that, for unadapted oblique saccades approximately 15° in magnitude, the peak component velocities exhibited identical skew at 42% of the total duration (Fig. 5.5D). But with training, vertical velocity became more symmetric while the horizontal velocity became skewed toward saccade onset. This misalignment of velocity profiles underlies the curvature seen in the path of saccade trajectories (Figs. 5.2 & 5.3). During training, although the vertical velocity component issued by the vertical saccadic channel grew with adaptation (Fig. 5.5F), the timing of this component was late compared to the horizontal motor output, suggesting that much of the vertical motor command was not generated at the start of saccade trajectory but added during the saccade.

5.4 Chord Slopes Display Multiple Timescales of Learning

Upon close examination of the trial-to-trial changes of S1 and S4 (Fig. 5.3B), a complex pattern of temporal dynamics is revealed. During the ~ 30 sec (5sec–1min) period between training sets when subjects rested in complete darkness, S1 was relatively unchanged, while S4 rapidly decayed toward S1. When the next training set resumed, S1 continued to climb slowly, while S4 rebounded rapidly toward its value at the end of the previous training set. Overall, S4 seemed to respond strongly to error but had poor memory retention, while S1 responded weakly to error but retained well what it had learned. Furthermore, when S4 decayed, it decayed toward but never fell below S1. This suggests that the two learning processes, one fast and one slow, are additive.

Recently, Smith et al. (2006) proposed and demonstrated through a reaching adaptation paradigm, that short-term motor learning consists of interacting adaptive processes with different learning rates. Our observations on the temporal dynamics of saccade chord slopes during adaptation confirms this idea. Additional evidence has come from a saccade gain adaptation study conducted by Kojima et al. (2004).

The fast decay of S4 between training sets can be understood through the competitive influence between error-driving adaptation and spontaneous decay. During these brief rest periods, subjects sat in complete darkness and made spontaneous saccades (observation through infrared video camera, no data was recorded) without information about

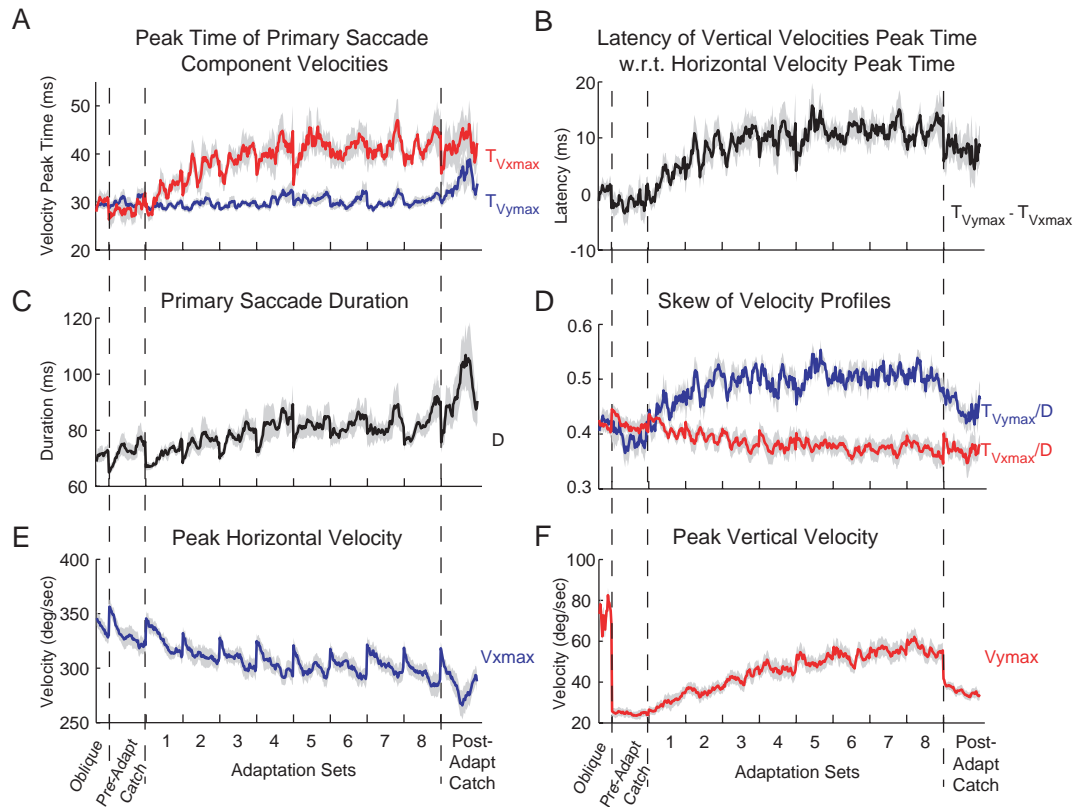


Figure 5.5 Characteristics of primary saccade component velocities. **A.** Average time of peak saccade velocities in the horizontal direction (blue) and vertical direction (red) over the course of the experiment. **B.** Average difference between peak times of vertical and horizontal component velocities. **C.** Average primary saccade duration. **D.** Skew of vertical velocity profile measured as the percentage of saccade duration at which the velocity reaches peak. **E.** Primary saccade's peak horizontal velocity. **F.** Primary saccade's peak vertical velocity. Grey shades indicate standard error of mean. Data in all three panels are moving averages with bin width = 8.

the accuracy of these saccades. Absence of error feedback meant that no stimulus was available to drive learning, hence the state of the memory would be dominated by decay. Indeed, multiple studies have demonstrated significant memory decay when error feedback was either not supplied or clamped to zero (Cohen et al., 2004; Kassardjian et al., 2005; Smith et al., 2006).

Chapter 6

Modeling Cross-Axis Saccade Adaptation

6.1 Simulating a Single Saccade Trajectory

6.1.1 Starting Point: Signal-Dependent Noise

In primates, saccades are highly stereotyped: the peak speed and duration of saccade increase monotonically with amplitude of the movement (see §1.6.1), and velocity profile of saccades are bell-shaped. Similar stereotypy is observed in reaching movement: point-to-point reaching movements have smooth, bell-shaped velocity profiles (Morasso, 1981), and tend to be straight in (Cartesian) visual coordinates even for congenitally blind individuals (Sergio & Scott, 1998). These empirical findings have led to the theory that the central nervous system operates on certain optimization principles when planning and executing goal-directed movements. Many optimization criteria have been proposed to account for the stereotypy: minimum jerk (Flash & Hogan, 1985), minimum torque change (Uno et al., 1989), minimum command change (Kawato, 1996), and minimum endpoint variance (Harris & Wolpert, 1998). As a starting point of our simulation, we have chosen the Harris & Wolpert minimum endpoint variance model because it is based on an important insight about physiological noise.

The Harris & Wolpert Minimum Endpoint Variance Model

In their model, Harris and Wolpert began with the assumption that neural control signals are corrupted by *signal-dependent* noise — noise with an amplitude that rises with the size of motor output. The idea of signal-dependent noise stemmed from the empirical observation that the standard deviation of motor-neuronal firing increases with the mean level (Clamann, 1969; Matthews, 1996), and the psychophysical observations that the variability of motor errors increases with the amplitude of the movement. This property about noise in the motor system imposes an unavoidable trade-off between movement speed and endpoint accuracy: on one hand, larger motor output, hence higher speed, would result in less accuracy; on the other hand, smaller motor output would ensure better accuracy but movements would take longer. Harris and Wolpert proposed that, to make a point-to-point movements of a given amplitude and duration, the optimal strategy for the central nervous system is to select the trajectory, i.e., the neural command, that minimizes the final positional variance of the effector.

This model’s prediction of saccade trajectories of various lengths is reproduced in Figure 6.1. These trajectories compared very well with saccades made by human subjects (see Figure 2 in Collewyn et al. 1988). The model also accurately captures a known property of saccades — the asymmetry in the velocity profile increases with saccade amplitude. Figure 6.1E displays the motor commands that drive the example saccades. Each command function, $u(t)$, can be considered as the sum of the neural signals controlling the agonist and the antagonist eye muscles (see Figure 1e of Harris & Wolpert 1998), and the overall shape gives away the three phases of a saccade: burst of agonist activity to accelerate the eye, burst of antagonist activity to terminate movement and sustained agonist activity to keep the eye on target. Figure 6.1C provides the weighting function of the control signal, $L(t)$, for every example saccade, derived from the cumulative endpoint variance over a post-movement “hold period” of 50ms. It specifies the relative contribution of the motor command, u , at any given time t , to the total endpoint variance over the hold period. It is a non-monotonic function that peaks near the end of the movement just before the antagonist burst begins. The total control cost is $u^T L u$.

Limitations of the Minimum Endpoint Variance Model

Although the minimum endpoint variance model is able to produce realistic trajectories, it has notable limitations. At the practical level, the predicted trajectories are highly sensitive to the length of the hold period (simulation not shown). Theoretically, the agonist activity during the holding period should not affect the shape of the velocity profile, since it would be the same for a given target eccentricity regardless how the eye gets to the target. But the shape of $L(t)$ amplifies the role of motor command during the hold period. The fundamental limitation of the model is that the optimization is open-loop based; the control law, $u(t)$, is *on average* the optimal solution for short duration movements. But for any given trajectory, the motor command generated by the model cannot adjust to compensate for the signal-dependent noise. In reality, neither saccades nor reaching movements are performed open-loop: both use forward models, and reaching movements depend additionally on sensory feedback (see §1.6.1).

6.1.2 New Framework: Stochastic Optimal Feedback Control

Fortunately, this problem was recently solved using the computational framework of stochastic optimal control (Todorov & Jordan, 2002; Todorov, 2005). Optimal feedback control is distinct from previous optimization principles in that it does not separate trajectory planning from execution. Given an initial position and final goal, instead of deriving a fixed command function, $u(t)$, which optimizes some property about the trajectory (e.g. smoothness, torque, endpoint variance), optimal feedback control derives a control policy which provides the optimal motor output throughout the movement. This control policy (Eq. 6.3) is a vector field dependent on the plant dynamics, movement goal and a quadratic cost (Eq. 6.4) associated with both the movement error (tracking cost) and the motor output (control cost, or energetic cost). At every time point the motor command is generated according to the optimal control policy and the current sensory estimates about the effector — the command is specific to the effector’s current state — hence feedback control has been incorporated into feedforward control. To account for physiological noise, Todorov derived solution for signal-dependent noise (Todorov, 2005). We have adopted this solution in our simulation (Eq. 6.3).

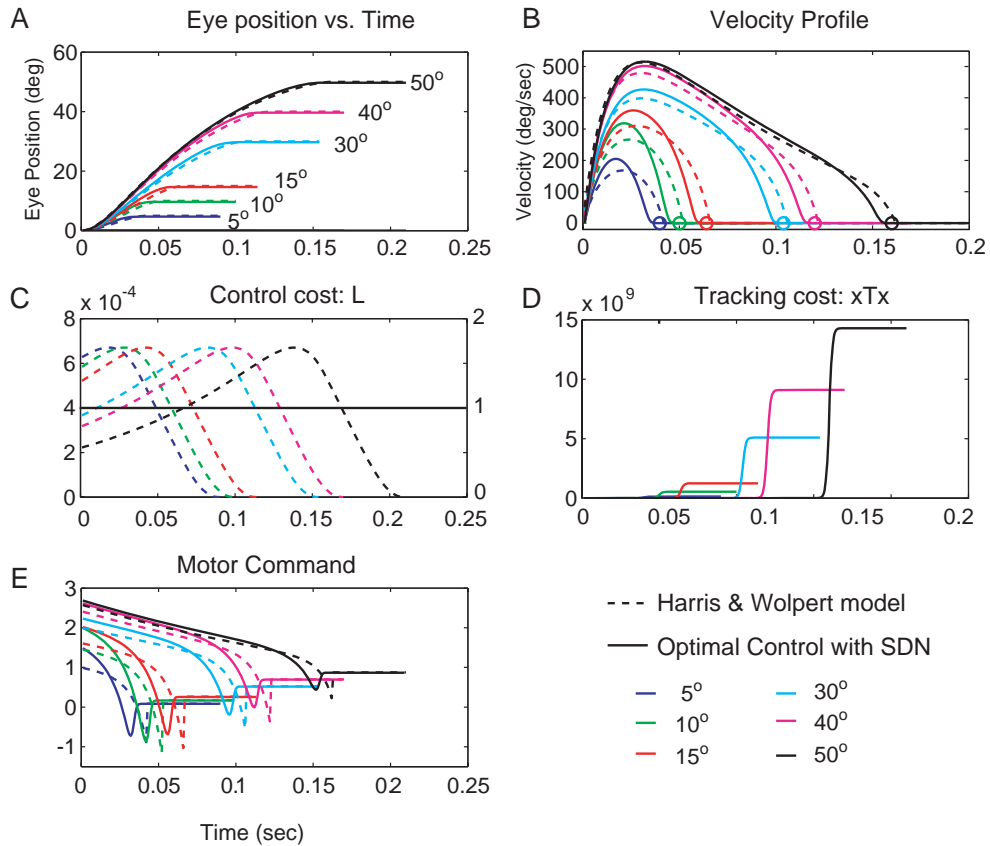


Figure 6.1 Comparison of optimal saccade trajectories predicted by the Harris & Wolpert's minimum endpoint variance model (dashed lines) and stochastic optimal control model with signal-dependent noise (SDN) structure (solid lines). **A.** Predicted paths of saccades. **B.** Predicted velocity profiles of saccades. Circles are movement durations approximated from empirical data from (Collewyn et al., 1988): 40, 50, 64, 104, 120, and 160ms for saccade lengths indicated in A. **C.** Weighting function for command signal. The ordinate scale on the left side is for the H&W model, the right side is for the optimal control model. **D.** Tracking costs for the optimal control model. **E.** Motor commands applied.

Model Description

We modeled saccade system-dynamics with a discrete, second-order linear set of equations:

$$\mathbf{x}_{t+1} = A\mathbf{x}_t + B\mathbf{u}_t \quad (6.1)$$

where \mathbf{x}_t is the two-dimensional state of the eye at time t , augmented by the saccade goal, \mathbf{r} : $[e_x, \dot{e}_x, e_y, \dot{e}_y, r_x, r_y]^T$ (all variables are in Cartesian coordinates). The system-matrices A and B are:

$$A = \begin{bmatrix} 0 & 1 & 0 & 0 & 0 & 0 \\ \frac{-1}{\tau_1\tau_2} & \frac{-(\tau_1+\tau_2)}{\tau_1\tau_2} & 0 & 0 & 0 & 0 \\ 0 & 0 & 0 & 1 & 0 & 0 \\ 0 & 0 & \frac{-1}{\tau_1\tau_2} & \frac{-(\tau_1+\tau_2)}{\tau_1\tau_2} & 0 & 0 \\ 0 & 0 & 0 & 0 & 1 & 0 \\ 0 & 0 & 0 & 0 & 0 & 1 \end{bmatrix}, \quad B = \frac{1}{\tau_1\tau_2} \begin{bmatrix} 0 & 0 \\ 1 & 0 \\ 0 & 0 \\ 0 & 1 \\ 0 & 0 \\ 0 & 0 \end{bmatrix},$$

where the time constants τ_1 and τ_2 are 224 and 13ms (Robinson et al., 1986). The forward model,

$$\hat{\mathbf{x}}_{t+1} = A\hat{\mathbf{x}}_t + B\mathbf{u}_t. \quad (6.2)$$

predicts the state of the eye in absence of external sensory feedback. The output of the optimal controller at a given time, t , is:

$$\mathbf{u}_t = G_t(A, B, T, \mathbf{r})\hat{\mathbf{x}}_t \quad (6.3)$$

where the control policy, G_t , provided by Todorov, 2005, is a function of the system dynamics, the goal and the weighting function associated with the tracking cost (T , defined below). The cost function used to find the optimal control policy is a scalar quadratic function of eye state error and oculomotor output:

$$J = \mathbf{y}^T T \mathbf{y} + \mathbf{u}^T \mathbf{u} \quad (6.4)$$

where T is a sigmoid function that rises at the desired time of the movement termination, \mathbf{y} is the state error vector, defined by,

$$\mathbf{y} = H\mathbf{x}, \quad H = \begin{bmatrix} -1 & 0 & 0 & 0 & 1 & 0 \\ 0 & 1 & 0 & 0 & 0 & 0 \\ 0 & 0 & -1 & 0 & 0 & 1 \\ 0 & 0 & 0 & 1 & 0 & 0 \end{bmatrix}.$$

Results of the simulation are shown in Figure 6.1. Compared with the minimum endpoint variance model, the speed profiles (Fig. 6.1B) produced by the stochastic optimal feedback control model begin and end smoothly and therefore are closer to empirical data. Also, the optimal control model does not require a weighting function, L , for the control cost, and therefore does not make any assumption about the energetic distribution along the trajectory, whereas the minimum endpoint variance model inherently specifies such a function (Fig. 6.1C). But the most important distinction is that the minimum endpoint variance model generates the entire sequence of control signals *en masse*, while optimal control provides a feedback control law and thus access to the computational components underlying the dynamical system throughout the course of a movement. This opens up the possibility to explore the mechanism of trajectory change during adaptation.

6.2 Modeling Adaptation

6.2.1 Trajectory Curvature Reflects Suboptimality in the Saccadic System

As shown in Chapter 5, cross-axis adaptation produced increasingly curved saccades. From the optimality point of view, curvature implies that parts of the saccadic system must operate sub-optimally, as the optimal trajectory would bring the eye straight to the intended target. Since curvature develops with adaptation, components in the saccadic system that drive the curvature should also adapt. The computational components of the saccadic system, as discussed in §1.1, are the controller, the forward model, and a process that specifies saccadic goal (Fig. 1.1B&C).

We imagined that when one makes a saccade in complete darkness and observes an error, there are two possible interpretations that the brain might make: either the target

moved, or the dynamics of the eyes changed (or some combination of the two). Both are sensory consequences that depend on oculomotor commands. This suggests that the forward model may play two roles in this situation: estimating the state of the eye, and setting an internal goal for the trajectory after a saccade has been initiated. This internal goal might be either the initial target location, T1, or the displaced target location, T2, in which cases saccades would aim from the start at either T1 or T2. Our data, however, suggest neither is true — throughout adaptation, the initial aim (first chord slope, S1) of saccade trajectories is moving from T1 toward T2, though never reaching T2 (Fig. 5.3) — arguing that the saccadic system may in fact create an internal saccadic goal and furthermore, the goal may change with time. We included this feature in our forward model by adapting the internal goal over trials as follows:

$$\hat{r}_y[n + 1] = (1 - a_r)\hat{r}_y[n] + b_r y[n], \quad (6.5)$$

where n is the trial number, a_r and b_r are the forgetting and learning rates for the goal, and y is the vertical visual error at the end of the primary saccade.

We simulated a saccadic system with this adaptive feature, an example trajectory is illustrated in Figure 6.2A. It demonstrates that adapting the goal specification process alone cannot explain why trajectories curve.

6.2.2 Adapting the Controller and the Forward Model

We next conjectured that saccade adaptation relied on dynamic calibration of sensorimotor maps encoded by forward model and inverse model of eye dynamics, any changes in one model that are not matched by the other would result in sub-optimality – trajectory curvature in saccades.

Coupling the Horizontal and Vertical Channels

We implemented trial-by-trial adaptation of the controller and the forward model of the eye dynamics by introducing coupling between the horizontal and the vertical saccadic system. Specifically, a cross-talk term was added in the system matrix B of the controller

and the forward model:

$$\mathbf{u}_t = G_t(A, B_{\text{OC}}, T, \mathbf{r})\hat{\mathbf{x}}_t, \quad (6.6a)$$

$$\hat{\mathbf{x}}_{t+1} = A\hat{\mathbf{x}}_t + B_{\text{FM}}\mathbf{u}_t, \quad (6.6b)$$

$$\text{where } B_{\text{OC}} = \frac{1}{\tau_1\tau_2} \begin{bmatrix} 0 & 0 \\ 1 & 0 \\ 0 & 0 \\ c_{\text{OC}} & 1 \\ 0 & 0 \\ 0 & 0 \end{bmatrix}, \text{ and } B_{\text{FM}} = \frac{1}{\tau_1\tau_2} \begin{bmatrix} 0 & 0 \\ 1 & 0 \\ 0 & 0 \\ c_{\text{FM}} & 1 \\ 0 & 0 \\ 0 & 0 \end{bmatrix}.$$

When $B_{\text{OC}} \neq 0$, any horizontal motor command would be associated with a vertical motor command. When $B_{\text{FM}} \neq 0$, any horizontal command would be *interpreted* by the forward model (FM) to cause a vertical displacement of the eye as well as the desired length of horizontal displacement. Specifically, $B_{\text{OC}} < 0$ characterizes a dynamical system in which a rightward horizontal command would result in rightward and downward eye movement. In order for the eye to reach the goal optimally, the optimal controller (OC) for such a system would generate a vector field G_t that counteracts the system's natural tendency. Similarly, when $B_{\text{FM}} < 0$, a rightward horizontal command would be estimated to cause both rightward and downward eye movement, which would then cause corrective action from OC to generate upward motor output. In short, coupling the horizontal and the vertical channels at either the OC or the FM level would result in trajectory changes in the vertical direction.

Figure 6.2 illustrates four scenarios of how relative adaptation rates of FM and OC affect saccade trajectories. (1) When neither FM nor OC adapt, saccade trajectory is straight (Fig. 6.2A). (2) When FM adapts faster than OC (or in the limit, FM adapts and OC does not), discrepancy between their models of the eye dynamics renders OC unable to fully compensate the cross-talk predicted by FM, thus resulting in curvature toward the new target position, T2 (Fig. 6.2B). (3) When OC adapts faster than FM (or in the limit, only OC adapts), OC overcompensates any cross-talk predicted by the forward model, resulting in curvature toward the original target position, T1 (Fig. 6.2C). (4) Lastly, if FM and OC adapt simultaneously to the same level, while FM predicts the eye to be below its

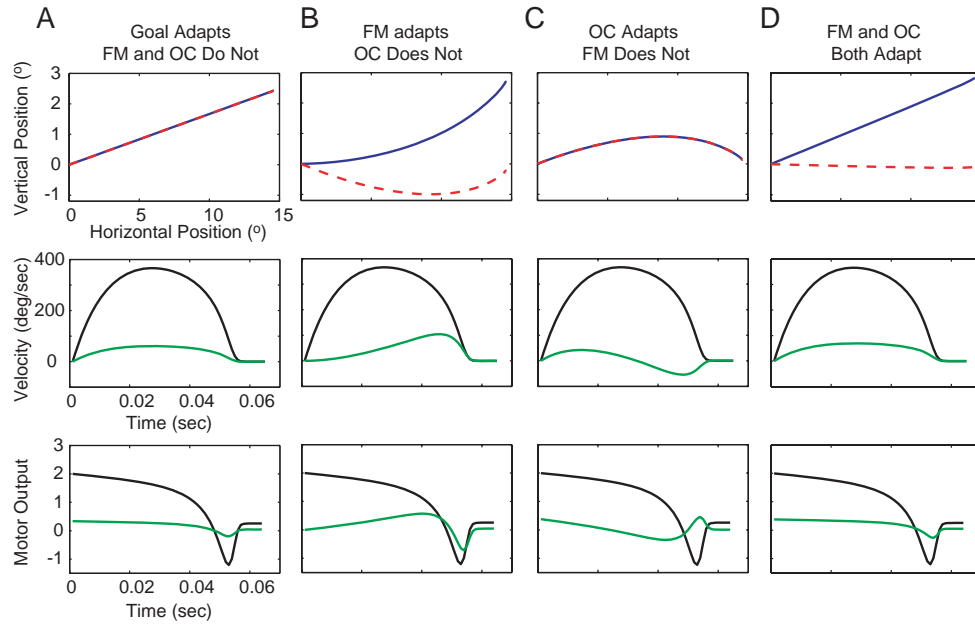


Figure 6.2 Comparisons of four implementations of cross-axis saccade adaptation. Top row: Trajectories executed (solid blue) by the model and predicted by FM (dashed red). Middle row: horizontal (black) and vertical (green) velocity profiles. Bottom row: horizontal (black) and vertical (green) motor commands. **A.** Internal goal adapts to the level of 2.5° . FM (of the eye dynamics) and OC do not adapt. **B–D** Internal goal does not adapt. **B.** FM adapts ($c_{FM} = 0.2$), the controller stays un-adapted. **C.** OC adapts ($c_{OC} = 0.2$), FM does not. **D.** Both FM and OC adapt, ($c_{FM} = c_{OC} = 0.2$).

actual position, the controller compensates appropriately so that the trajectories remained optimal, i.e., straight (Fig. 6.2D).

Our data showed strong agreement with the second scenario where the forward model adapts faster than the controller, or in the limiting case, only the forward model adapts and the controller stays unchanged.

Rationale For Adapting the Saccadic Internal Model and Coupling the Horizontal and Vertical Channels

Saccade adaptation can be induced either naturally or experimentally (reviewed in (Hopp & Fuchs, 2004)). Naturally occurring adaptation has been observed in patients with weakened eye muscles due to cranial nerve (CNIII or CNVI) palsy (Kommerell et al., 1976; Abel et al., 1978), and in monkeys that have undergone resection of either tendons or nerves of eye muscles (Optican & Robinson, 1980; Snow et al., 1985). Experimentally induced (e.g. by intra-saccadic target step) saccade adaptation are behaviorally similar to naturally occurring adaptation. This has led to the idea that perhaps during an adaptation experiment, the brain interprets, at least in part, the unexpected visual errors as indication of weakness or miscalibration of the eye muscles. Such interpretation of error — miscalibration of eye dynamics or sensory estimation— will then drive adaptation of the internal model.

During a cross-axis adaptation experiment, adaptation requires the saccade to have an increased vertical component but no change to the horizontal component. As mentioned in §5.3.1, the horizontal and the vertical components of saccades are encoded separately downstream of the superior colliculus. Since no change is required in the horizontal saccadic channel, it is possible that the vertical channel could adapt independently, and generate a growing vertical component with a velocity profile that is stretched in time (see §5.3.1) but appropriate for a straight oblique saccade. But our data showed otherwise (Fig. 5.5) — the vertical component is not stereotypical. We argue therefore, that it could not have developed independently of the horizontal channel, but rather developed as a function of the horizontal motor output.

6.3 Characteristics of Forward Model Adaptation

6.3.1 Forward Model Involves Multiple Time-Scales of Plasticity

This framework for single-trial trajectory control provided us a foundation for modeling the trial-by-trial adaptation. If trajectory curvature results from a rapidly adapting forward model, then the multiple timescales of adaptation we observed in the chord slopes (Fig. 5.3B) is a signature of the temporal dynamics governing forward model learning. We hypothesized that the forward model of the eye dynamics is comprised of two learning processes: a fast process that learns quickly but also forgets quickly, and a slow process that learns slowly but does not forget much (see §5.4). We applied this idea to trial-by-trial learning of the cross-talk term in the forward model:

$$c_{\text{FM}}[n + 1] = c_{\text{fast}}[n + 1] + c_{\text{slow}}[n + 1] \quad (6.7a)$$

$$c_{\text{fast}}[n + 1] = (1 - a_{\text{fast}})c_{\text{fast}}[n] + b_{\text{fast}}y[n] \quad (6.7b)$$

$$c_{\text{slow}}[n + 1] = (1 - a_{\text{slow}})c_{\text{slow}}[n] + b_{\text{slow}}y[n]. \quad (6.7c)$$

In equations 6.7b&c, the constants a_{fast} and a_{slow} are forgetting rates of the fast and the slow systems, b_{fast} and b_{slow} are the learning rates of the two systems. They are constrained by $a_{\text{fast}} > a_{\text{slow}}$ and $b_{\text{fast}} > b_{\text{slow}}$. The visual error, $y[n]$, provides the driving force to the adaptation. This formulation is the same as that in Smith et al. (2006), where the concept of interacting fast- and slow-learning systems underlying short-term motor learning was first proposed.

We further simulated the ~ 30 sec break between adaptation training sets with 5 catch trials in which no visual feedback was given at the end of a saccade. Without the driving force, $y[n]$, memories of learning will be left to decay (Eq. 6.7b&c).

6.3.2 Error Interpretation Dictates Motor Learning

Last but not least, we consider a central question to any learning paradigm – the driving force of learning. What drives cross-axis or other types of saccade adaptation? Multiple studies have shown that saccade adaptation is mostly driven by visual error that exists at the end of the primary saccades; corrective saccades following the primary saccades do not seem to be necessary for the adaptive process in either humans or monkeys (Wallman

& Fuchs, 1998; Noto & Robinson, 2001). As mentioned above (§6.2.1), we hypothesized that the brain may interpret each visual error two different ways: either its model of the dynamics of the eye was inaccurate (changes in the body), or the target had jumped (changes in the environment). How the brain explains this error at the end of each trial necessarily dictates subsequent adaptive actions. We explored two possibilities of error interpretation, one in which error drives forward model adaptation of the internal goal and eye dynamics separately, and the other in which error is split up among the two possible contributing sources according to their likelihood.

Model 1: Error Drives Forward Models of the Target and the Eye Equally

Figure 6.3A summarizes the model we have described so far, in which the visual error observed at the end of each saccade drives adaptation of the goal through a single timescale of plasticity (Eq. 6.5), and the forward model through two timescales of plasticity (Eq. 6.7). Altogether, this model contains 6 parameters ($a_r, b_r, a_{\text{fast}}, b_{\text{fast}}, a_{\text{slow}}, b_{\text{slow}}$). We fit these parameters to data on primary saccades of all adaptation trials as well as the post-adaptation catch trials (540 trials total). We simulated the short breaks between sets with 5 additional catch trials each. Thus altogether, 580 saccade trajectories were simulated, of which, the aforementioned 540 trajectories were used to compare with actual data. Three aspects of each primary saccade trajectory were used in the fit: the vertical extent of the saccade, the first chord slope (S1) and the fourth chord slope (S4), thus yielding a total of 1620 data points. A nonlinear least-squares solver (Matlab, Mathworks Inc.) was used to find the parameter set that minimized the squared residual between the model and the average data across all 11 subjects. The goodness of fit for the model was evaluated with the statistic r^2 (defined by equation 3.4), and the statistic *reduced* χ^2 , the sum of squared-ratio between residual and measurement uncertainty normalized by the degree of freedom in the model, where standard deviation across subjects was used as the uncertainty about the mean.

Figure 6.4 displays the results of this model. Panels A provide examples of simulated trajectories from both adaptation trials and post-training catch trials. The simulation showed that the forward model consistently under-predicted the vertical extent of the trajectories, as discussed in §6.2.2. Also as expected, the vertical motor output increased throughout the course of adaptation (panel B). We found the learning rates for the fast and

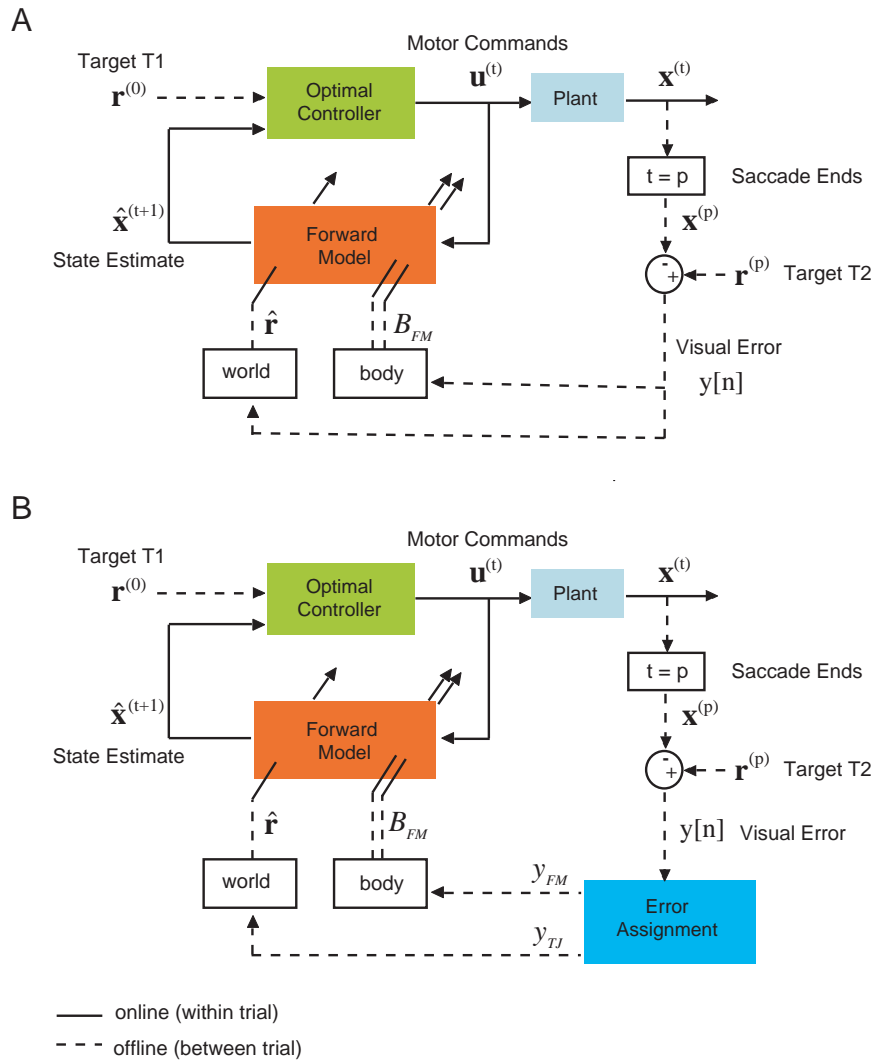


Figure 6.3 Two Scenarios of error-driven forward model adaptation **A**. Error drives adaptation of target jump and eye dynamics separately. **B** Error assignment model.

slow system of the forward model to be 1.04×10^{-3} and 7.43×10^{-5} , respectively, and the forgetting rates 0.296 and 0.00290, respectively. The learning and forgetting rates for the goal adaptation were 0.00138 and 0.00119, respectively. Panels C & D show the model's fit to the initial and final chord slopes, and to the adaptation level. While the model predicted the overall trends in the data, it failed to capture the fast decay occurring between sets and therefore greatly overestimated the data in the post-training catch trial set (goodness of fit for 1620 data points together: $r^2 = 0.574$, *reduced* $\chi^2 = 4.64$). This is also reflected in panel E which displays the progression of chord slopes of the simulated saccade trajectories in the same format as Figure 5.3.

In summary, Model 1 was only able to partially explain the data. The key features of Model 1 were:

- Forward model adapts its expectation of both the goal and the eye
- Both adaptations are driven equally by error feedback
- Adaptation of the forward model of the eye dynamics involves two timescales

The model failed to predict the fast decay of curvature (S4) and adaptation during the rest period between sets, the characteristic in the data that had led us to consider the multiple timescales of plasticity (two-state) formulation. Yet the two-state feature alone was not sufficient to explain this characteristic.

Model 2: Error Assignment Depending on Likelihood of Source

The simple two-state model's failure to predict the observed sharp drop-off between sets led us to develop a more complex model (Fig. 6.3B), in which the saccadic system is able to differentially attribute errors to the two sources, depending on the magnitude of the post-saccadic visual error. When the error is very large, it is more believable that it is caused by unexpected changes in the external environment (the displacement of the target in this case). Small errors are presumed to be dominated by imperfections in the internal model of the effector (an inaccurate forward model of the eye in this case). We model the likelihood that a visual error is attributed to a target jump as a sigmoid function that increases with the error magnitude. The remainder of the error is attributed to the forward model of the eye and drives its adaptation. These ideas are encapsulated in the following

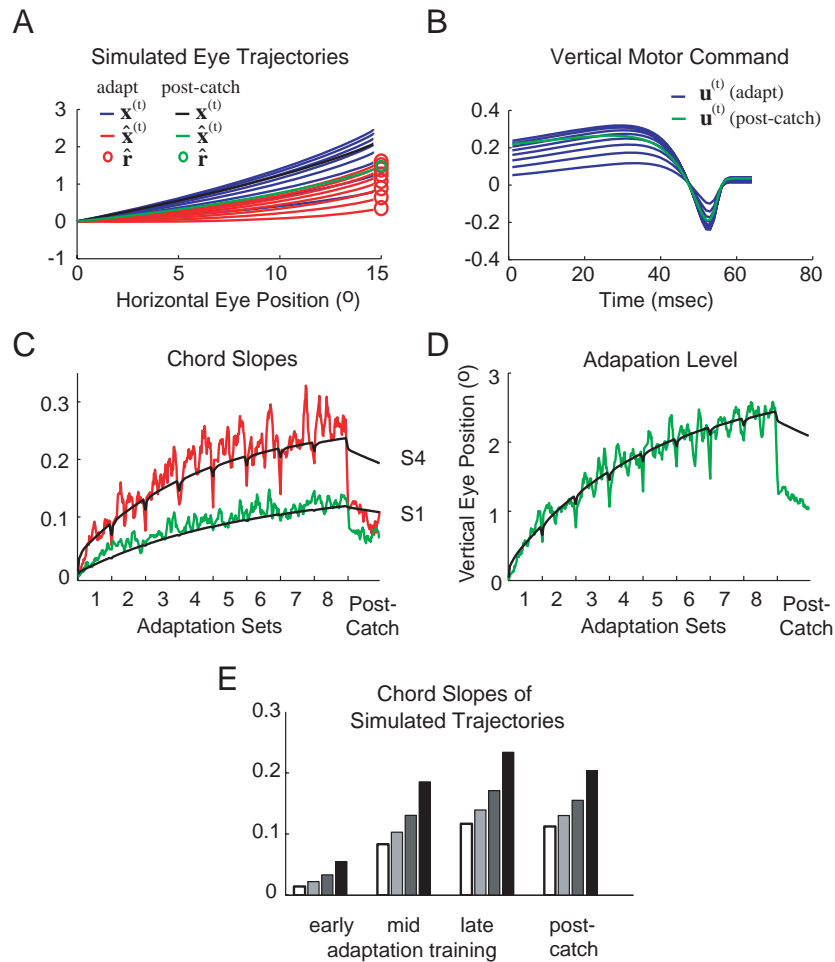


Figure 6.4 Results of the two-state model. **A.** Trajectories produced by the model (blue and black) and estimated by FM (red and green) at the last trial of each training set as well as the post-training catch trial set. Circles indicate the internal goal of each of these trials. **B.** Vertical motor command produced for the trials displayed in **C.** **C.** Initial and final chord slopes of simulated trajectories (black) overlaid on average experimental results (red and green) across 11 subjects. Moving average over trials (described in Fig. 5.3B legend) was applied to both the simulation and experimental results. **D.** Vertical endpoint of simulated trajectories (black) overlaid on averaged experimental results (green). Again, moving average has been applied to both data and simulation results. **E.** Average chord slopes of the simulated trajectories at various stages of the experiment. The shades, from white to black, correspond to S1–S4.

mathematical expressions:

$$y[n] = y_{\text{TJ}}[n] + y_{\text{FM}}[n] \quad (6.8a)$$

$$p_{\text{TJ}}[n] = y_{\text{TJ}}[n]/y[n] = (1 + e^{k\sigma} e^{-ky[n]})^{-1} \quad (6.8b)$$

$$p_{\text{FM}}[n] = 1 - p_{\text{TJ}}[n] \quad (6.8c)$$

In equations 6.8, p_{TJ} and p_{FM} are the fractions of error attributed to target jump and forward model of the eye, respectively, σ is the magnitude of error at which target jump and the forward model contribute equally, and k describes the shape (steepness) of the sigmoid. The subscriptes TJ and FM stand for target jump and forward model, respectively. The full model, after incorporating the concept of error-assignment, is now:

$$\hat{r}_y[n + 1] = (1 - a_r)\hat{r}_y[n] + b_r y_{\text{TJ}}[n] \quad (6.9a)$$

$$c_{\text{FM}}[n + 1] = c_{\text{fast}}[n + 1] + c_{\text{slow}}[n + 1] \quad (6.9b)$$

$$c_{\text{fast}}[n + 1] = (1 - a_{\text{fast}})c_{\text{fast}}[n] + b_{\text{fast}}y_{\text{FM}}[n] \quad (6.9c)$$

$$c_{\text{slow}}[n + 1] = (1 - a_{\text{slow}})c_{\text{slow}}[n] + b_{\text{slow}}y_{\text{FM}}[n] \quad (6.9d)$$

In total, the full model contained 8 parameters (a_r , b_r , a_{fast} , b_{fast} , a_{slow} , b_{slow} , σ , and k). Results of the model is displayed in Figure 6.5. The error-assignment functions for target jump and FM are shown in panel A. The two sigmoid functions intersect at 1.57° , which means when a visual error of 1.57° is observed, the error will be equally distributed to the two possible sources. Panel B displays the actual magnitude of error assigned to target jump (world) and FM (body) by the model throughout the experiment. As expected from the shapes of the error-assignment functions, early in the experiment when error was large, most of the error was attributed to target jump, hence was used to drive goal adaptation. This assignment decreased over trials as the total size of the visual error decreased, while the assignment of error to inaccuracy associated with the forward model increased. Overall, more error was blamed to have come from target jump than FM. We found the learning rates for the fast and slow system of the forward model to be 0.104 and 0.000896, respectively, and the forgetting rates 1 (complete forgetting) and 0.0260, respectively. The learning and forgetting rates for the internal goal were 0.00147 and 0.00189, respectively. Panel C provides examples of simulated trajectories from both adaptation trials and post-

training catch trials. Model-predicted saccade trajectories produced highly significant fits to empirical results of chord slopes and adaptation level (panels E&F, goodness of fit for 1620 data points: $r^2 = 0.829$, *reduced* $\chi^2 = 1.892$). Panel G displays the progression of chord slopes of the simulated saccade trajectories in the same format as Figure 5.3, further confirming the success of the error-assignment model.

The error-assignment features of Model 2 provide much a better fit to the data than Model 1. Next, we considered alternative optimization techniques to see if the fit could be further improved. So far we have solved the model parameters by minimizing the squared residuals between model and data, where the data sequence consists of the values of S1, S4 and the vertical amplitude (adaptation level) of primary saccades for all trials. But in terms of numerical value, adaptation level is almost ten times that of chord slopes. This difference is carried over to the residuals, which could cause the least-squares solver, hence the model, to preferentially minimize residuals of the adaptation-level portion of the data, at the expense of fitting the chord slopes. A better choice of minimization quantity would be χ^2 , which weights the data points by the inverse of their uncertainty. But this would only make a big difference if the distinct portions of the data sequence were independent. Adaptation level, however, is not independent of S1 or S4. When we solved for the model parameters by minimizing χ^2 , we observed that the model fit improved in some early trials but was worse in later trials, without significant increase in the quality of the overall fit (though the minimization statistic, χ^2 , did improve: *reduced* $\chi^2 = 1.60$, $r^2 = 0.795$). We further tested a model where adaptation of the internal goal involved two timescales. But the quality of the fit was, again, not significantly improved (*reduced* $\chi^2 = 1.576$, $r^2 = 0.797$) with the additional two parameters.

In conclusion, Model 2 — the error-assignment model — seems to be a good model for our cross-axis saccade adaptation data.

6.4 Neural Correlates of the Model

If our model (Fig. 6.3B) indeed underlies saccade trajectory guidance and adaptation, how might the brain implement such a model? As discussed in §1.6.2 and §1.6.3, the cerebellum plays an important role in both steering and adapting saccades. Neuroanatomically, the cerebellum exerts its influence on saccades via two output pathways leaving the cFN. The short pathway projects directly to the burst generators (BBG), while the long

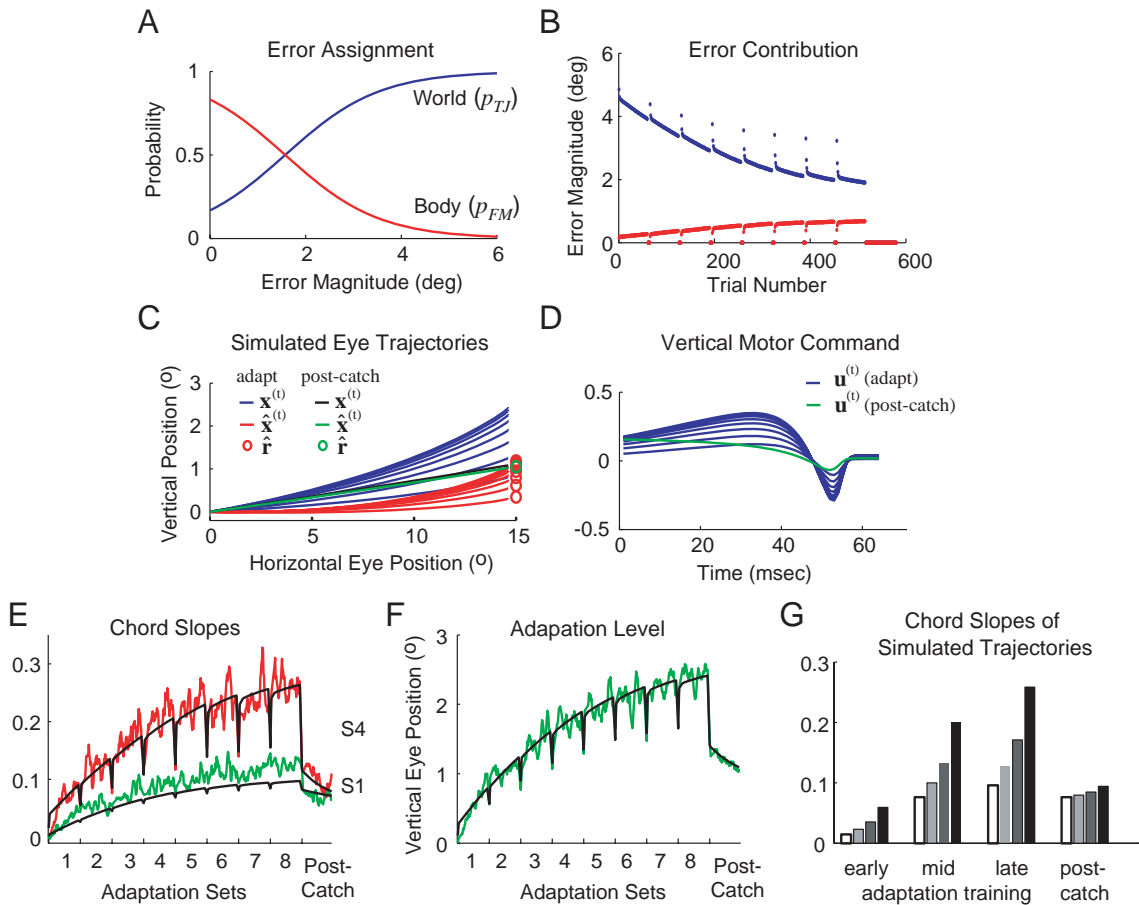


Figure 6.5 Results of the error-assignment model. **A.** Error assignment sigmoid resulted from the fit. They describe, at any given visual error, the fraction of error the brain attributes to the body (FM estimation) and the world (target jump). **B.** The magnitude of error attributed to goal (blue) and FM (red) throughout the adaptation experiment. **C.** Trajectories produced by the model (blue and black) and estimated by FM (red and green) at the last trial of each training set as well as the post-training catch trial set. Circles indicate the internal goal of each of these trials. **D.** Vertical motor command produced for the trials displayed in **C.** **E.** Initial and final chord slopes of simulated trajectories (black) overlaid on average experimental results (red and green) across 11 subjects. Moving average over trials (described in Fig. 5.3B legend) was applied to both the simulation and experimental results. **F.** Vertical endpoint of simulated trajectories (black) overlaid on averaged experimental results (green). Again, moving average has been applied to both data and simulation results. **G.** Average chord slopes of the simulated trajectories at various stages of the experiment. The shades, from white to black, correspond to S1–S4.

pathway ascends via the thalamus to various cortical eye fields, which then influence the superior colliculus and the BBG. The superior colliculus (SC) is mostly likely to issue the feedforward saccadic commands, S1. The adaptation of S1 may depend on the long pathway involving the cortex. Gaymard et al. (2001) reported that patients with lesions in the cerebellar thalamus show reduced saccade adaptation. They suggest that the thalamus relays adaptation-related information from the cerebellum to cerebral cortical oculomotor areas. The short output pathway is part of the superior colliculus-cerebellar-brainstem side-loop, which has been implicated in several other curvature studies and is a likely candidate for carrying out S4. Robinson et al. (1993) showed that unilateral lesion to cFN causes vertical saccades to curve toward the lesioned side late in the saccade. Microstimulation of the oculomotor vermis evokes curved saccades in oblique directions (Fujikado & Noda, 1987). Anatomically, this pathway is suitable for computing the forward model: the collicular input to the cerebellum may provide the efference copies of recent motor commands. On the output end, cFN has direct, descending projection to BBG, which allows it to have a rapid influence on saccadic accuracy (Hopp & Fuchs, 2004), as well as ascending projection back to SC (Noda et al., 1990; Sugita & Noda, 1991), which may carry sensory estimation to SC for further computation of the optimal motor command (Fig. 1.1C). Together, this side loop seems important for steering saccade trajectories, influencing saccades on a short timescale, and carrying out the necessary computation for the forward model. It therefore is a likely candidate for acting on the forward model to produce mid-flight corrective feedback. Several works in the manual motor control literature also suggest the cerebellum as the site where the forward model is computed (Miall et al., 1996; Diedrichsen et al., 2005b).

Bibliography

- Abel, L. A., Schmidt, D., Dell'Osso, L. F., & Daroff, R. B. 1978, Saccadic system plasticity in humans, *Ann Neurol*, 4, 313
- Anderson, M. E., Postupna, N., & Ruffo, M. 2003, Effects of high-frequency stimulation in the internal globus pallidus on the activity of thalamic neurons in the awake monkey, *J Neurophysiol*, 89, 1150
- Bahill, A. T., Clark, M. R., & Stark, L. 1975, The main sequence, a tool for studying human eye movements, *Math. Biosci.*, 24, 191
- Bahill, A. T. & Stark, L. 1977, Oblique saccadic eye movements. Independence of horizontal and vertical channels, *Arch Ophthalmol*, 95, 1258
- Barash, S., Melikyan, A., Sivakov, A., Zhang, M., Glickstein, M., & Thier, P. 1999, Saccadic dysmetria and adaptation after lesions of the cerebellar cortex, *J Neurosci*, 19, 10931
- Bastian, A. J., Martin, T. A., Keating, J. G., & Thach, W. T. 1996, Cerebellar ataxia: abnormal control of interaction torques across multiple joints, *J Neurophysiol*, 76, 492
- Becker, W. & Jurgens, R. 1990, Human oblique saccades: quantitative analysis of the relation between horizontal and vertical components, *Vision Res*, 30, 893
- Berkley, K. J. 1980, Spatial relationships between the terminations of somatic sensory and motor pathways in the rostral brainstem of cats and monkeys. I. Ascending somatic sensory inputs to lateral diencephalon, *J Comp Neurol*, 193, 283
- Butler, E. G., Bourke, D. W., & Horne, M. K. 2000, The activity of primate ventrolateral thalamic neurones during motor adaptation, *Exp Brain Res*, 133, 514

- Butler, E. G., Harvey, M. C., Finkelstein, D. I., & Horne, M. K. 1998, Neuronal activity in the monkey ventrolateral thalamus following perturbations of voluntary wrist movements, *Exp Brain Res*, 118, 393
- Butler, E. G., Horne, M. K., & Hawkins, N. J. 1992, The activity of monkey thalamic and motor cortical neurones in a skilled, ballistic movement, *J Physiol*, 445, 25
- Ceballos-Baumann, A. O., Boecker, H., Fogel, W., Alesch, F., Bartenstein, P., Conrad, B., Diederich, N., von Falkenhayn, I., Moringlane, J. R., Schwaiger, M., & Tronnier, V. M. 2001, Thalamic stimulation for essential tremor activates motor and deactivates vestibular cortex, *Neurology*, 56, 1347
- Clamann, H. P. 1969, Statistical analysis of motor unit firing patterns in a human skeletal muscle, *Biophys J*, 9, 1233
- Cohen, M. R., Meissner, G. W., Schafer, R. J., & Raymond, J. L. 2004, Reversal of motor learning in the vestibulo-ocular reflex in the absence of visual input, *Learn Mem*, 11, 559
- Collewijn, H., Erkelens, C. J., & Steinman, R. M. 1988, Binocular co-ordination of human horizontal saccadic eye movements, *J Physiol*, 404, 157
- Coltz, J. D., Johnson, M. T., & Ebner, T. J. 1999, Cerebellar Purkinje cell simple spike discharge encodes movement velocity in primates during visuomotor arm tracking, *J Neurosci*, 19, 1782
- Conrad, B., Matsunami, K., Meyer-Lohmann, J., Wiesendanger, M., & Brooks, V. B. 1974, Cortical load compensation during voluntary elbow movements, *Brain Res*, 71, 507
- Deuschl, G. & Bergman, H. 2002, Pathophysiology of nonparkinsonian tremors, *Mov Disord*, 17 Suppl 3, S41
- Diedrichsen, J., Hshambhoy, Y., Rane, T., & Shadmehr, R. 2005a, Neural Correlates of Reach Errors, *J Neurosci.*, in press.
- Diedrichsen, J., Verstynen, T., Lehman, S. L., & Ivry, R. B. 2005b, Cerebellar involvement in anticipating the consequences of self-produced actions during bimanual movements, *J Neurophysiol*, 93, 801

- Donchin, O., Francis, J. T., & Shadmehr, R. 2003, Quantifying generalization from trial-by-trial behavior of adaptive systems that learn with basis functions: theory and experiments in human motor control, *J Neurosci*, 23, 9032
- Donchin, O., Sawaki, L., Madupu, G., Cohen, L. G., & Shadmehr, R. 2002, Mechanisms influencing acquisition and recall of motor memories, *J Neurophysiol*, 88, 2114
- Dowsey-Limousin, P. 2002, Postoperative management of Vim DBS for tremor, *Mov Disord*, 17 Suppl 3, S208
- Duncan, R., Bone, I., & Melville, I. D. 1988, Essential tremor cured by infarction adjacent to the thalamus, *J Neurol Neurosurg Psychiatry*, 51, 591
- Dupuis, M. J., Delwaide, P. J., Boucquey, D., & Gonsette, R. E. 1989, Homolateral disappearance of essential tremor after cerebellar stroke, *Mov Disord*, 4, 183
- Elble, R. & Koller, W. 1990, *Tremor* (Baltimore: Johns Hopkins University Press)
- Elble, R. J. 1998, Animal models of action tremor, *Mov Disord*, 13 Suppl 3, 35
- . 2000, Origins of tremor, *Lancet*, 355, 1113
- Fabre, M. & Buser, P. 1979, [Visually guided movement in the cat: difference in the effects of a bilateral lesion of the thalamic nucleus ventralis lateralis performed either before or after training], *C R Seances Acad Sci D*, 288, 417
- Fernandez-Ruiz, J., Diaz, R., Hall-Haro, C., Vergara, P., Mischner, J., Nunez, L., Drucker-Colin, R., Ochoa, A., & Alonso, M. E. 2003, Normal prism adaptation but reduced after-effect in basal ganglia disorders using a throwing task, *Eur J Neurosci*, 18, 689
- Findlay, J. M. & Harris, L. R. 1984, in *Theoretical and Applied Aspects of Eye Movement Research.*, ed. A. G. Gale & F. Johnson (North-Holland: Elsevier)
- Flash, T. & Hogan, N. 1985, The coordination of arm movements: an experimentally confirmed mathematical model, *J Neurosci*, 5, 1688
- Fuchs, A. F., Robinson, F. R., & Straube, A. 1993, Role of the caudal fastigial nucleus in saccade generation. I. Neuronal discharge pattern, *J Neurophysiol*, 70, 1723

- Fujikado, T. & Noda, H. 1987, Saccadic eye movements evoked by microstimulation of lobule VII of the cerebellar vermis of macaque monkeys, *J Physiol*, 394, 573
- Garonzik, I. M., Hua, S. E., Ohara, S., & Lenz, F. A. 2002, Intraoperative microelectrode and semi-microelectrode recording during the physiological localization of the thalamic nucleus ventral intermediate, *Mov Disord*, 17 Suppl 3, S135
- Gaymard, B., Rivaud-Pechoux, S., Yelnik, J., Pidoux, B., & Ploner, C. J. 2001, Involvement of the cerebellar thalamus in human saccade adaptation, *Eur J Neurosci*, 14, 554
- Gengo, F. M., Kalonaros, G. C., & McHugh, W. B. 1986, Attenuation of response to mental stress in patients with essential tremor treated with metoprolol, *Arch Neurol*, 43, 687
- Georgopoulos, A. P., Kalaska, J. F., Caminiti, R., & Massey, J. T. 1982, On the relations between the direction of two-dimensional arm movements and cell discharge in primate motor cortex, *J Neurosci*, 2, 1527
- Goldberg, M. E., Musil, S. Y., Fitzgibbon, E. J., Smith, M. A., & Olson, C. R. 1993, in *Role of the Cerebellum and Basal Ganglia in Voluntary Movement*, ed. N. Mano, I. Hamada, & M. R. Delong (New York: Elsevier), 203–211
- Guietton, D. & Mandl, G. 1980, Oblique saccades of the cat: a comparison between the durations of horizontal and vertical components, *Vision Res*, 20, 875
- Halbig, T. D., Gruber, D., Kopp, U. A., Scherer, P., Schneider, G. H., Trottenberg, T., Arnold, G., & Kupsch, A. 2004, Subthalamic stimulation differentially modulates declarative and nondeclarative memory, *Neuroreport*, 15, 539
- Hallet, P. E. & Lightstone, A. D. 1975, in *Proc of the Assoc for Res in Vision and Ophthalmol*, Sarasota, 1
- Hallett, M. & Dubinsky, R. M. 1993, Glucose metabolism in the brain of patients with essential tremor, *J Neurol Sci*, 114, 45
- Harris, C. M. & Wolpert, D. M. 1998, Signal-dependent noise determines motor planning, *Nature*, 394, 780
- Hasan, Z. 1983, A model of spindle afferent response to muscle stretch, *J Neurophysiol*, 49, 989

- Hashimoto, T., Elder, C. M., Okun, M. S., Patrick, S. K., & Vitek, J. L. 2003, Stimulation of the subthalamic nucleus changes the firing pattern of pallidal neurons, *J Neurosci*, 23, 1916
- Haslinger, B., Boecker, H., Buchel, C., Vesper, J., Tronnier, V. M., Pfister, R., Alesch, F., Moringlane, J. R., Krauss, J. K., Conrad, B., Schwaiger, M., & Ceballos-Baumann, A. O. 2003, Differential modulation of subcortical target and cortex during deep brain stimulation, *Neuroimage*, 18, 517
- Hershey, T., Revilla, F. J., Wernle, A., Gibson, P. S., Dowling, J. L., & Perlmutter, J. S. 2004, Stimulation of STN impairs aspects of cognitive control in PD, *Neurology*, 62, 1110
- Hopp, J. J. & Fuchs, A. F. 2004, The characteristics and neuronal substrate of saccadic eye movement plasticity, *Prog Neurobiol*, 72, 27
- Hua, S. E. & Lenz, F. A. 2005, Posture-related oscillations in human cerebellar thalamus in essential tremor are enabled by voluntary motor circuits, *J Neurophysiol*, 93, 117
- Iwamoto, Y. & Yoshida, K. 2002, Saccadic dysmetria following inactivation of the primate fastigial oculomotor region, *Neurosci Lett*, 325, 211
- Jeljeli, M., Strazielle, C., Caston, J., & Lalonde, R. 2003, Effects of ventrolateral-ventromedial thalamic lesions on motor coordination and spatial orientation in rats, *Neurosci Res*, 47, 309
- Jenkins, I. H., Bain, P. G., Colebatch, J. G., Thompson, P. D., Findley, L. J., Frackowiak, R. S., Marsden, C. D., & Brooks, D. J. 1993, A positron emission tomography study of essential tremor: evidence for overactivity of cerebellar connections, *Ann Neurol*, 34, 82
- Jurgens, R., Becker, W., & Kornhuber, H. H. 1981, Natural and drug-induced variations of velocity and duration of human saccadic eye movements: evidence for a control of the neural pulse generator by local feedback, *Biol Cybern*, 39, 87
- Kassardjian, C. D., Tan, Y. F., Chung, J. Y., Heskin, R., Peterson, M. J., & Broussard, D. M. 2005, The site of a motor memory shifts with consolidation, *J Neurosci*, 25, 7979
- Kawato, M. 1989, Adaptation and learning in control of voluntary movement by the central nervous system, *Adv. Robotics*, 3, 229

- . 1996, in *Advances in Motor Learning and Control*, ed. H. N. Zelaznik (Champaign, IL: Human Kinetics)
- Keller, E. L. & Robinson, D. A. 1971, Absence of a stretch reflex in extraocular muscles of the monkey, *J Neurophysiol*, 34, 908
- King, W. M., Lisberger, S. G., & Fuchs, A. F. 1986, Oblique saccadic eye movements of primates, *J Neurophysiol*, 56, 769
- Kojima, Y., Iwamoto, Y., & Yoshida, K. 2004, Memory of learning facilitates saccadic adaptation in the monkey, *J Neurosci*, 24, 7531
- Koller, W. C., Pahwa, P. R., Lyons, K. E., & Wilkinson, S. B. 2000, Deep brain stimulation of the Vim nucleus of the thalamus for the treatment of tremor, *Neurology*, 55, S29
- Kommerell, G., Olivier, D., & Theopold, H. 1976, Adaptive programming of phasic and tonic components in saccadic eye movements. Investigations of patients with abducens palsy, *Invest Ophthalmol*, 15, 657
- Krebs, H. I., Hogan, N., Hening, W., Adamovich, S. V., & Poizner, H. 2001, Procedural motor learning in Parkinson's disease, *Exp Brain Res*, 141, 425
- Li, C. S., Padoa-Schioppa, C., & Bizzi, E. 2001, Neuronal correlates of motor performance and motor learning in the primary motor cortex of monkeys adapting to an external force field, *Neuron*, 30, 593
- Macchi, G. & Jones, E. G. 1997, Toward an agreement on terminology of nuclear and subnuclear divisions of the motor thalamus, *J Neurosurg*, 86, 670
- Marsden, C. D., Merton, P. A., & Morton, H. B. 1976, Stretch reflex and servo action in a variety of human muscles, *J Physiol*, 259, 531
- Martin, T. A., Keating, J. G., Goodkin, H. P., Bastian, A. J., & Thach, W. T. 1996, Throwing while looking through prisms. I. Focal olivocerebellar lesions impair adaptation, *Brain*, 119 (Pt 4), 1183
- Maschke, M., Gomez, C. M., Ebner, T. J., & Konczak, J. 2004, Hereditary cerebellar ataxia progressively impairs force adaptation during goal-directed arm movements, *J Neurophysiol*, 91, 230

- Matthews, P. B. 1996, Relationship of firing intervals of human motor units to the trajectory of post-spike after-hyperpolarization and synaptic noise, *J Physiol*, 492 (Pt 2), 597
- McIntyre, C. C., Grill, W. M., Sherman, D. L., & Thakor, N. V. 2004, Cellular effects of deep brain stimulation: model-based analysis of activation and inhibition, *J Neurophysiol*, 91, 1457
- Miall, R. C., Malkmus, M., & Robertson, E. 1996, Sensory prediction as a role for the cerebellum (commentary), *Behav. Brain Sci.*, 19, 466
- Mohadjer, M., Goerke, H., Milios, E., Etou, A., & Mundinger, F. 1990, Long-term results of stereotaxy in the treatment of essential tremor, *Stereotact Funct Neurosurg*, 54-55, 125
- Morasso, P. 1981, Spatial control of arm movements, *Exp Brain Res*, 42, 223
- Morton, S. M. & Bastian, A. J. 2006, Cerebellar contributions to locomotor adaptations during splitbelt treadmill walking, *J Neurosci*, 26, 9107
- Nagaratnam, N. & Kalasabail, G. 1997, Contralateral abolition of essential tremor following a pontine stroke, *J Neurol Sci*, 149, 195
- Noda, H., Sugita, S., & Ikeda, Y. 1990, Afferent and efferent connections of the oculomotor region of the fastigial nucleus in the macaque monkey, *J Comp Neurol*, 302, 330
- Nolte, J. & Angevine, J. 2000, *The Human Brain in photographs and diagrams*, 2nd edn. (Mosby, Inc.)
- Noto, C. T. & Robinson, F. R. 2001, Visual error is the stimulus for saccade gain adaptation, *Brain Res Cogn Brain Res*, 12, 301
- Optican, L. M. & Robinson, D. A. 1980, Cerebellar-dependent adaptive control of primate saccadic system, *J Neurophysiol*, 44, 1058
- O'Suilleabhain, P. E., Frawley, W., Giller, C., & Dewey, R. B., J. 2003, Tremor response to polarity, voltage, pulsewidth and frequency of thalamic stimulation, *Neurology*, 60, 786
- Padoa-Schioppa, C., Li, C. S., & Bizzi, E. 2002, Neuronal correlates of kinematics-to-dynamics transformation in the supplementary motor area, *Neuron*, 36, 751

- . 2004, Neuronal activity in the supplementary motor area of monkeys adapting to a new dynamic environment, *J Neurophysiol*, 91, 449
- Pare, M. & Hanes, D. P. 2003, Controlled movement processing: superior colliculus activity associated with countermanded saccades, *J Neurosci*, 23, 6480
- Paz, R., Boraud, T., Natan, C., Bergman, H., & Vaadia, E. 2003, Preparatory activity in motor cortex reflects learning of local visuomotor skills, *Nat Neurosci*, 6, 882
- Perlmutter, J. S., Mink, J. W., Bastian, A. J., Zackowski, K., Hershey, T., Miyawaki, E., Koller, W., & Videen, T. O. 2002, Blood flow responses to deep brain stimulation of thalamus, *Neurology*, 58, 1388
- Robinson, D. A. 1963, A Method of Measuring Eye Movement Using a Scleral Search Coil in a Magnetic Field, *IEEE Trans Biomed Eng*, 10, 137
- . 1975, in *Basic Mechanisms of Ocular Motility and Their Clinical Implications.*, ed. P. Bach-y Rita & G. Lennerstrand (Oxford, UK: Pergamon), 337–374
- Robinson, D. A., Gordon, J. L., & Gordon, S. E. 1986, A model of the smooth pursuit eye movement system, *Biol Cybern*, 55, 43
- Robinson, F. R., Fuchs, A. F., & Noto, C. T. 2002, Cerebellar influences on saccade plasticity, *Ann N Y Acad Sci*, 956, 155
- Robinson, F. R. & Noto, C. T. 2005, in *Society for Neuroscience*
- Robinson, F. R., Straube, A., & Fuchs, A. F. 1993, Role of the caudal fastigial nucleus in saccade generation. II. Effects of muscimol inactivation, *J Neurophysiol*, 70, 1741
- Sakai, S. T., Inase, M., & Tanji, J. 2002, The relationship between MI and SMA afferents and cerebellar and pallidal efferents in the macaque monkey, *Somatosens Mot Res*, 19, 139
- Schuurman, P. R., Bosch, D. A., Bossuyt, P. M., Bonsel, G. J., van Someren, E. J., de Bie, R. M., Merkus, M. P., & Speelman, J. D. 2000, A comparison of continuous thalamic stimulation and thalamotomy for suppression of severe tremor, *N Engl J Med*, 342, 461

- Schwartz, A. B., Kettner, R. E., & Georgopoulos, A. P. 1988, Primate motor cortex and free arm movements to visual targets in three-dimensional space. I. Relations between single cell discharge and direction of movement, *J Neurosci*, 8, 2913
- Schweighofer, N., Arbib, M. A., & Kawato, M. 1998, Role of the cerebellum in reaching movements in humans. I. Distributed inverse dynamics control, *Eur J Neurosci*, 10, 86
- Sergio, L. E. & Scott, S. H. 1998, Hand and joint paths during reaching movements with and without vision, *Exp Brain Res*, 122, 157
- Shadmehr, R. & Mussa-Ivaldi, F. A. 1994, Adaptive representation of dynamics during learning of a motor task, *J Neurosci*, 14, 3208
- Shahzadi, S., Tasker, R. R., & Lozano, A. 1995, Thalamotomy for essential and cerebellar tremor, *Stereotact Funct Neurosurg*, 65, 11
- Smit, A. C., Van Opstal, A. J., & Van Gisbergen, J. A. 1990, Component stretching in fast and slow oblique saccades in the human, *Exp Brain Res*, 81, 325
- Smith, M. A., Brandt, J., & Shadmehr, R. 2000, Motor disorder in Huntington's disease begins as a dysfunction in error feedback control, *Nature*, 403, 544
- Smith, M. A., Ghazizadeh, A., & Shadmehr, R. 2006, Interacting adaptive processes with different timescales underlie short-term motor learning, *PLoS Biol*, 4, e179
- Smith, M. A. & Shadmehr, R. 2005, Intact Ability to Learn Internal Models of Arm Dynamics in Huntington's Disease But Not Cerebellar Degeneration, *J Neurophysiol*, 93, 2809
- Snow, R., Hore, J., & Vilis, T. 1985, Adaptation of saccadic and vestibulo-ocular systems after extraocular muscle tenectomy, *Invest Ophthalmol Vis Sci*, 26, 924
- Soetedjo, R. & Fuchs, A. F. 2006, Complex spike activity of purkinje cells in the oculomotor vermis during behavioral adaptation of monkey saccades, *J Neurosci*, 26, 7741
- Sommer, M. A. & Wurtz, R. H. 2004, What the brain stem tells the frontal cortex. II. Role of the SC-MD-FEF pathway in corollary discharge, *J Neurophysiol*, 91, 1403

- Stepniewska, I., Sakai, S. T., Qi, H. X., & Kaas, J. H. 2003, Somatosensory input to the ventrolateral thalamic region in the macaque monkey: potential substrate for parkinsonian tremor, *J Comp Neurol*, 455, 378
- Straube, A., Deubel, H., Ditterich, J., & Eggert, T. 2001, Cerebellar lesions impair rapid saccade amplitude adaptation, *Neurology*, 57, 2105
- Sugita, S. & Noda, H. 1991, Pathways and terminations of axons arising in the fastigial oculomotor region of macaque monkeys, *Neurosci Res*, 10, 118
- Takagi, M., Zee, D. S., & Tamargo, R. J. 1998, Effects of lesions of the oculomotor vermis on eye movements in primate: saccades, *J Neurophysiol*, 80, 1911
- Thiele, A., Henning, P., Kubischik, M., & Hoffmann, K. P. 2002, Neural mechanisms of saccadic suppression, *Science*, 295, 2460
- Thomas, E. L. & O'Beirne, H. 1967, Curvature in the saccadic movement, *Arch Ophthalmol*, 77, 105
- Thoroughman, K. A. & Shadmehr, R. 1999, Electromyographic correlates of learning an internal model of reaching movements, *J Neurosci*, 19, 8573
- . 2000, Learning of action through adaptive combination of motor primitives, *Nature*, 407, 742
- Todorov, E. 2005, Stochastic optimal control and estimation methods adapted to the noise characteristics of the sensorimotor system, *Neural Comput*, 17, 1084
- Todorov, E. & Jordan, M. I. 2002, Optimal feedback control as a theory of motor coordination, *Nat Neurosci*, 5, 1226
- Uno, Y., Kawato, M., & Suzuki, R. 1989, Formation and control of optimal trajectory in human multijoint arm movement. Minimum torque-change model, *Biol Cybern*, 61, 89
- Urushitani, M., Inoue, H., Kawamura, K., Kageyama, T., Fujisawa, M., Nishinaka, K., Udaka, F., & Kameyama, M. 1996, [Disappearance of essential neck tremor after pontine base infarction], *No To Shinkei*, 48, 753

- Vaillancourt, D. E., Sturman, M. M., Verhagen Metman, L., Bakay, R. A., & Corcos, D. M. 2003, Deep brain stimulation of the VIM thalamic nucleus modifies several features of essential tremor, *Neurology*, 61, 919
- Van Gisbergen, J. A., Van Opstal, A. J., & G, R. J. 1987, in *Eye Movements: From Physiology to Cognition*, ed. J. K. O'Regan & A. Levy-Schoen (Amsterdam: Elsevier), 27–36
- Vaziri, S., Diedrichsen, J., & Shadmehr, R. 2006, Why does the brain predict sensory consequences of oculomotor commands? Optimal integration of the predicted and the actual sensory feedback, *J Neurosci*, 26, 4188
- Vilis, T. & Hore, J. 1980, Central neural mechanisms contributing to cerebellar tremor produced by limb perturbations, *J Neurophysiol*, 43, 279
- . 1981, Characteristics of saccadic dysmetria in monkeys during reversible lesions of medial cerebellar nuclei, *J Neurophysiol*, 46, 828
- Waespe, W. & Baumgartner, R. 1992, Enduring dysmetria and impaired gain adaptivity of saccadic eye movements in Wallenberg's lateral medullary syndrome, *Brain*, 115 (Pt 4), 1123
- Wallman, J. & Fuchs, A. F. 1998, Saccadic gain modification: visual error drives motor adaptation, *J Neurophysiol*, 80, 2405
- Weiner, M. J., Hallett, M., & Funkenstein, H. H. 1983, Adaptation to lateral displacement of vision in patients with lesions of the central nervous system, *Neurology*, 33, 766
- Westheimer, G. 1989, in *The Neurobiology of Saccadic Eye Movements*, ed. R. H. Wurtz & M. E. Goldberg, Vol. 3 (Amsterdam: Elsevier), 3–12
- Wolpert, D. M. & Ghahramani, Z. 2000, Computational principles of movement neuroscience, *Nat Neurosci*, 3 Suppl, 1212
- Zee, D. S., Optican, L. M., Cook, J. D., Robinson, D. A., & Engel, W. K. 1976, Slow saccades in spinocerebellar degeneration, *Arch Neurol*, 33, 243

H A I Y I N C H E N

haiyin.chen@gmail.com

EDUCATION

Johns Hopkins University School of Medicine, 1999-2006

- Ph.D in Biomedical Engineering
- Dissertation title: Cerebellar and Cerebellar Thalamic Contributions to Motor Adaptation
- Advisor: Dr. Reza Shadmehr, Department of Biomedical Engineering
- Co-advisors:
 - Dr. David Zee, Department of Neurology
 - Dr. Frederick Lenz, Department of Neurosurgery

Princeton University, 1994-1998

- B.S.E in Electrical Engineering
- Certificate in Applied and Computational Mathematics
- magna cum laude

PUBLICATIONS

- Chen H, Joiner WM, Zee DS., Shadmehr R. Adaptive control of saccades via forward models (submitted).
- Chen H, Hua, SE, Smith MA, Lenz FA, Shadmehr R. Effects of human cerebellar thalamus disruption on adaptive control of reaching. *Cerebral Cortex* 2006, 16:1464-73.
- Chen H, Smith MA, Shadmehr R. Effects of human deep brain stimulation on adaptive control of reaching. *Proc IEEE EMBS* 2005:5445-48.

HONORS

- Selected for NIH National Graduate Student Research Festival (2006)
- Ruth L. Kirschstein National Research Service Award Individual Fellowship (2004 -2006)
- Society for Neural Control of Movement Travel Scholarship (2006)
- Johns Hopkins University Graduate Student Association Student Travel Award (2005)
- Winner of Abstract Award for the best abstract at the American Society for Stereotactic and Functional Neurosurgery meeting (2004)
- Princeton University Scholarship (1994-1998)

MEETING ABSTRACTS (POSTERS/TALKS)

- Chen H: Adaptation induces curvature in saccades, revealing multiple time-scales of plasticity. Advances in Computational Motor Control meeting 2006 (talk)
- Chen H, Hua SE, Lawson, HC, Lenz FA, Shadmehr, R. Intra-operative recordings of neurophysiological activities of the human motor thalamus during reaching adaptation. Society for Neuroscience 2006 (poster)
- Chen H, Joiner WM, Shadmehr R, Zee DS. Cross-axis saccade adaptation, curved eye trajectories and forward models. Society for Neuroscience 2006 (poster)
- Chen H: Psychophysical and neurophysiological evidence on the role of human cerebellar thalamus on adaptive control of reaching. Society for Neural Control of Movement 2006 (invited talk)
- Chen H, Joiner WM, Shadmehr R, Zee DS. Cross-axis saccade adaptation induces curvature in saccade trajectories. Society for Neural Control of Movement 2006 (poster)
- Chen H, Joiner WM, Smith MA, Shadmehr R, Zee DS. Cross-axis saccade adaptation induces curvature in saccade trajectories. Society for Neuroscience 2005 (poster)
- Chen H, Smith MA, Shadmehr R. Effects of deep brain stimulation on adaptive control of reaching. Institute of Electrical and Electronics Engineers (IEEE), Engineering in Medicine and Biology Society 2005 (poster)
- Chen H, Hua SE, Shadmehr R, Lenz FA. Thalamotomy and thalamic DBS in a voltage dependent manner impairs motor adaptation in patients with essential tremor. American Society for Stereotactic and Functional Neurosurgery 2005 (talk)
- Hua SE, Chen H, Lenz FA, Shadmehr R. Vim thalamotomy disrupts motor adaptation. Society for Neuroscience 2003 (poster)
- Chen H, Hua SE, Lenz, FA, Shadmehr R. Effect of thalamic deep brain stimulation on motor learning. Society for Neuroscience 2003 (poster)

WORK EXPERIENCE

- Teaching Assistant in the Department of Biomedical Engineering, Johns Hopkins University. Biomechanics and Computational Motor Control (2001) and Circuit and Systems (2002).
- Lecturer, Temasek Polytechnic Department of Telecommunication, Singapore (1998-1999). Taught courses in Differential Equations, Circuits and Systems, Digital Communication and Telecommunication.
- Software Engineer, KLA-Tencor, San Jose, CA (Summer 1997). Designed quality control user interface software using Excel Visual Basic.

- Research Assistant, Department of Electrical Engineering, Princeton University. (Summer 1996). Programmed in C to perform face detection and recognition in digital video.
- Summer Intern, Oak Ridge National Laboratory, Oak Ridge, TN (1995). Assisted with computer simulation of nuclear fusion reaction.